TU Delft Delft University of Technology

Environmental Engineering Master Thesis

NOVEL MULTI FACADE DESIGN: The design of a insulated bioreceptive facade panel for retrofitting buildings

Author:
Salvör Svanhvít Björnsdóttir (6077781)

Supervisor :
M. Ottelé (Chair)
Max Veeger (Daily supervisor)
Jagoda Cupać (External supervisor)

November 6, 2025

Preface

I want to thank my supervisors, Marc, Max, and Jagoda, for their guidance and encouragement throughout this project. Your support, patience, and knowledge have been essential in helping me finish this thesis, and you made the process not only manageable but also enjoyable. A big thank you as well to Maiko and Martin for their extra help and guidance along the way.

To my family and friends back home in Iceland, thank you for always being there for me and for believing in me no matter what. I am so grateful for your constant encouragement and support.

I also want to thank my "Delft family," as I like to call them. Without you, these last two years would have been a lot harder and definitely a lot less fun. I feel lucky to have met such amazing people here, and I know we'll keep making memories together for years to come.

Finally, I would like to dedicate this thesis and my degree in Environmental Engineering to my late brother, Sigurður Darri Björnsson. Sigurður was one semester away from completing his bachelor's degree in Civil and Environmental Engineering at the University of Iceland, a field in which he would no doubt have achieved great things. As little sisters often do, I followed in his footsteps in many things, and pursuing a degree in Civil and Environmental Engineering was no exception. Without him, I might never have chosen this path. a path I now know is truly right for me. This degree is for us, Siggi. We did it.

Summary

This thesis investigates the design and performance of a multilayered bioreceptive facade system intended for retrofitted infrastructure. The system combines concrete, cork insulation, waterproof membrane and moss layers, with the aim of balancing thermal performance, bioreceptivity, and circularity. The research addresses the question: How can an exterior facade system be optimized for bioreceptivity, circularity, and thermal performance by selecting the best performing moss species and suitable insulation material?

The study implemented heat flux measurements in a hot-box setup to assess the thermal conductivity and resistance of bioreceptive concrete panels colonized by three moss species: *Grimmia pulvinata*, *Ptychostomum capillare*, and *Brachythecium rutabulum*. A life cycle assessment and multi-criteria analysis guided the selection of insulation materials, with cork identified as the optimal option due to its renewable origin, thermal efficiency, and negative shadow cost. Circularity principles were included in the design through mechanical fastening systems, reversible installation methods, and clean material separation to support reuse and recycling.

Results demonstrate that the combined system can achieve Dutch building regulation requirements for external facade R-values. While moss layers only provide moderate improvements in thermal insulation, their ecological and aesthetic benefits further enhance facade multifunctionality. Trade-offs were observed, as *Ptychostomum capillare* achieved the lowest thermal conductivity under dry conditions, whereas *Grimmia pulvinata* proved to be more resilient under saturated condictions. A life cycle assessment confirmed that cork insulation provides significant environmental advantages, including biogenic carbon storage, while concrete production remains the main contributor to impacts. Overall, the system achieved a relatively low shadow cost per square meter, further reduced by ecological co-benefits such as carbon sequestration and pollutant capture from moss layers.

The findings also highlight limitations of the study, including the reliance on simplified laboratory experiments that cannot fully replicate outdoor conditions, and the need for long-term durability testing of the proposed assembly methods. Material selection revealed trade-offs between technical performance and environmental goals, with cork favored over technically stronger rock wool due to its circularity and carbon storage potential. The system is particularly suited for retrofitting existing masonry buildings, though cork's thickness and sensitivity to moisture present design challenges.

This research highlights the feasibility of integrating renewable insulation materials and bioreceptive surfaces in facade systems, offering a pathway to improving the energy efficiency of existing buildings while supporting circular construction practices.

Contents

List of Figures

List of Tables

Chapter 1

Introduction

Since the Industrial Revolution, the global economy has relied heavily on cheap energy, raw materials, and other resources. This overexploitation has pushed the Earth's capacity to a critical threshold, approaching a point of no return (Kunič, 2017). By 2050, it is estimated that 70% of the world's population will live in urban areas (United Nations, 2014). Rapid urbanization intensifies environmental challenges, placing additional pressure on energy systems, material resources, and the livability of cities. Figure 1.1 summarizes the negative environmental impacts of urbanization that future solutions must address.

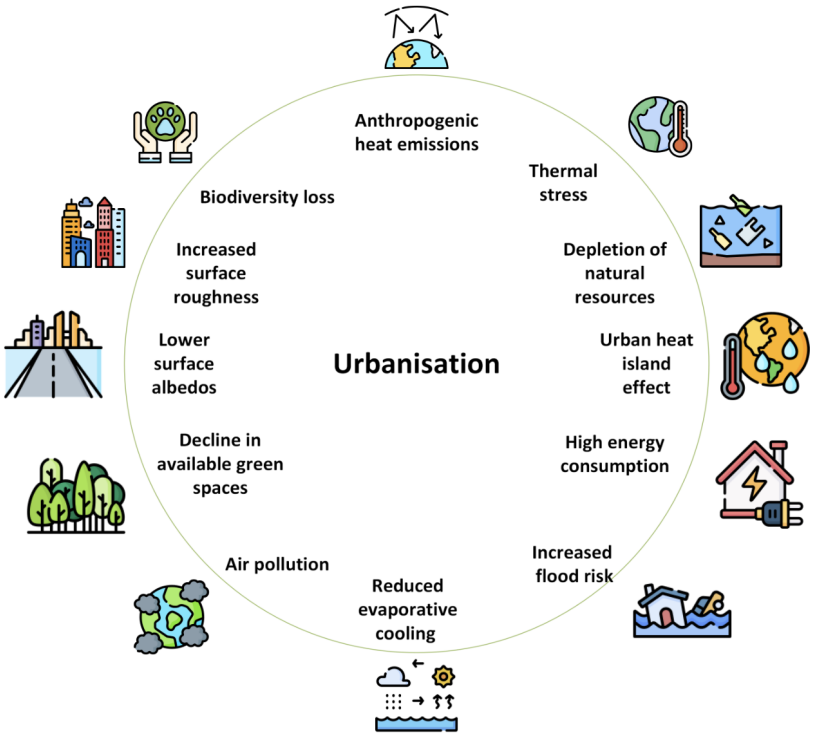

Figure 1.1: Negative environmental impact of urbanisation

High energy consumption in buildings further exacerbates these challenges. Climate change and population growth are expected to increase building energy demand in the coming decades, making energy efficiency a critical aspect of sustainable development (Jamilu et al., 2024). The building envelope, in

particular, offers significant potential for energy savings. High-performance insulation not only reduces energy use but also mitigates urban issues such as noise pollution, which affects approximately 65% of European citizens and is linked to serious health impacts (Asdrubali et al., 2015).

Improving the energy efficiency of existing buildings is therefore a crucial strategy for reducing greenhouse gas emissions and mitigating climate change. Retrofitting older buildings can achieve reductions in energy consumption, with some studies reporting up to a 50% decrease (Iwuanyanwu et al., 2025). Beyond operational energy, retrofitting existing buildings is oftena a more sustainable option than new construction. The embodied carbon emissions associated with demolishing and rebuilding structures can be substantial. Enhancing the energy efficiency of existing buildings therefore aligns closely with principles of sustainability and circular economy (Bienert, 2023).

The building and construction industry contributes roughly 40% of global energy consumption and CO_2 emissions, while generating substantial material and solid waste (Azariy et al., 2023; Jamilu et al., 2024). To mitigate these impacts, sustainable strategies must be implemented throughout the entire building lifecycle, including reducing both its energy and material consumption, improving resource efficiency, and promoting recycling and effective waste management (Kunič, 2017).

One promising approach to address these challenges is the implementation of green wall systems, also known as living walls or vertical gardens. These facade systems integrate vegetation directly into the building envelope, offering multiple benefits such as thermal insulation, noise reduction, material protection, improved air quality, and enhanced visual appeal (Fernando et al., 2023; Stohl et al., 2023). For instance, Fernando et al. (2023) reports that green walls can reduce external wall surface temperatures by up to 20.9°C and decrease indoor temperatures by approximately 11°C. Beyond environmental performance, green walls also provide social and health benefits, including stress reduction and faster recovery rates for hospital patients.

Despite these advantages, integrating green walls into buildings often presents challenges in plant selection, material sustainability, and long-term resilience (M. Manso & Castro-Gomes, 2015). Moss-based facades offer a promising alternative to these challenges, as moss species are resilient to outdoor conditions, require minimal maintenance, and contribute to both thermal regulation and urban biodiversity (Rotondi et al., 2024). By combining moss with carefully selected insulation materials, it is possible to create multilayered, bioreceptive facade systems. This approach introduces the concept of *bioreceptivity*, which describes the ability of building materials to support biological colonization and provides the theoretical foundation for this research (Hueck, 1965; Stohl et al., 2023).

1.1 Objective

The primary objective of this project is to design a multilayered facade system suitable for retrofitted infrastructure, combining high thermal performance with bioreceptive properties. The system will support the growth of selected moss species, chosen based on their resilience to outdoor conditions and their contribution to the facades thermal performance. In addition, the project prioritizes circularity and sustainability by selecting materials with low environmental impact, ensuring that the facade system aligns with principles of sustainable construction, by choosing circular assembly and dissasembly methods.

To meet these objectives, material selection will be guided by specific performance criteria, including thermal insulation, circularity, and the ability to support biological growth. Laboratory experiments will

be carried out to evaluate the thermal conductivity of the concrete mixture and various moss species commonly found on built structures in the Netherlands. The performance of the combined system as a whole will also be assessed.

1.2 Scope and delimitations

This research focuses on the design of a moss based multilayered facade system for retrofitted buildings. The study includes the selection of insulation materials, moss species, and concrete mixtures, as well as laboratory testing to evaluate thermal performance and bioreceptivity. Durability testing, large scale implementation, long term maintenance, and full urban scale environmental impact assessments are beyond the scope of this project.

1.3 Research question

The following research question is proposed to guide the project towards an optimized facade system that balances bioreceptivity and thermal performance:

How can an exterior facade system be optimized for **bioreceptivity**, **circularity** and **thermal performance** by selecting the best performing moss species and suitable insulation material?

The following sub-questions are proposed to guide the research process in a systematic manner toward addressing the main research question.

1. Which insulation material provides the optimal balance of thermal performance, sustainability, and compatibility with a bioreceptive concrete facade system?
2. Which selected moss species most effectively contributes to enhancing the thermal performance of the facade system?
3. What is the overall thermal conductivity of the optimized facade system, and does it meet current building regulations for thermal resistance ($\geq 4.7\ (m^2 \cdot K)/W$)?

Chapter 2

Literature review

2.1 Bioreceptive concrete

Concrete is a widely used building material in various construction practices today. This is mainly due to its affordability, easy production methods, versatility and accessibility to raw materials. Concrete consists of cement, water, differently grained aggregates, and various binders. Additionally, additives or substitutions can be introduced to the concrete mixture in order to modify its properties and even further reduce its environmental impact (Stohl et al., 2023).

Therefore, concrete is a highly suitable material to facilitate bioreceptivity, since the concrete mix design can be modified to tailor specific properties that ensure bioreceptivity. To do so effectively, it is essential to first identify the key parameters that influence bioreceptivity of concrete beforehand, and then adjust the mix design accordingly based on these desirable parameters (Stohl et al., 2023).

2.1.1 Bioreceptivity

The neutral term "hylobiology" was first used to describe biological colonization, but the term was quickly changed to "biodeteriation" and "biodegradation" in the late 1960s. These terms stuck for this phenomenon until research performed by Guillete changed the negative perception of biological colonization of a building material for the better (Hueck, 1965; Stohl et al., 2023). The term *bioreceptivity* was now defined by Guillitte as: *"The aptitude of a material (or any object) to be colonized by one or several groups of living organisms without necessarily undergoing any biodeterioration"* (Guillitte, 1995). Today, recent studies have further explored and refined the concept of bioreceptivity for the better (Stohl et al., 2023).

Bioreceptivity is a rather complex concept, and much is yet to be defined and explored. It is a dynamic parameter that changes over time and can be defined over a few stages. Primary bioreceptivity, or intrinsic bioreceptivity of a new material, is before the material is exposed to the outdoor environment and before being associated weathering mechanisms. Once it has been exposed, the material reaches secondary bioreceptivity, which is then quickly followed by tertiary bioreceptivity. That is when the addition of coatings are formed, which act as a measure of maintenance. The last stage is extrinsic bioreceptivity, or

when materials, such as dust on the surface, accumulate on the surface of the material (Sanmartín et al., 2021; Stohl et al., 2023).

As expected, numerous factors influence bioreceptivity. First and foremost, it depends on the building material itself, particularly its physical and chemical properties (Stohl et al., 2023). The surrounding environment is another major factor, with climate, microclimate, and local conditions all playing significant roles. Lastly, biological factors also can contribute bioreceptivity, where the type of microorganisms or biodiversity already present can be of great influence, as well as their abundance or biomass (Stohl et al., 2023). These three contributing factors are summarized in Figure 2.1 here below.

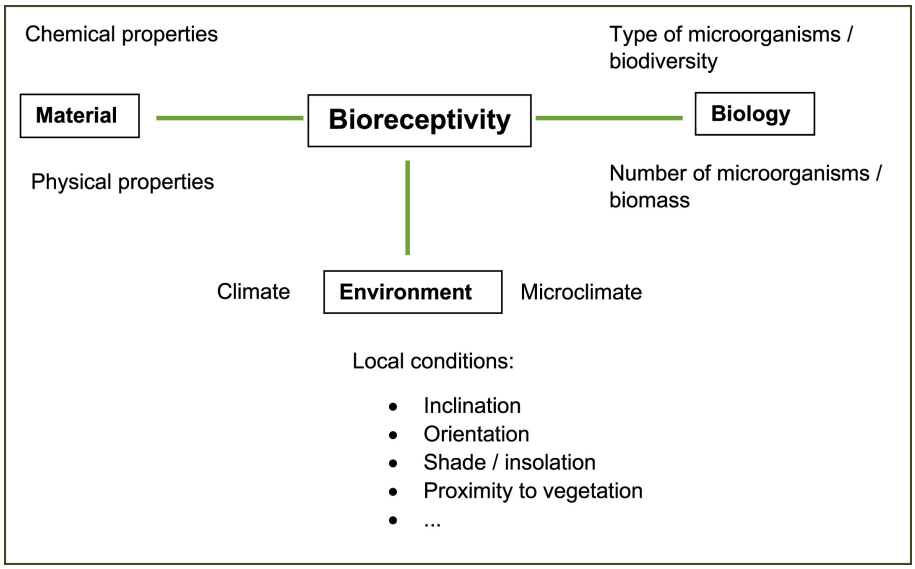

Figure 2.1: Influencing parameters of bioreceptivity(Stohl et al., 2023).

Moss

Mosses exhibit unique characteristics that make them particularly suitable for bioreceptive surfaces. They differ from vascular plants because they lack roots and instead use rhizoids for their attachment to a surface (Glime, 2017c). They absorb water and nutrients directly through their thin, cuticle covered leaves and stems (Glime, 2017b). Additionally, rather than utilizing seeds for reproduction, the reproduction of moss occurs via spores, vegetative propagules, or fragmentation (Glime, 2017a; Veeger et al., 2023).

One of the key adaptations of mosses is *poikilohydry*, a process when mosses suspend metabolic activity during desiccation and resume function when rehydration occurs. Their capacity to absorb water and nutrients directly through their leaves and stems is facilitated by a thin cuticle, which allows them to survive in fluctuating moisture conditions (Proctor et al., 2007; Veeger et al., 2023).

Veeger et al. (2025) investigated 137 moss communities across three Dutch cities: Amsterdam, Rotterdam, and The Hague. Through both exploration and analysis, seven primary colonizing species were identified (Veeger et al., 2025). Table 2.1 includes the 7 pioneering moss species identified, along with the type of species and the common name of the species.

Species	Type of species	Common name
Tortula muralis	Acrocarp	Wall Screw moss
Grimmia pulvinata	Acrocarp	Grey cushioned Grimmia
Ptychostomum cappillare	Acrocarp	Holyoak N. Pedersen
Orthotrichum diaphanum	Acrocarp	White-tipped Bristle moss
Rhynchostegium confertum	Pleurocarp	Clustered feathermoss
Hypnum cupressiforme	Pleurocarp	Cypress-leaved plait-moss
Brachythecium rutabulum	Pleurocarp	Rough-stalked Feather-moss

Table 2.1: Identified primary colonizing species (Veeger et al., 2025)

Acrocarp species tend to thrive in more exposed environments, while pleurocarp species prefer shaded habitats. Therefore, for bioreceptive concrete structures, acrocarp pioneers are recommended for sun-exposed locations, whereas pleurocarp pioneers are better suited for shaded areas (Veeger et al., 2025).

2.1.2 Factors that influence the bioreceptivity of concrete

Due to its ability to be tailored through mix design, concrete is considered a highly suitable material for enhancing bioreceptivity. To do so effectively, it is essential to first identify the key parameters that influence the materials bioreceptivity beforehand, and then adjust the mix design according to these desirable parameters (Stohl et al., 2023).

Bioreceptivity is influenced by both chemical and physical properties of the chosen material. While physical properties play a dominant role, chemical properties must also be carefully considered when optimizing bioreceptivity. Chemical factors include mineralogical composition, nutrient content and pH levels, while physical properties encompass surface roughness, texture, porosity, permeability, water absorption, water retention, wettability and drying characteristics (Stohl et al., 2023).

pH level

Since concrete is a alkaline building material with rather high initial pH levels, the materials pH level is a chemical property that highly influences bioreceptivity of the material. Fresh concrete can exhibit extremely high pH levels, often exceeding levels of 12 or even 13. Over time, carbonation lowers this initial pH, which makes the surface more hospitable for biological colonization. Most organisms prefer lower pH values, but it has also been proven that high or low pH levels are not as influential as initially thought (Stohl et al., 2023).

Ordinary Portland Cement (OPC) is commonly used in concrete mixtures, but its high initial pH can reduce bioreceptivity (Natanzi et al., 2021) . Alternative binders, such as magnesium phosphate cement (MPC), have been explored for their potential to improve water retention and bioreceptivity (S. Manso et al., 2014). However, research on these alternatives remains limited, and current findings suggest they may not perform well in outdoor environments (Veeger et al., 2023).

Nutrient content

Photoautotrophic organisms, such as moss, require only minimal amounts of additional nutrients, as they primarily rely on CO_2, sunlight, and water for survival (Stirbet et al., 2020). The small amount of nutrients they do need can be obtained from the surrounding environment via aerosols. Key additional nutrients, such as phosphate and nitrogen, are typically present in sufficient quantities in surrounding environments and can be deposited onto the concrete surface through aerosol transport (Katarzyna et al., 2015; Stohl et al., 2023). .

Furthermore, adding nutrients such as phosphate to the concrete mixture can enhance its bioreceptivity (S. Manso et al., 2014). While this approach shows significant potential, it still requires further research to fully understand its link to bioreceptivity (Veeger et al., 2023). Magnesium-phosphate cement (MG-P cement) and bone-ash have been investigated to a certain extent, with research indicating its suitability for bioreceptivity. For MG-P cement, results show that it maintains a low pH and provides nutrients for microorganisms but at the expense of lower comparative strength (Stohl et al., 2023; Veeger et al., 2023).

Surface roughness and geometry

Surface roughness has been directly linked to bioreceptivity, where increased roughness enhances surface area of microorganisms by providing anchoring points for microorganisms, and improves nutrient and water retention. Additionally, roughness aids in biofilm formation by protecting microorganisms from shear stress caused by wind and water flow (Stohl et al., 2023).

Mustafa et al. (2021) identified that the most effective macro-geometry for enhancing bioreceptivity in facade panels involves the use of continuous "along-the-flow" obstacles. These obstacles, arranged in a structured alternating patter, extend the water flow path, promoting sustained moisture availability and encouraging moss growth. This leads to a prolonged flow path, ranging from varying lengths and promoting a continuous trail of growth.

2.1.3 Porosity and permeability

Enhancing water storage and retention within concrete is a crucial factor to improve bioreceptivity. Therefore, porosity and permeability are two crucial parameters for the bioreceptivity of concrete (Stohl et al., 2023) . For traditional concrete, increasing porosity is generally avoided due to its negative impact on compressive strength and increased susceptibility to freeze-thaw damage (Veeger et al., 2023).

Concrete mixture composition significantly influences porosity and pore size distribution, where key factors include the water/binder ratio, binder composition, mixing procedure, and compaction intensity (Veeger et al., 2023). Several measures can be undertaken to achieve the increase of water storage and retention within concrete, they are the following according to Veeger et al. (2023):

1. Increasing the porosity of the concrete's aggregates
2. Raising the water-to-binder ratio
3. Incorporation of superabsorbent polymers (SAPs)
4. Combination of measures (1), (2) and/or (3)

Water absorption and retention

For facade system applications, it is important to consider what types of pore systems can be found in the concrete material, as it controls water and surface interactions. Aditionally, pores and their connectivity withing the substrate greatly influence bioreceptivity (Stohl et al., 2023).

Concrete pores are classified by size into gel pores, micropores, mesopores, capillary pores, and macropores. However, pore size classifications vary, making comparisons rather difficult. Capillary pores have the most significant influence on bioreceptivity, as they regulate vapor and fluid transfer within the material. Without capillary pores, microorganisms on the surface would struggle to obtain sufficient water for survival (Stohl et al., 2023). Beyond pore size, the connectivity of pores is also crucial. A well-connected pore network enhances water retention, absorption, and drying characteristics, which directly impacts bioreceptivity (Stohl et al., 2023).

Types of pores, pore systems and permeability found in Concrete is shown in Figure 2.2. As can be seen, there are three types of pores, open blind pores, closed pores and interconnected pores. Closed pores are non-permeable and interconnected pores are permeable, increasing the the permeability of the concrete. The network of interconnected pores is crucial for bioreceptivity, as it is decisive for water absorption, water retention and drying of the material (Li et al., 2021; Nikaido & Vaara, 1985; Stohl et al., 2023).

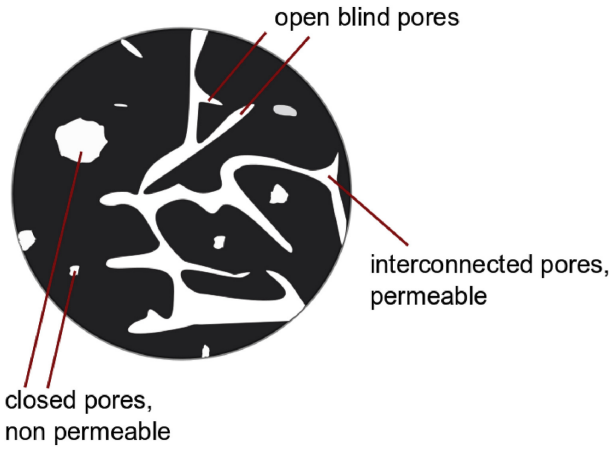

Figure 2.2: Types of pore systems, pores and permeability found in concrete substrates and other materials (Stohl et al., 2023)

Ideally, to improve bioreceptivity, the pore system should be able to store rain and dew water near the surface, ensuring accessibility for the microorganisms. Rapid water transport into deep layers of the material can lead to decreased bioreceptivity (Stohl et al., 2023; von Werder et al., 2015).

Additionally, high relative humidity creates ideal conditions for microorganisms (Häubner et al., 2006). Prolonged surface wetness is beneficial and can be achieved by modifying the material's surface structure to enhance water retention, allowing water droplets to adhere and remain on the surface for longer periods (Stohl et al., 2023).

Surface texture has been found to increase water capacity and retention. The employment of a surface retarder has been found to increase water absorption of concrete (Veeger et al., 2023).

There is a clear correlation between local water retention and patterns of biological growth (Solga et al., 2007; Stohl et al., 2023). To enhance the material's bioreceptivity, surfaces with low surface energy and

appropriate microstructures are required, as they promote water spreading and retention. Low-energy surfaces allow water droplets to spread out, minimizing surface tension and achieving a lower energy state (Feng et al., 2008; Stohl et al., 2023).

2.2 Insulation properties

A key strategy for reducing the total energy consumption of a building is by improving the insulation properties of building envelopes. Heat loss through walls and roofs directly impacts a buildings energy consumption.

Thermal conductivity of traditional building materials is usually higher than that of thermal building insulation materials, resulting in the application of thermal building insulation materials (Jelle, 2011). Thermal conductivity values for traditional building materials can be seen in Table 2.2, where it is clear that aluminum has the highest thermal conductivity value, followed by carbon steel, stainless steel, stone, brick, concrete, glass, and lightweight concrete.

Material	**Thermal conductivity [W/(mK)]**
Wood	0.1 – 0.2
Carbon Steel	55
Stainless steel	17
Aluminium	220
Concrete	0.15 – 2.5
Lightweight aggregate	0.10 – 0.70
Brick	0.40 – 0.80
Stone	1 – 2
Glass	0.80

Table 2.2: Thermal conductivity of traditional building materials (Jelle, 2011)

Thermal conductivity (λ) represents the steady-state heat flow passing through a unit area of a homogeneous material with a thickness of 1 meter, induced by a 1K temperature difference across its surfaces (Asdrubali et al., 2015). Refer to Appendix A.1.2 for more information on the concept of thermal conductivity.

2.2.1 Factors that influence insulation properties of concrete

Energy loss of buildings can be minimized with the consideration of thermal conductivity (λ-value) of concrete. Several factors influence the thermal conductivity of concrete, including moisture content, aggregate type, cementious material type, and overall concrete density (Asadi et al., 2018).

Moisture content

It has been proven that concrete in a saturated state exhibits higher thermal conductivity, compared to dry concrete, due to water's thermal conductivity being approximately 25 times greater than that of air, leading to an overall increase in heat transfer (Asadi et al., 2018; Bessenouci et al., 2014; Shin & Kodide, 2012).

According to Valore (1980), with each 1 % increment in the moisture content of concrete, the λ rises by approximately 6%. This effect has been confirmed for various type of concrete. For instance, in fly-ash concrete at 350 °C, the λ increased from 1.151 to 1.603 W/mK as the relative humidity of the micro-environment was enhanced from 20% to 100% (Wang et al., 2017). Similarly, in autoclave aerated concrete (AAC), a notable increase in thermal conductivity was observed as moisture content increased (Asadi et al., 2018).

Aggregates

As aggregates make up approximately 60-80% of concrete's volume, their type and proportion significantly influence the materials thermal conductivity (Asadi et al., 2018). Increasing the volume fraction of coarse aggregate while keeping the sand fraction constant results in higher thermal conductivity (Ahmed & Kamau, 2017; Asadi et al., 2018).

Normal weight concrete exhibits a thermal conductivity range from 0.6-3.3 W/mK, while lightweight concrete lowers this range to 0.2-1.9 W/mK. Therefore, by using lightweight concrete in both structural and non-structural building envelopes, heat transfer and energy consumption can be reduced significantly (Asadi et al., 2018).

Phase change material (PCM)

Due to the ability of Phase Change Materials (PCMs) to store and regulate heat, they are widely used in building applications to improve thermal comfort and reduce energy consumption (Sá et al., 2012; Zhang et al., 2013). The thermal conductivity of PCM-modified cementitious materials is lower than that of conventional concrete. For example, adding around 5% PCM by total weight can reduce the value by approximately 5% (Aguayo et al., 2017; Asadi et al., 2018).

Density of concrete

A strong correlation exists between concretes unit weight and thermal conductivity (Sengul et al., 2011). Reducing the density of concrete can effectively lower its thermal conductivity, which can be, for example, achieved by (Asadi et al., 2018) :

1. Introducing artificial air voids using foaming agents or aluminum powder in foamed concrete (FC)
2. Replacing conventional aggregates with lightweight aggregates (LWAs).

Porosity

Porosity plays a significant role in determining a material's thermal conductivity. Increasing porosity by 1% can reduce thermal conductivity by approximately 0.6% (Asadi et al., 2018; Real et al., 2016).

2.2.2 Thermal insulation materials

The primary function of thermal insulation materials is to reduce heat transfer through building envelopes, thereby enhancing energy efficiency (Asdrubali et al., 2015). In recent years, the benefits of insulation materials have gained increasing recognition where previously, the focus was primarily placed on improving thermal and sound insulation. However, there is now a growing awareness of their role in reducing environmental impact, enhancing indoor air quality, and increasing overall energy efficiency of building (Erzen et al., 2025). .

Today, it is possible to choose from a wide variety of insulation materials, where they vary in chemical composition (organic or inorganic), origin (partially or completely recycled, or derived from new raw materials), specific weights (from 12-600 kg/m^3), thermal conductivity (λ ranges from 3-45 mw/(mK), and resistance to physical (moisture, elevated temperature, presence of UV radiation, pressure, shear, laminated or other strength), and chemical factors (presence of organic solvents, moisture, oxidation and reaction to fire) (Kunič, 2017).

In the following subsections, traditional and recently developed thermal building insulation materials will be discussed, along with a few chosen state-of-the-art insulation materials. Traditional thermal building insulation materials are commonly manufactured from petrochemical derived materials, such as polystyrene, or from natural sources like glass and rock wool. However, these conventional materials often come with high energy consumption costs during production (Asdrubali et al., 2015). Currently, the insulation material market is dominated by a few categories of thermoacoustic insulators, including mineral wool, extruded polystyrene (XPS), and expanded polystyrene (EPS). At the end of their lifespan, these materials are challenging to recycle or reuse, which poses environmental concerns (Asdrubali et al., 2015). Luckily, research and development in sustainable construction materials have led to advancements in thermal and acoustic insulation by utilizing either natural or recycled materials. The incorporation of recycled synthetic materials or industrial byproducts presents an environmentally friendly alternative, reducing dependence on virgin resources and minimizing landfill waste. Several innovative insulation materials have been successfully developed in recent years, including recycled glass foam and fibers, cork, recycled plastics, recycled cotton and denim, and recycled textile fibers (Asdrubali et al., 2015). Other state-of-the-art thermal building materials include vaccum insulation panels (VIP), aerogels and phase change materials (PCM) (Jelle, 2011)

Mineral wool

There are two types of mineral wool, glass wool and rock wool. Glass wool is produced at high temperatures (approximately 1400°C) from borosilicate glass, while rock wool is made by melting stone, such as diabase or dolerite, at even higher temperatures (around 1500°C). In both cases, additional materials, such as abatement oil and phenolic resin, are incorporated to bind the fibers and enhance their properties. The final product can be perforated, cut, and adjusted on-site without compromising its thermal resistance (Jelle, 2011) Figure 2.3 provides an example of glass wool as a thermal building insulation material and its application to building panel insulation.

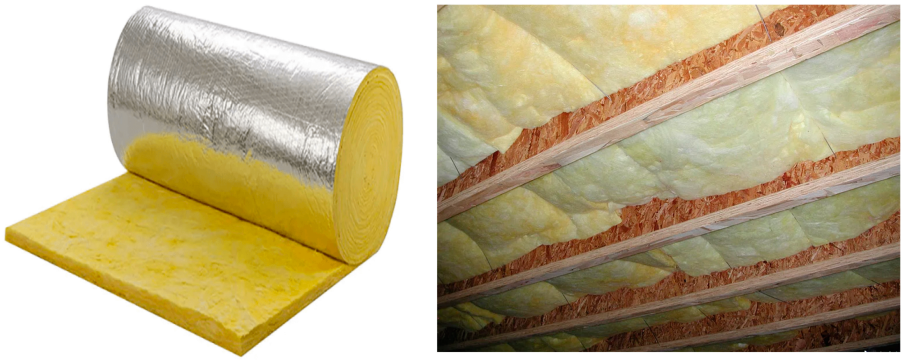

(a) (b)

Figure 2.3: Example of glass wool as a thermal building insulation material and its application to building panel insulation (Ali et al., 2024)

Typical thermal conductivity of mineral wool ranges from 0.030 to 0.040 W/(m· K). However, this value can vary depending on factors such as temperature, moisture content, and mass density. For instance, an increase in moisture content from 0 vol% to 10 vol% can raise thermal conductivity from 37 to 55 mW/(m· K) (Jelle, 2011).

Cellulose

A thermal insulation material made from cellulose (plyasccharide ($(C_6H_{10}O_5)_n$) includes recycled paper or wood fiber mass. The consistency of this thermal insulation material is that similar to that of wool. Additional materials used are boric Acid (H_3BO_3) and Borax (sodium borates $Na_2B_4O_7 \cdot 10H_2O$, added in order to improve neccessary properties of the product. Typical thermal conductivity for cellulose insulation is between 0.040 and 0.050 W/(mK) (Jelle, 2011).

Cork

The primary material of cork thermal insulation is cork oak. It can be produced as both a filler material or boards, Figure 2.4 provides an example of cork as a thermal building insulation material produced as a board (Jelle, 2011).

Figure 2.4: Example of cork insulation boards (MaterialDistrict, 2025)

The boards can be perforated, cut and adjusted at the building site, without any loss of thermal resistance. Typical thermal conductivity of cork boards are between 0.040-0.050 W/(mK) (Jelle, 2011).

Polyurethane (PUR)

Polyurethane (PUR) is made from natural and synthetic polymers, where the formation of the material is when a reaction between isocyanates and polyols occurs (Jelle, 2011; Kunič, 2017). During the expansion process, closed pores are filled with an expansion gas (HFC, CO_2, or C_6H_{12}). The resulting product is either insulation boards or expanding foam (Jelle, 2011).

PUR is known for its low thermal conductivity, high strength and lightweight structure. Typical thermal conductivity of polyurethane is between 0.020-0.030 W/(mK), which is the lowest thermal conductivity value when compared with other traditional insulation materials such mineral wool, polystyrene and celllose thermal insulation boards (Jelle, 2011).

It should be noted that PUR has given cause for serious health concerns and hazards in case of a fire. If a fire occurs, PUR will release hydrogen cyanide (HCN) and isocyanets, which is very poisonous (Jelle, 2011).

Expanded polystyrene (EPS)

Expanded polysterene (EPS) is made out of small spheres of polystyrene, which is derived from crude oil, containing an expansion agent (pentane C_6H_{12} (Jelle, 2011). The material is know for is economic benefits and for being a relatively lightweight material (Kunič, 2017). The material is usually casted as boards but can also be continuously casted on a production line. EPS can be perforated, cut and adjusted at the building site, without any loss of thermal resistance (Jelle, 2011). Figure 2.5 provides an example of expanded polystyrene (EPS) as a thermal building insulation material and its application to building panel insulation.

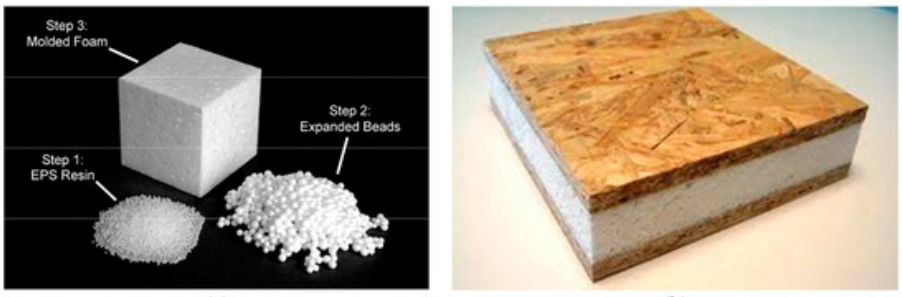

Figure 2.5: Example of expanded polystyrene (EPS) and EPS insulation boards (Ali et al., 2024)

Typical thermal conductivity of EPS ranges from 0.030 to 0.040 mW/(m· K), similar to that of rockwool. The thermal conductivity value of EPS varies with temperature, moisture content and mass density (Jelle, 2011).

Extruded polystyrene (XPS)

Extruded polystyrene (XPS) is made from melted polystyrene, which is made from crude oil. Expansion gas (HFC, CO_2 or C_6H_{12}) is added to the material in ordered mass expand the material, resulting in insulation boards as shown in Figure 2.6 . XPS is produced in continuous length and cut after cooling. The material can be both cut and adjusted at the building site, without any loss of thermal resistance. Typical thermal conductivity of EPS ranges from is the same as EPS, which is in the range of 0.030 to 0.040 mW/(m· (Jelle, 2011).

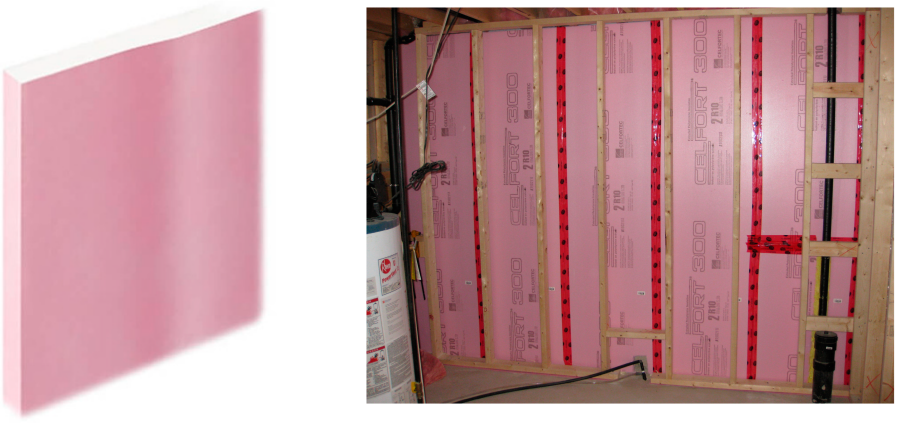

(a) (b)

Figure 2.6: Example of extruded polystyrene (XPS) as a thermal building insulation material (right Figure) and its application to building panel insulation (left Figure)) (Ali et al., 2024)

Kenaf and wood fiber

Sustainable insulation materials that have been developed and commercialized usually include kenaf or wood fiber. Despite their eco-friendly nature, their thermal performance remains comparable to that of synthetic insulation materials and could benefit from further improvements (Asdrubali et al., 2015).

Moss

Mosses can trap small pockets of stagnant air between their leaves, exhibiting promising thermal properties. In dry conditions, bioreceptive concrete can achieve a temperature reduction of 0–5°C, while in wet conditions, the reduction ranges between 5–10°C (Veeger et al., 2023).

Glass

Waste glass can be recycled into thermal and acoustic insulation materials through a foaming process. Several commercialized products based on this technology exhibit thermal conductivity values between 0.038 and 0.050 W/(m· K) and densities ranging from 100 to 165 kg/m^3 (Asdrubali et al., 2015) . Insulation materials incorporating recycled glass demonstrate thermal and mechanical properties similar to those of rock wool (Asadi et al., 2018).

Polythylene terephtalate (PET)

Polyethylene terephthalate (PET) is produced in large quantities worldwide, primarily for packaging and bottle manufacturing. As one of the most commonly used plastic materials, developing effective recycling strategies for PET can significantly reduce oil consumption and mitigate environmental impacts associated with improper disposal (Asdrubali et al., 2015).

Intini and Kühtz (2011), developed innovative thermal insulation panels incorporating 75% recycled PET bottles and 25% virgin thermo-bonding PET. These panels exhibit low thermal conductivity (0.035 W/(m· K)) and a density of 30 kg/m^3 created innovative thermal insulation panels made with recycled PET (75% PET bottles and 25% virgin thermobonding PET). The panels were characterized by low thermal conductivity with a density of 30 kg/m^3 (Asdrubali et al., 2015).

Cotton

Several manufacturers currently produce thermal and acoustic insulation materials using recycled cotton fibers. Figure 2.7 provides an example of recycled cotton as a thermal building insulation material and its application to building panel insulation. These type of insulation materials exhibit thermal conductivity values ranging from 0.039 to 0.044 W/mW/(m· K), with densities between 25 and 45 kg/m^3 (Asdrubali et al., 2015).

Figure 2.7: Example of insulation boards made from recycled cotton its application to building panel insulation. (Ali et al., 2024)

Vaccum insulation panels (VIP)

Vacuum Insulation Panels (VIPs) consist of an open-porous fumed silica core enclosed within multiple layers of metallized polymer laminates. The thermal conductivity of a VIP typically ranges between 0.003 and 0.004 mW/(m·K) when newly manufactured but can increase to approximately 0.008 mW/(m·K) after 25 years of aging. This increase is primarily due to the diffusion of water vapor and air through the panel's envelope into its open-pore core material (Jelle, 2011). Figure 2.8 includes two figures, the left figure includes a typical VIP structure and its main components, and the right figure shows a comparison of equivalent thermal resistance thickness of traditional thermal insulation and VIP,

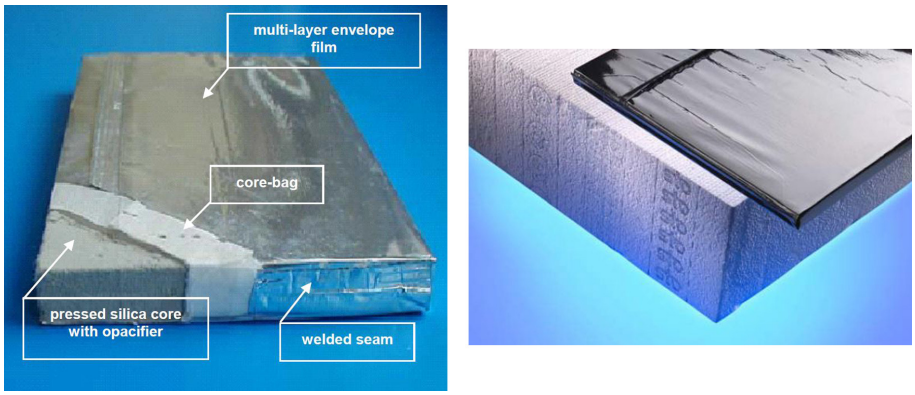

Figure 2.8: Typical VIP structure (right Figure) and comparison of equivalent thermal resistance thickness of traditional thermal insulation and VIP (left Figure) (Jelle, 2011)

Since VIPs are still under active research and development, they present several disadvantages. Most notably, they cannot be cut or perforated on-site, as doing so significantly reduces their thermal insulation performance. Additionally, if punctured, by nails for example, their thermal conductivity can rise up to 0.020 W/(m·K). Another drawback of this material is their relatively high cost. Despite these limitations, the exceptionally low thermal conductivity of VIPs makes them highly valuable for meeting the energy efficiency standards of passive houses, zero-energy buildings, and zero-emission buildings (Jelle, 2011).

Gas-filled panels (GFP)

Gas-filled panels (GFPs) utilize gases with lower thermal conductivity than air, such as argon (Ar), krypton (Kr), and xenon (Xe) through a barrier foil and baffle structure. In principle, GFPs and vacuum insulation panels (VIPs) are similar, but they differ in their insulation mechanisms. While VIPs rely on a vacuum for insulation, GFPs use low-conductivity gases. Since a vacuum is a more effective thermal insulator than gas, VIPs generally have lower thermal conductivity. GFPs, however, still offer good insulation, with a thermal conductivity of approximately 0.040 W/(m·K) (Jelle, 2011). Figure 2.9 includes an example of an GFP, including the barrier foil and baffle structure inside the GFP.

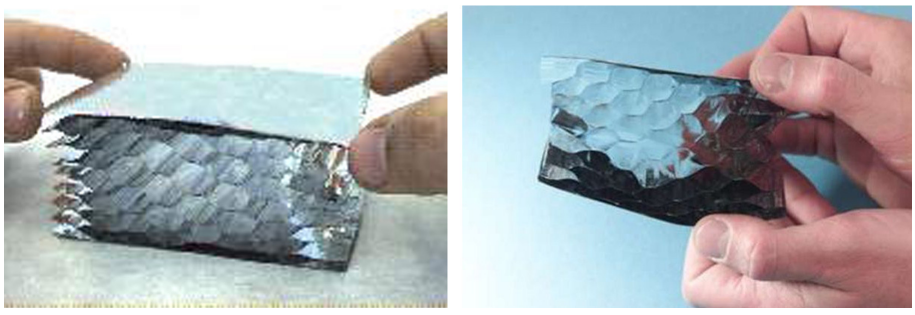

Figure 2.9: Example of an Gas Filled Panel (GFP) insulation material, including the barrier foil and baffle structure inside the GFP. (Jelle, 2011)

Aerogels

Aerogels are considered one of the most promising state-of-the-art thermal insulation solutions, offering superior performance compared to other materials. In aerogel insulation, carbon black is added to sup-

press radiative heat transfer. When subjected to a pressure of 50 mbar, aerogels achieve an exceptionally low thermal conductivity of 0.004 W/(m·K). They can be produced in opaque, translucent, or transparent forms (Jelle, 2011).

Despite their advantages, aerogels still face challenges that must be addressed before they can compete with conventional insulation materials. The primary drawbacks include high production costs and low tensile strength, making them fragile and difficult to handle (Jelle, 2011). Nonetheless, aerogels have been shown to possess low embodied energy per specific U-value, and their market price is expected to decrease in the foreseeable future. Aerogels are widely used in the space and aviation sector, where high performance is required (Kunič, 2017).

2.3 Building facade

The facade of a building, often seen as the skin of a building, plays a vital role in the thermal efficiency, aesthetics, and sustainability performance of a building (Azariy et al., 2023; Fernando et al., 2023). It can act as a mediator between interior and exterior environments by further regulating temperatures, facilitating ventilation, contribution to energy conservation and public health through air and water filtration (Sung, 2016).

Apart from its aesthetic value, the facade influences daylight, views, ventilation, occupant comfort, and may also serve structural functions. Modern facades are no longer viewed as isolated components of a building, but rather as multifunctional systems that can integrate load-bearing capacities, environmental controls, and architectural expression. This evolution of facades reflects changing building requirements, and rising demands for comfort, insulation, air tightness, and weather protection (Knaack et al., 2014).

2.3.1 Facade classification

Facade classification is primarily determined on panel modularity and connection details between the panels and the primary structure Panel modularity refers to whether the system consists of single units (mono-panels) or multiple integrated units (multi-panels). Connection details further describe the method by which panels are attached to the main structural framework (Bianchi et al., 2024).. Figure 2.10 provides an overview of the primary facade typologies and subtypologies currently employed today.

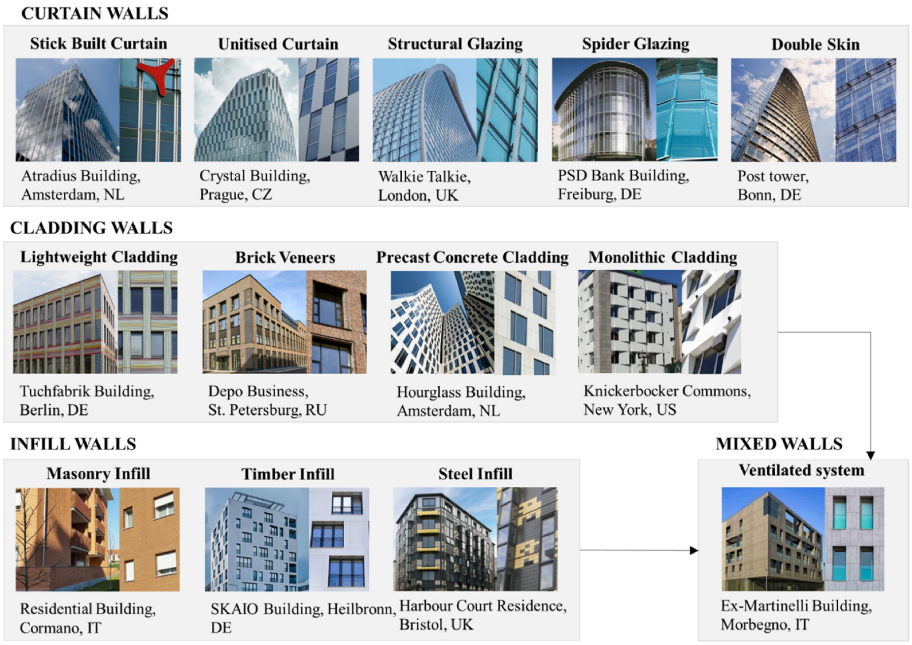

Figure 2.10: Primary facade typologies and subtypologies (Bianchi et al., 2024)

Curtain walls

Curtain walls are non-loadbearing façade systems that hang from the building's structure, typically suspended from the roof or floor slabs. This type of system is structurally independent of the primary loadbearing system, where they are usually designed to resist wind loads and their own weight (Knaack et al., 2014).

These systems are commonly constructed from prefabricated units or assembled on site from individual components. This modular approach allows for greater design flexibility, enabling panels to be configured for both aesthetic and functional purposes (Knaack et al., 2014).

Curtain walls are commonly found in high-rise buildings, due to their efficient installation, modularity, and suitability for repetitive architectural elements (Knaack et al., 2014).

Cladding walls

Cladding walls are attached to the building's loadbearing structure but do not carry any structural loads themselves. Their primary functions are to provide weather protection, thermal insulation, and aesthetic expression. Cladding materials vary widely, but commonly include metal, stone, fiber cement, or composites. These materials are selected based on performance requirements and visual appearance (Knaack et al., 2014).

Infill walls

Infill walls are non-loadbearing panels positioned between structural elements such as beams and columns within a frame. Their primary role is to provide enclosure and spatial partitioning. Historically derived

from timber frame constructions filled with various materials, modern infill walls often incorporate thermal insulation and cladding layers to enhance performance (Knaack et al., 2014).

2.3.2 Design considerations

The design of a facade can vary based on aesthetic, climate, cultural, technological, and safety factors. Due to continuous exposure to external conditions, facades typically experience more wear and tear than other building components, often resulting in increased maintenance needs and potential replacement costs over time. Designers must therefore balance structural integrity, environmental performance, and suitable aesthetics within the built context (Fernando et al., 2023).

Recently, a new phase in facade systems design has emerged, where decorative, functional, or environmentally friendly aspects coexist. This evolution is largely due to the technical revolution, which has made it possible for architects to implement various design concepts that were previously unattainable (Azariy et al., 2023). A facade is now inseparable from the buildings overall design, structure, use, and services (Knaack et al., 2014).

The design process of a buildings facede typically involves:

1. Initial conception
2. Functional definition
3. Design development
4. Implementation coordination
5. Assembly

At each stage mentioned here above, the integration of the facde with the buildings structural, mechanical, and safety systems must be carefully considered as well (Knaack et al., 2014).

Figure 2.11 illustrates the life cycle of a building facade system and highlights key design considerations. The lifecycle of a facade system includes design, construction, operation, rehabilitation, and demolition phases (Fernando et al., 2023).

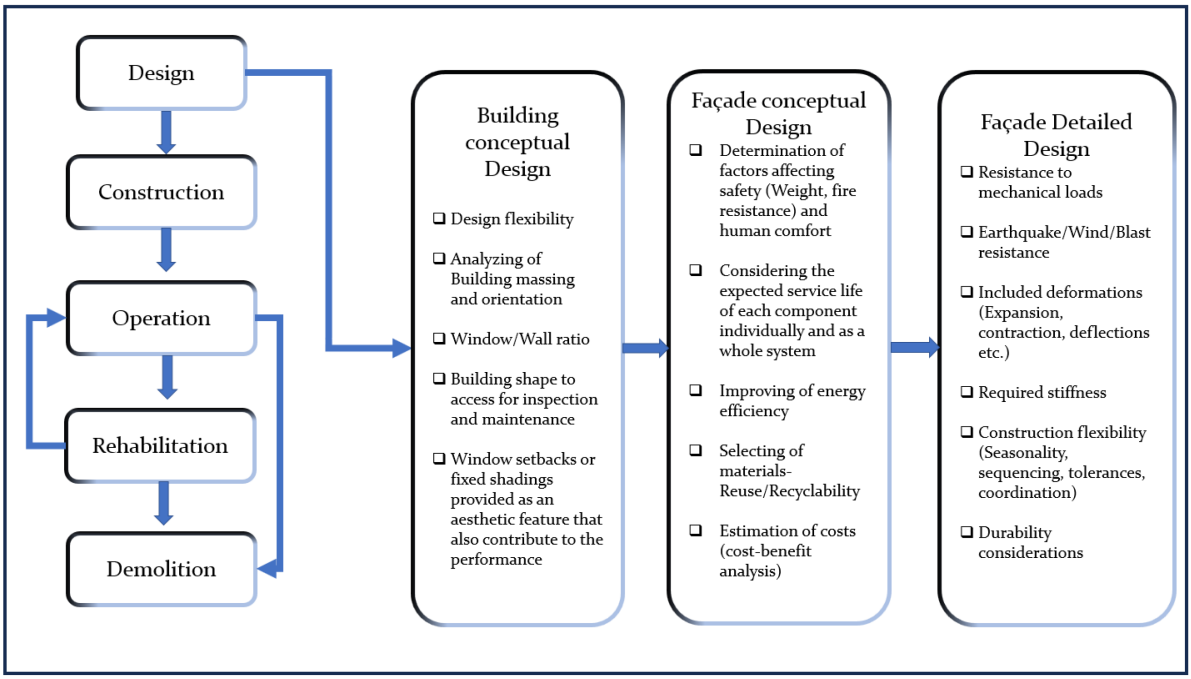

Figure 2.11: Life cycle of building facade system and necessary design considerations (Fernando et al., 2023)

2.3.3 Performance criteria

Functional, technical, and design requirements of facades are shaped by climatic conditions and basic construction principles, which have evolved from the lifestyles adapted to each specific climate. A facade separates interior from exterior and serves various roles, such as (Knaack et al., 2014),

- Define architectural identity
- Shaping interior and exterior views
- Resisting wind loads
- Supporting their own weight
- Resisting rain and humidity
- Provide thermal/acoustic insulation
- Enabling energy generation
- Durability and easy maintenance

Figure 2.12 includes the three performance criteria categories that facades are more or less subject to. These catagories include functional (structural safety, human comfort, durability), environmental (energy and material efficiency), and financial (cost-effectiveness) (Bianchi et al., 2024). Each of these categories includes a main criterion and related sub-criteria, as seen in Figure 2.12.

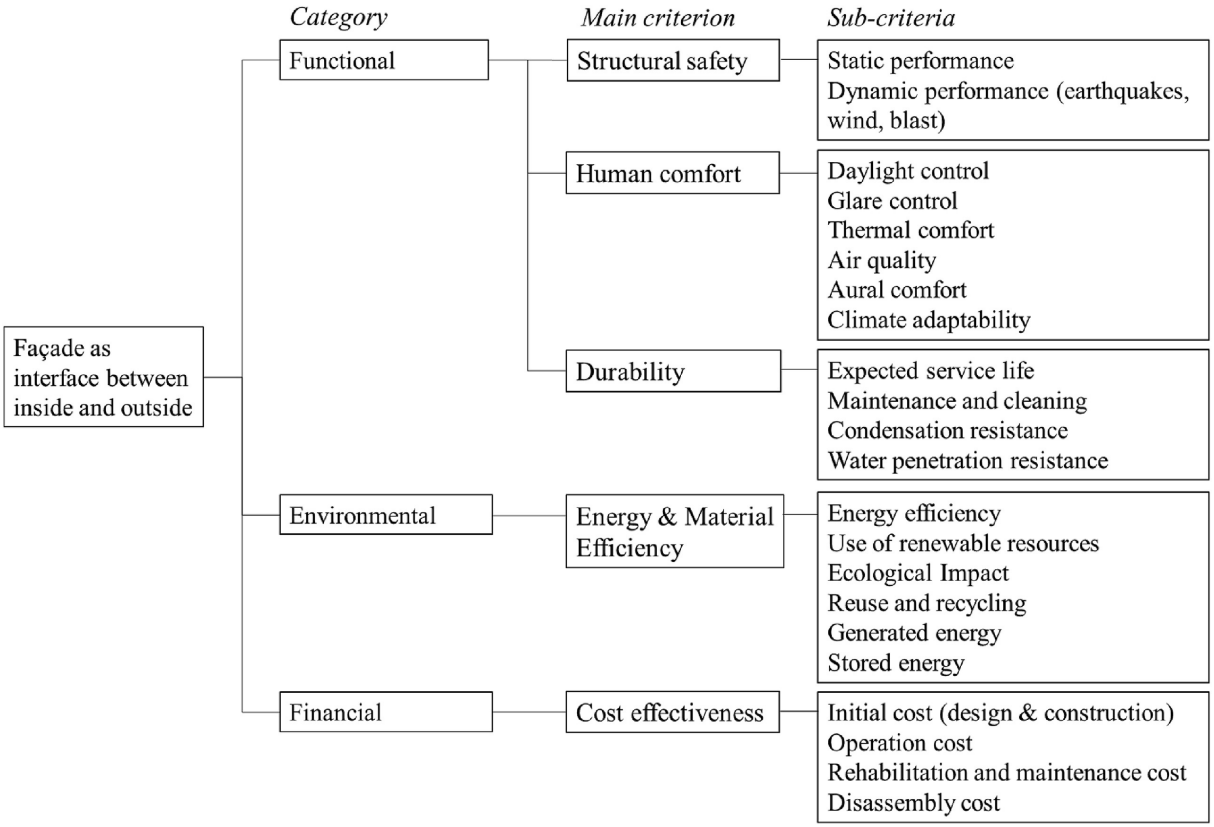

Figure 2.12: Performance criteria of a facade (Bianchi et al., 2024)

Functional

Facades must fulfill several essential functional requirements. Structurally, they must support their own weight and accommodate differential deformations caused by moisture, temperature changes, and structural movements. Additionally, facades must resist environmental loads such as wind, rain, and snow (Bianchi et al., 2024).

To ensure human comfort, the facade must meet heating and cooling needs of the occupants, control of the buildings thermal environment, support of occupant comfort, productivity and well-being. Minimizing air leakage through the building envelope is also essential to maintain indoor air quality (Bianchi et al., 2024).

Facades are highly sensitive to weathering and degradation, which leads to a loss of functionality. Therefore, durability is another critical functional criterion. The facade system must meet its expected service life, which requires proper maintenance and cleaning (Bianchi et al., 2024). To further ensure longevity, the system must resist water penetration and prevent condensation. Building use, environmental conditions, shape and details of components and quality of installation must be carefully accounted for to ensure facade durability (Moghtadernejad, 2013).

Environmental

To meet environmental performance goals, a facade system must prioritize energy and material efficiency. This includes reducing energy consumption, integrate renewable energy options, and maximizing reuse

and recyclability to lower ecological footprint (Bianchi et al., 2024).

Energy efficient facade panels should minimize heat gain and loss, maximize insulation in opaque areas, and reduce air leakage to control temperature and condensation (Boswell, 2013). Key design considerations include:

1. Local climate and geography
2. Building orientation and form
3. Material choice, quantity, and placement

To reduce operational energy use, several design strategies can be implemented (Fernando et al., 2023):

- Natural ventilation
- Daylight optimization
- Renewable energy integration (e.g., solar/wind)
- Smart adaptive devices
- Vegetated systems
- Sustainable materials

Current facade systems rarely incorporate design strategies for disassembly or reuse. Adhesive connections, for example, hinder component separation and recycling. To meet carbon reduction goals, better understanding of how facade assembly methods affect disassembly and material recovery is needed (Hartwell et al., 2021). Design for Disassembly (DfD) offers a promising approach for this problem, aiming to reduce waste and support a circular economy (see Appendix A.1.5). However, effective reuse also depends on disassembly ease, remanufacturing potential, market availability, and regulatory frameworks. While research has largely focused on single-material facades, multi-material, multi-layered systems remain underexplored and present unique challenges (Hartwell et al., 2021).

Financial

To meet the financial performance category, a facade system must be cost-effective. This includes evaluatng initial costs, which includes design and construction phases. Additionally, operational, maintenance, and rehabilitation costs must be carefully considered and reduced where possible. Finally, disassembly costs should also be evaluated to enable a comprehensive cost assessment, spanning the entire lifecycle of the system, i.e. from design to end-of-life disassembly (Bianchi et al., 2024).

Chapter 3

Material selection

The layers of the facade system must be selected with care, taking into account both technical requirements and the overall objectives of the project. Key layers include the insulation material, waterproof membrane, concrete mix design, and moss species. In addition, assembly methods need to be defined, covering both the connections between layers and the installation of panels onto an existing structure.

This chapter is structured as follows, the first section presents the process of choosing a suitable insulation material, including the multi-criteria analysis, product comparison, and final selection. The second section introduces the waterproof membrane, outlining material choices and their respective properties. The third section discusses the concrete layer, focusing on the selected mix design and performance considerations. The fourth section addresses the moss selection, where an evaluation of species suitable for colonization of the concrete substrate are considered. The fifth section explores possible assembly and installation methods, covering both connections between layers and on-site attachment methods.

3.1 Insulation material

This chapter presents the selection and evaluation of different thermal insulation materials for the proposed facade system. A systematic approach was applied to ensure that the chosen material balances thermal performance, durability, low environmental impact, and circularity. A multi-criteria analysis (MCA) was conducted to compare various insulation options against multiple performance indicators. The most promising candidates were then further assessed an their alignment with the projects sustainability objectives evaluated. Finally, a commercially available product was selected as the preferred insulation material for the facade system design.

3.1.1 Multi-criteria analysis

A multi-criteria analysis (MCA) was carried out to compare different insulation materials in a structured way. First, an overview of available options was gathered from literature. The MCA then assessed the materials based on a set of performance indicators and assigned weights, helping to highlight those best suited to the projects main priorities, particularly circularity and low environmental impact.

Specific indicators

A total of 10 specific indicators was selected to evaluate the performance and applicability of different thermal insulation materials for the facade system. These indicators are: thermal conductivity, perforation vulnerability, building site adaptability and cuttability, mechanical strength, fire resistance, water resistance, cost, environmental impact (global warming potential), water vapor resistance factor, and circularity. Table 3.1 explains their relevance for selecting an insulation material for exterior facades.

Specific indicator	**Reasoning**
Thermal conductivity [W/(mK)]	Measures how well a material conducts heat. Lower values indicate better insulation properties, which reduces a building's total energy consumption for heating and cooling.
Perforation vulnerability	Indicates how susceptible a material is to being damaged or weakened by drilling, cutting and adjusting. This indicator gives an idea of whether puncturing the envelope causes an increase in thermal conductivity.
Building site adaptability and cutability	Reflects how easily a material can be modified or fitted on-site. High adaptability and ease of cutting reduce labor time and costs, and improve feasibility for complex designs or retrofits. Also important if the insulation material needs to be cut to facilitate specific designs of the facade system or altered on site for the specific needs of the building.
Mechanical strength	Describes the ability to withstand loads and stresses without breaking or deforming. Essential for structural stability, long-term durability, and safety of facade systems.
Fire resistance	Measures how well a material resists ignition and limits fire spread. Extremely important for building occupant safety and compliance in building construction.
Water resistance	Indicates resistance to water penetration or degradation when exposed to moisture. Important for preventing mold, corrosion, or structural weakening, especially in exterior applications.
Cost	A key factor in material selection for ensuring project affordability and economic feasibility.
Environmental impact (Global warming potential)	Quantifies greenhouse gas emissions throughout the material's life cycle. Lower GWP supports climate-friendly building practices.
Water vapor resistance factor	Indicates how much a material resists water vapor diffusion. Important for moisture management in building envelopes.
Circularity	Reflects potential for reuse, recycling, or biodegradation. Encourages sustainable resource use and supports circular economy principles.

Table 3.1: Specific indicators for multi-criteria analysis of thermal insulation materials

Score system

Each indicator was scored to quantify how well each material performed in relation to the facade system requirements. A scale from 0.5 (no information available) to 5 (best performance) was used, where by summing the individual scores, a maximum total of 50 points could be achieved. The scoring ranges for each indicator are summarized in Table 3.2.

Points	0.5	1	2	3	4	5
Thermal conductivity [W/(mK)]	No information found	40-50	30-40	20-30	10-20	0-10
Perforation vulnerability	No information found	No - puncturing the envelope causes an increase in thermal conductivity	–	–	–	Yes - Can be perforated, cut and adjusted on site without loss of thermal resistance
Building site adaptability and cutability	No information found	No	–	–	–	Yes
Mechanical strength	No information found	No load bearing capability	–	–	–	Load bearing capability
Fire resistance	No information found	F	C/E	B	A2	A1
Water resistance	No information found	Very Low	Low	Medium	high	Very high
Cost	No information found	Very high (40–50€/m²)	High (30–40 €/m²)	Medium (20–30 €/m²)	Low (10–20 €/m²)	Very low (0–10€/m²)
Environmental impact (GWP)	No information found	15-18	11-14	8–11	4-7	0-3
Water vapor resistance factor	No information found	Very low (0–50)	Low (50–100)	Medium (100–150)	High (150–200)	Very high (200+)
Circularity	No information found	No recycled material content and recycling not possible at end of life	Recycling only performed by specialized industries	No recycled material content but recycling possible by specialized industries	Recycling only performed by specialized industries	Use of recycled materials and recycling possible at end of lifetime

Table 3.2: Assessment system used for specific indicators

Weights

Weights were next assigned in order to reflect the priorities of this project, and are summarized in Table 3.3. Circularity was given the highest weight (25%), followed by thermal conductivity and environmental impact (20% each). The remaining indicators were assigned 5–10% each, depending on their relative importance.

Factor	Weight
Thermal conductivity [W/(mK)]	20.00%
Perforation vulnerability	5.00%
Building site adaptability and cutting adaptability	5.00%
Mechanical strength	5.00%
Fire resistance	5.00%
Water resistance	5.00%
Cost	10.00%
Environmental impact (Global warming potential [kg CO_2 per functional unit])	20.00%
Circularity	25.00%
Water vapor diffusion resistance factor	5.00%
TOTAL	100.00%

Table 3.3: Specific weights for each performance indicator

MCA results

The materials assessed in the MCA included mineral wool (rock wool, glass wool), expanded polystyrene (EPS), extruded polystyrene (XPS), cellulose, cork, polyurethane, vacuum insulation panels (VIP), gas-insulated panels, and aerogels. Data on these materials were collected from literature and product descriptions. Scores were calculated according to the system in Table 3.2 and weighted using Table 3.3. Full results are provided in Appendix D.2.

The overall results are shown in Table 3.4. Rock wool scored highest both before and after applying the weights, followed by glass wool. Cork also performed well, particularly in environmental categories, although its thermal performance was slightly lower.

Material	Score before weights	Score after weights
Rock wool	39	3.8
Glass wool	38	3.7
Expanded polystyrene (EPS)	33	3.2
Cork	33	3.2
Extruded polystyrene (XPS)	31	3.2
Polyurethane	31.5	3.1
Aerogels	31	2.7
Cellulose	28	2.5
Vacuum insulated panels	12	1.5
Gas insulated panels	12	1.5

Table 3.4: Comparison of insulation materials: raw scores before weighting and weighted scores after applying performance indicator weights

3.1.2 Material selection

Based on the MCA results and the project's emphasis on circularity and low environmental impact, two materials were selected for further evaluation: rock wool and cork. Rock wool scored highest in the MCA and is widely used in construction, offering strong thermal and acoustic performance. Cork was selected for its natural origin and low embodied energy, making it well aligned with circular design principles.

A comparison of the information gathered from literature for cork and rock wool is summarized in Table 3.5. Rock wool outperforms cork in fire resistance and thermal conductivity. Cork, on the other hand,

provides significant environmental benefits, including carbon negativity, biodegradability, and reintegration into natural cycles. Although rock wool can be recycled through specialized manufacturers, its higher embodied energy and frequent disposal to landfills reduce its environmental advantage.

Specific indicator	**Cork**	**Rockwool**
Thermal conductivity [W/(mK)]	40-50	30-40 (High)
Perforation vulnerability	Yes	Yes
Building site adaptability and cuttability	Yes, lightweight structure	Yes, easily handled without losing thermal performance
Mechanical strength	No load bearing capabilities (NO), high strength	No load bearing capabilities (NO)
Fire resistance	E	Very high class (A1), A1-A2
Water resistance	Water resistant	Medium
Cost [€/m^2]	Medium (20–30)	Low
Environmental impact (GWP, kg CO_2/unit)	5.72–5.93	1.45 (commercial stone wool)
Circularity	High, no additional binders or chemicals used	Can be recycled by manufacturers or disposed in landfills
Water vapor diffusion resistance factor	5–30	1–1.3

Table 3.5: Comparison table of gathered information for cork and rock wool

Overall, cork is considered to be the more sustainable and circular option, while rock wool is a strong choice in cases where fire resistance and high thermal performance are needed.

Comparison of available cork and rockwool roducts

To validate the findings further and make an informed design decision, representative products found on the market today for cork and rockwool were found. The chosen products are the following:

- Facade Cork Insulation Boards by Pro Suber (Pro Suber, 2023; Suber, 2022)
- Frontrock Max E Stone Wool boards by ROCKWOOL (ROCKWOOL Polska Sp. z o.o., 2025)

Their properties are compared in Table 3.6. The results confirm the sustainability advantages of cork, while rock wool has notable advantages is fire safety and slightly better thermal conductivity.

Property	Pro Suber Cork	ROCKWOOL Stone Wool
Material composition	100% natural cork	Basalt (volcanic rock) + 2–3% resin binder
Thermal conductivity [W/(mK)]	0.040	0.032
Density [kg/m³]	140 +/- 10	28 (for 39 mm thickness)
Fire classification	Euroclass E	Euroclass A1
Moisture resistance	High (vapor-permeable)	High (water-repellent)
Acoustic insulation	Excellent	Good
Recyclability	100% recyclable	100% recyclable
Service life [years]	75	50
Embodied carbon	Carbon negative	Carbon neutral

Table 3.6: Comparison of product specifications and thermal properties for Pro Suber cork and ROCKWOOL stone wool insulation

Representative Environmental Product Declarations (EPDs) were retrieved for both products, and their environmental impacts and shadow costs were estimated based on the provided data. The calculation procedure is outlined in Chapter 5.4. Figure 3.1 presents a comparison of the shadow costs, while Table 3.7 summarizes the calculated environmental impacts.

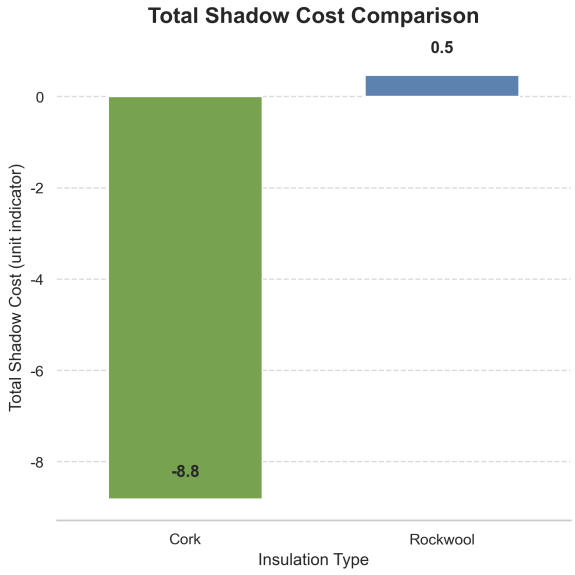

Figure 3.1: Shadow cost comparison for Pro Suber Cork and ROCKWOOL Stone Wool

Impact Category	Cork	Rockwool
CC total (kg CO_2 eq)	-8.8	0.40
CC fossil (kg CO_2 eq)	0,5	0,43
CC biogenic (kg CO_2 eq)	-9,3	-0,03
CC luluc (kg CO_2 eq)	0,0	0,00
ODP (kg CFC 11 eq)	0,0	0,00
AP (mol H+ eq)	0,0	0,01
EP freshwater (kg P eq)	0,0	0,00
EP marine (kg N eq)	0,0	0,01
EP terrestrial (mol N eq)	0,0	0,03
POCP (kg NMVOC eq)	0,0	0,01
ADP Elements (kg Sb eq)	0,0	0,00
ADP fossil fuels (MJ)	0,0	0,01
WDP (m^3 water eq deprived)	0,1	0,00
Total	-8.8	0,47

Table 3.7: Shadow cost comparison values for Pro Suber Cork and ROCKWOOL Stone Wool

Cork insulation demonstrates a significantly lower shadow cost compared to Rockwool, which is primarily due to its biogenic carbon sequestration.

Final Insulation Material Selection

Based on the results of the multi-criteria analysis and the project's emphasis on circularity and low environmental impact, cork was selected as the most suitable insulation material for the proposed facade system. Cork demonstrates clear advantages in circularity, embodied carbon, durability, and recyclability. While rock wool performs better in some technical aspects, such as fire classification, thermal conductivity, and moisture resistance, these benefits are outweighed by cork's lower environmental impact and stronger alignment with circular design principles.

The selected product is the *Facade Cork Insulation Boards* manufactured by Pro Suber. Produced in Portugal and distributed in the Netherlands, these boards are carbon neutral, free of adhesives, and supported by a verified Environmental Product Declaration (EPD) (Pro Suber, 2023). An example of the insulation boards is shown in Figure 3.2.

Figure 3.2: Pro Suber facade Cork Insulation Boards, showing typical board dimensions and texture.

The boards are made entirely of natural cork (Falca Cork). Details of the production process, relevant for assessing sustainability and circularity, are provided in Appendix B.2. Key technical properties of the material, as reported in the product datasheet, are summarized in Table 3.8.

Property	**Value**	**Unit**
Density	140 ± 10	kg/m^3
Thickness	≤200	mm
Reaction to fire	Euroclass E	–
Thermal conductivity (λ)	0.043	W/m·K
Short-term water absorption (W_p)	0.18	kg/m^2
Water vapor transmission rate (g)	455.54	$mg/(h{\cdot}m^2)$
Water vapor permeance (W)	0.3	$m^2h{\cdot}Pa/mg$
Water vapor resistance (Z)	3.09	mg/(m·h·Pa)
Water vapor permeability (δ)	0.01	mg/(m·h·Pa)
Water vapor diffusion resistance factor (μ)	54.61	–
Water vapor equivalent air layer thickness (S_d)	2.19	m
Shear strength (τ)	110	kPa
Compressive strength (σ)	185	kPa

Table 3.8: Key technical properties of Pro Suber cork insulation boards

The table highlights the material's density, fire performance (Euroclass E), and thermal conductivity,

which are relevant for thermal efficiency and safety. Moisture-related properties, including water absorption, vapor transmission, and diffusion resistance, ensure reliable hygrothermal behavior in facade applications. Mechanical properties such as shear and compressive strength confirm the material's suitability as a stable and durable insulation layer.

3.2 Membrane

To protect the cork insulation from moisture while maintaining vapor permeability, a breathable, watertight, and windproof membrane was included between the cork and the concrete layer. The system will not incorporate an air gap (non ventilated facade system) and therefore the membrane is included to allow vapor diffusion. This will prevent condensation, while simultaneously providing water resistance. UV resistance is of minor importance, though the material should tolerate temporary exposure during installation.

After comparing several alternatives (see Table B.1 in Appendix B.3), Solitex Fronta Humida (SFH) was selected for its high vapor permeability (S_d = 0.05 m), moderate UV resistance of up to 3 months, and proven suitability for direct contact with insulation materials. A sample of this type of membrane is shown in Figure 3.3.

Figure 3.3: Solitex Fronta Humida waterproof membrane

Other membranes listed in Appendix B.3 were not selected due to incompatibility with non ventilated facade systems or because their application required adhesives or liquid coatings, which would hinder disassembly and conflict with circular design principles. In contrast, the SFH membrane can be mechanically fastened and removed without damaging adjacent layers, supporting both system durability and design-for-disassembly.

3.3 Concrete layer

A concrete mixture usually includes cement, differently grained aggregates, and water. Cement can be replaced by alternative binders and thus decreasing the total negative environmental impact of the substrate. Additional additives and admixtures can also be added additionally to the mixture to further refine specific properties.

Functionalization refers to when a specific material is tailored to a specific application and the specific properties required (Stohl et al., 2023). Thus, the concrete mixture design can be functionalized to improve bioreceptivity of the material itself. This can include the addition of more porous aggregates, filler or binder, or a combination of these three options. More specifically, the concrete mixture design can be designed in such a way that hydraulic properties, surface roughness, substrate pH and phosphorus content are used as performance indicators to increase bioreceptivity of the material (Veeger et al., 2023).

Coarse aggregates

According to Veeger et al. (2023), it is recommended to use crushed expanded clay for the use of coarse aggregates, for improved bioreceptivity. Argex 4/8 is a suitable material choice for this purpose, and has therefore been incorporated to the concrete mix design.

Argex is widely used in various sectors, including construction, green infrastructure, and utility projects. In the concrete industry, it enhances lightweight, self-compacting, and pumpable concrete (Transport- en Aannemingsbedrijf Van der Waal B.V., 2025). Refer to Appendix B.1 for more detailed information on Argex 4/8. Figure 3.4 includes and example of the Argex 4/8 used for this project.

Figure 3.4: Argex 4/8 (coarse aggregates)

Fine aggregates

In order to decrease the environmental impact of the concrete material and increase the circularity of the system itself, recycled sand was chosen. This sand comes from recycled concrete that is acquired from demolition rubble (Urban Mine, 2025), see Appendix B.1 for more information on the recycling process. The size of recycled sand used in the concrete mixture for this project is from 0-4mm.

CEMIII/B 42.5N LH SR

CEM III/B 42.5N is a Portland slag cement commonly used in mass or reinforced concrete structures. Blast furnace cement CEM III/B 42.5 N LH R is produced by blending ground granulated blast furnace slag with Portland cement clinker. The blast furnace slag is a by-product generated during iron production in blast furnaces (Stichting MRPI and Hollandse Cement Maatschappij B.V., 2025)

This type of cement is particularly suitable for bioreceptivity due to the pozzolanic content of the blast furnace slag, which lowers the surface pH of the concrete substrate (Natanzi et al., 2021; Veeger et al., 2023).

Nutrients

To improve bioreceptivity and nutrient content of the concrete, the addition of bone ash was added to the concretes mix design. This specific nutrient has been proven to improve bioreceptivity, as it is an pozzolanic material that contains phosphorus (Veeger et al., 2023).

Surface roughness

To increase surface roughness of the concrete, the selected approach for the combined facade system involves applying a surface retarder during casting. With this employment, the material's surface roughness and water absorption can be increased. The result creates a more favorable environment for organisms, by forming micro-habitats that support their initial establishment and long-term survival.

Due to time constraints, surface retarder was not applied to all panels made for this project. Specifically, it was not used on the panels designated for heat flux experiments. This proved to be beneficial for glueing the moss to the panels, as a smoother surface made it easier to glue the moss to the panels, minimized air gaps and thus further improving the accuracy of the heat flux results.

3.4 Moss

As mentioned in Section 2.1.1, seven main colonizing species of concrete were identified after exploration of 137 moss communities growing on concrete in three Dutch cities. These identified species are the following: *Tortula muralis*, *Grimmia pulvinata*, *Ptychostomum capillare*, *Orhotrichum diaphanum*, *Brachythecium rutabulum*, *Hypnum cupressiforme*, and *Rhynchostegium confertum*. These species acted as the most common pioneers and formed a part of the climax community (Veeger et al., 2025)

For the facade panel, the selection of mosses was further decreased by choosing mosses that are the most spread around cities in North Holland. These species include *Grimmia pulvinata*, *Ptyschostomum cappilare* and *Brachythecium rutabulum,* and are shown in Figure 3.5.

(a) *Grimmia pulvinata* (British Bryological Society, 2025)

(b) *Ptyschostomum cappilare* (GBIF, 2025)

(c) *Brachythecium rutabulum* (Floral Images, 2025).

Figure 3.5: Three most common moss species found on stone surfaces in Dutch cities

These three species will be added to separate panel prototypes where their R-values will be further explored. Based on these results, the final decision for which moss specie is the most suitable for the facade system will be chosen

3.5 Assembly and installation

The performance of the facade system is highly dependent on how the facade layers and their respective materials are combined and attached. Proper assembly and installation are important to ensure thermal efficiency, weatherproofing and structural stability. The design choices presented in this chapter emphasizes circularity, where all assembly and installation methods are chosen to allow for easy maintenance, repair, and disassembly at the end of the facade's service life.

This section first describes the assembly of the different layers of the facade, highlighting strategies that support reversibility and future reuse. It then discusses a possible installation method of the prefabricated panels onto existing building walls.

3.5.1 Assembly

To support future reuse and recycling, the bioreceptive concrete layer, waterproof membrane, and insulation are assembled for clean separation. Chemical adhesives are avoided, as they create irreversible bonds that complicate disassembly and contaminate recycling streams. Instead, circular assembly methods with mechanical fixings are prioritized, allowing the layers to be detached at end of life.

The selected SFH membrane can be combined with the insulation using cap nail. These fasteners include wide plastic caps to prevent tearing of the membrane (see Figure 3.6b). Where necessary, Pro Clima tapes such as Tescon Vana may be used to seal overlaps and penetrations, though this should be minimized as it complicates disassembly. Gaskets or compression battens offer an alternative for joining the membrane and concrete layer without puncturing the membrane.

Following supplier recommendations for the cork insulation boards, the Fischer 6H NT Screw Washer is used to fix the combined insulation–membrane layer to the concrete. This fastening system is shown in Figure 3.6a.

(a) Fischer 6H NT Screw Washer (Fischer, n.d.)

(b) Cap nail (AFT Fasteners, 2025)

Figure 3.6: Mechanical fastening systems used for the facade system

3.5.2 Installation

The multilayered facade system is designed for retrofit onto existing exterior walls, supporting refurbishment projects with the goal of minimizing material waste and promoting circularity. In order to achieve these goals, the installation method must be reversible, and mechanical attachment methods are chosen that allow individual panels to be removed, replaced, or reused at the end of their service life. Adhesives or irreversible bonding methods are avoided to maintain the potential for disassembly and recycling (Bossche et al., 2015).

For this purpose, a clip-and-rail subframe system is proposed as the primary installation method. In this system, a lightweight subframe is attached to the exterior wall using clips that penetrate the insulation at specific points. Prefabricated facade panels are then mounted onto the rails using screws or other mechanical fasteners, allowing each panel to be removed, repaired, or replaced individually without affecting neighboring panels. Additional components such as gaskets or compression battens can be used to join layers like insulation and waterproof membranes without damaging the materials, further supporting circularity (RDH Building Science Inc., 2018).

This installation strategy aligns closely with the principles of circular construction. Panels can be maintained, repaired, or upgraded without dismantling the entire facade, and at the end of their life, individual layers or materials can be separated and recovered. The mechanical fastening method seeks that thermal performance, weatherproofing, and structural stability are maintained, supporting both functional and environmental objectives of the retrofit project (Bossche et al., 2015).

3.6 Final material selection

The facade system was designed and developed through a stepwise evaluation of insulation materials, membrane, concrete, moss species and assembly and installation. strategies. Each material choice was guided by the project's priorities of circularity, low environmental impact, and long-term performance. The outcome of this process is a system composed of biobased and recycled resources where possible, supported by reversible mechanical connections that facilitate maintenance and end-of-life disassembly.

Figure 3.7 summarizes the final selection of materials and their role in the multilayer facade panel. This schematic illustrates how the chosen layers interact within the system and highlights the key products and material categories that form the basis of the design.

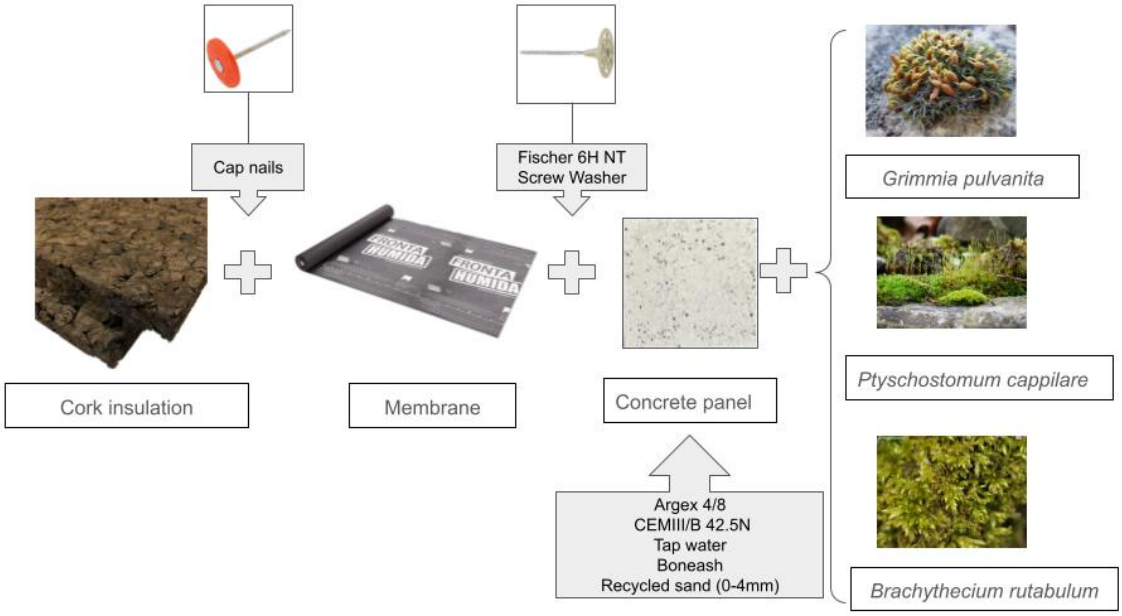

Figure 3.7: Overview of final material selection for the facade system.

Chapter 4

Facade design

The proposed facade system consists of four key components: insulation material, waterproof membrane, concrete substrate, and the moss species selected to colonize the concrete surface. These components are briefly summarized in Figure 4.1 below. Each component plays a critical role in the system's overall functionality and must be carefully selected to ensure compatibility, enhanced facade performance, and sustainability. The selection of insulation material, waterproof membrane, concrete mixture, and colonizing moss species has been described in detail in Chapter 4.

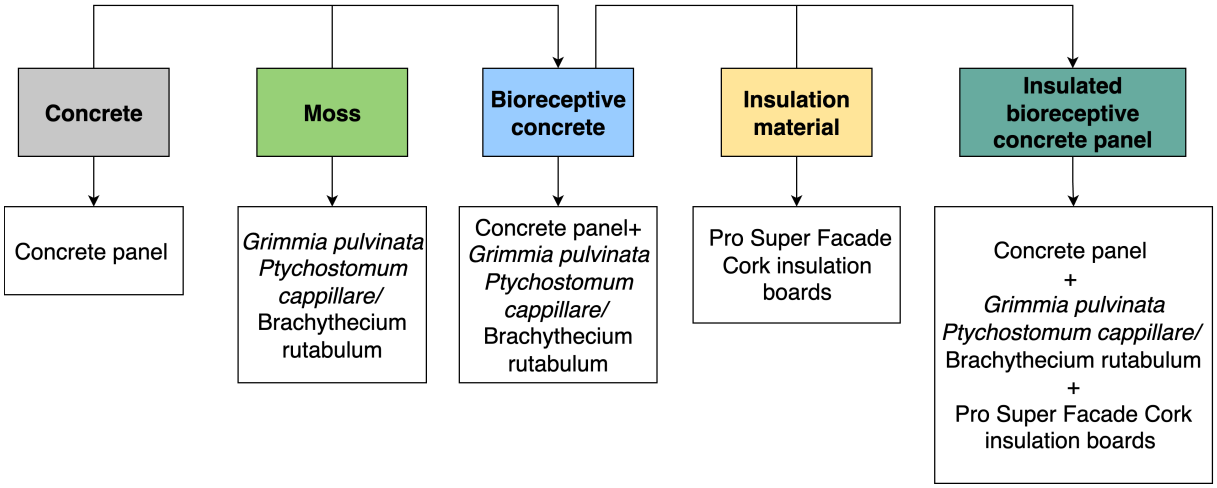

Figure 4.1: Facade system components

This chapter will further discuss how the facade system is designed with the chosen materials in mind. First, important design considerations are reviewed and linked to the specific requirements of this facade system. Next, the required thickness of the insulation layer is determined based on experimental and thermal performance results. Lastly, the assembly and installation methods for the selected materials are analyzed, emphasizing reversible, circular, and sustainable construction practices.

4.1 Design considerations

When designing a facade system, it is essential to consider factors that influence performance throughout its life cycle, as outlined in Chapter 2.3.2 and illustrated in Figure 2.11.

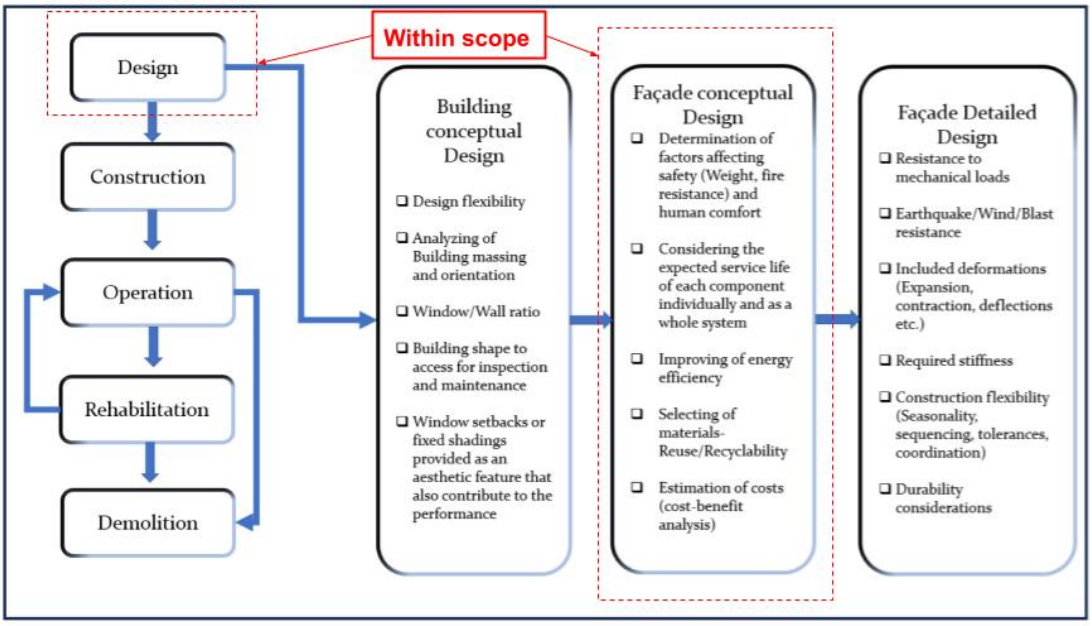

Figure 4.2: Design considerations within the scope of this project

This project focuses specifically on the conceptual design of the facade system. Broader aspects of building design and the detailed facade design are excluded from the scope. The following subchapters discuss the design considerations relevant to the facades conceptual design within the scope of this project.

Factors affecting safety and human comfort

Safety considerations such as weight and fire resistance are acknowledged during the design process but not the primary focus, as the project emphasizes circularity, bioreceptivity, and thermal performance. Nevertheless, design choices indirectly address these factors. For example, the concrete substrate is classified as lightweight concrete, since its density is less than < 2000 kg/m^3. This reduces the total weight of the system, while the insulation layer provides enhanced fire resistance in addition to the concrete's inherent properties. Full compliance with safety standards requires further study.

Human comfort factors include daylight control, glare, thermal comfort, indoor air quality, acoustic comfort, and climate adaptability. Among these, thermal comfort is prioritized, the concrete substrate and high performance insulation layer improve energy efficiency of the facade and stabilizes indoor temperatures. Additonal benefits are provided by the bioreceptive layer, which may further improve air quality, reduce urban heat stress, and manage rainwater run off (M. Manso et al., 2021; Veeger et al., 2023). Other comfort factors (e.g., daylight, glare, acoustic performance) are less relevant since the system is opaque.

Expected service life of individual components and the complete facade system

The facade system's service life depends on the durability of its layers (Table 5.1). The overall service life is 30 years if the waterproof membrane is not replaced, but can extend to 50+ years with replacement and proper maintenance.

Facade layer	Expected service life [years]	Notes
Moss	30+	Highly exposed layer where the lifespan depends on UV resistance, wind tolerance, and moisture retention. Regular inspection is necessary to assess health and coverage.
Concrete	50+	Long lasting if properly maintained.
Membrane	30 (pro clima, 2025b)	Requires replacement at ∼30 years.
Cork insulation	75 (Pro Suber, 2023)	Highly durable if protected from moisture and mechanical stress

Table 4.1: Expected service life of individual layers of the façade system with explanatory notes

It is imporant to highlight that these estimates are indicative, as real service life of each material is highly dependent on local climate, maintenance practices, and exposure conditions.

Energy efficiency improvement

A key design objective of this project is to enhance the thermal resistance of the facade system. Dutch regulations (Bouwbesluit) require an Rc-value of 4.7 mm^2K/W for exterior walls (Ministerie van Binnenlandse Zaken en Koninkrijksrelaties, 2022). Analysis of the concrete substrate and moss layer indicated that additional insulation was necessary, leading to the integration of cork insulation, which not only improves thermal performance but also supports the refurbishment of the existing building by reducing energy use, lowering operational costs, and minimizing embodied carbon compared to new construction, thus contributing to climate targets and circular economy principles (Bienert, 2023; Iwuanyanwu et al., 2025).

Selection of materials

Material selection is guided by principles of circularity, low environmental impact, and transparency. Priority is given to:

- Low embodied energy and non-toxic materials
- Natural or recycled resources
- Verified Environmental Product Declarations (EPDs)

The design promotes reuse, disassembly, and recycling, aligning with circular construction principles (Hartwell et al., 2021). The system favors direct reuse of panels where possible and, alternatively, easy disassembly for component reuse or material recycling. Mechanical and reversible connections are central to this strategy.

4.2 Insulation thickness

According to the Dutch Building Decree (Besluit bouwwerken leefomgeving, (Rijksoverheid, 2024)), the minimum thermal resistance (R_c-value) for external facade systems is dependent on whether the buildings is new constrution or an older structure set for renovation measures. For renovation or replacement of insulation, the requirement is at least $1.4\,m^2 \cdot K/W$. For new construction or large scale renovations exceeding 25% of the building envelope, the required minimum increases to $4.7\,m^2 \cdot K/W$.

Scenario	**Thermal resistance requirement (R_c)**	**Element**
Renovation / replacement of insulation	$\geq 1.4\,m^2 \cdot K/W$	Walls / facades
New construction / major renovation (>25% envelope)	$\geq 4.7\,m^2 \cdot K/W$	facades (vertical wall)

Table 4.2: Thermal resistance requirements for facades according to the Dutch Building Decree (Rijksoverheid, 2024)

To ensure the system is suitable for major renovations as well, the chosen method to determine the suitable thickness of the insulation material is based on a thermal thermal resistance requirement of $4.7\,m^2 \cdot K/W$.

Since the façade system is multilayered, each component contributes to the overall thermal resistance. The available thicknesses of the selected insulation material (Pro Suber façade Cork Insulation Board) were evaluated along with their corresponding resistance values. In addition, literature values were used to estimate the contribution of a typical existing external wall in the Netherlands, which was taken as $1.1\,m^2 \cdot K/W$, (Yu et al., 2024). An air gap was also included, contributing approximately $0.17\,m^2 \cdot K/W$ (Anderson & Kosmina, 2019).

The thermal resistance of the bare concrete panel and the colonizing moss species was measured and included as well, resulting in values of $0.16\,m^2 \cdot K/W$ for the concrete layer and $0.17\,m^2 \cdot K/W$ for *Ptychostomum cappilare* (see Chapter 6.3). Table 4.3 summarizes the estimated total R-values of the combined system for different insulation thicknesses.

Insulation thickness [mm]	**External wall**	**Air gap**	**Insulation**	**Concrete**	**Moss**	**Total R-value**
40	1.1	0.17	0.93	0.16	0.17	2.53
50	1.1	0.17	1.16	0.16	0.17	2.76
60	1.1	0.17	1.40	0.16	0.17	3
100	1.1	0.17	2.33	0.16	0.17	3.93
120	1.1	0.17	2.80	0.16	0.17	4.4
150	**1.1**	**0.2**	**3.49**	**0.16**	**0.17**	**5.09**
200	1.1	0.2	4.65	0.16	0.17	6.25
200	-	-	4.65	0.16	0.17	4.98

Table 4.3: Estimated thermal resistance of the multilayered facade system when added to an exterior wall, accounting for different insulation thicknesses

There are two results that are particularly promising, as shown in Table 4.3. First, a thickness of **120 mm** reaches a total thermal resistance of $4.4\,m^2 \cdot K/W$, which is close to the required minimum

of $4.7\,m^2 \cdot K/W$. This thickness could be applied in cases where other project-specific factors, such as improved wall performance or additional layers, increase the overall thermal resistance.

A thickness of **200 mm** could be considered for new construction, as it achieves $4.98\,m^2 \cdot K/W$. While this lies outside the scope of this project, which focuses on renovation projects, it demonstrates strong potential for new construction or other applications aiming at extremely high insulation performance and future oriented sustainable design.

As shown in Table 4.3, a thickness of **150 mm** is recommended, as it achieves $5.09\,m^2 \cdot K/W$. This not only ensures compliance with Dutch building envelope requirements but also provides a comfortable margin, balancing performance with material efficiency.

4.2.1 Assembly and installation

Several factors were considered when selecting suitable assembly methods for the layers of the proposed facade system and their installation on a exterior wall of an building. The primary goal is to ensure ease of on-site assembly while enabling circularity, including clean disassembly and reuse or recycling at the end of the facade's life cycle.

The proposed system aligns with modern ETICS principles and compact facade design (no air gaps). Figure 4.3 illustrates a typical ETICS composition for masonry/concrete and lightweight timber walls.

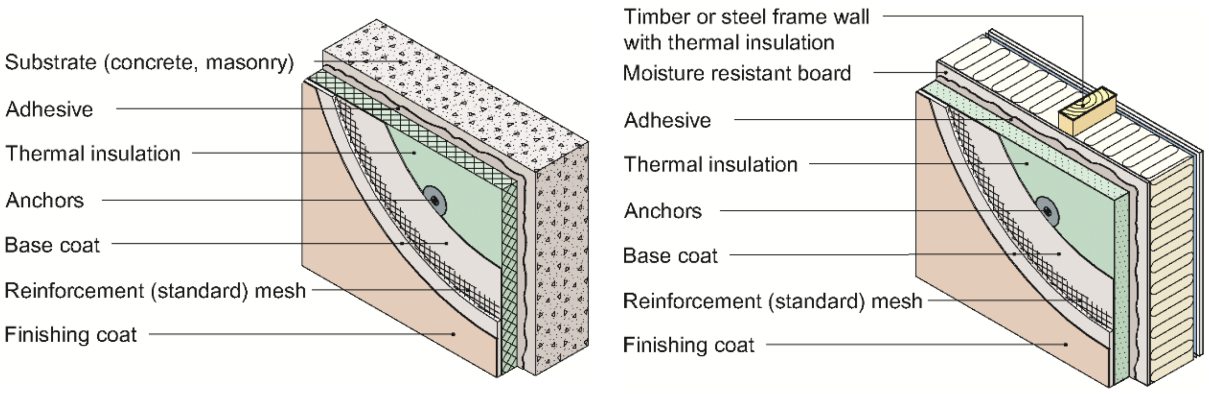

Figure 4.3: Example of a typical ETICS composition for masonry/concrete and lightweight timber walls (Kvande et al., 2018)

While this assembly and installation method provides a good starting point, it relies heavily on adhesives, mesh, and finishing coats, which do not fully meet circularity principles of this project. The following sections discuss alternative assembly methods for the proposed facade system design, intended for retrofitting existing exterior walls that prioritize mechanical fastening solutions and full disassembly.

Assembly

To enable full disassembly, each layer must be mechanically fixed, avoiding adhesives or permanent bonds. The following assembly sequence and methods are recommended for the assembly of the layers of the facade and recommnended assembly materials.

1. **Membrane to Cork Insulation** The waterproof membrane is mechanically fastened onto the cork insulation boards using corrosion resistant *cap nails*.

2. **Bioreceptive concrete to Membrane+Cork:** The bioreceptive concrete panels are attached to the membrane+cork assembly using *Fischer 6H NT screw washers*.

By keeping all layers independent and joined only by mechanical fasteners, the system allows for clean separation. This supports different end-of-life scenarios, such as whole-panel reuse, individual component reuse, or recycling to distinct material streams.

A key assembly consideration was whether to include an air gap between the concrete and insulation layers. After evaluation, the layers are placed in direct contact, separated only by the membrane to allow dry mechanical bonding and localized ventilation. This approach follows ETICS and cladding wall principles (Figure 2.10) and supports a compact facade design. Excluding an air gap in the design reduces the overall facade thickness, minimizes potential thermal bridges, and maximizes thermal resistance.

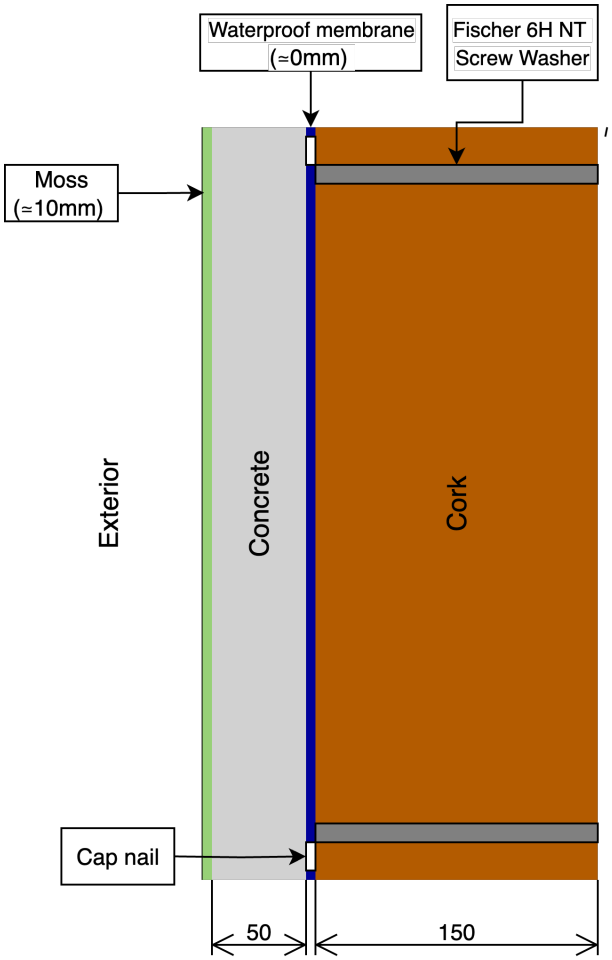

Figure 4.4: Cross section of the proposed multilayered facade system, combining bio-receptive concrete with cork insulation and exterior moss growth.

The panels can either be pre-assembled or assembled on site. For practical applications, the concrete panels should match the size of the cork insulation boards, which are 100cm long and 50cm wide. Therefore, it is recommended to prefabricate concrete panels in sizes of either 5×100×50cm or 5×50×50cm,

allowing each panel to either align with a single insulation board or combine two panels per board. These two options are summarized here below:

- **Option 1:** Two 5×50×50cm panels placed on top of one 10×100×50cm insulation board+membrane.
- **Option 2:** One 5×100×50cm panel placed on top of one 10×100×50cm insulation boards+membrane

The waterproof membrane should remain ascontinuous as possible. This can be achieved by either aligning with individual insulation boards or extending over multiple boards to maximize its protective properties.

Installation

For retrofitting existing masonry walls, the facade system can be implemented either as a fully on-site assembly or as a pre-assembled unit installed on-site. The choice of method depends on the building's structural conditions, logistical constraints, and desired level of off-site prefabrication. Both approaches rely fully on mechanical fastening for installation measures.

Figure 4.5 shows a cross section of the multilayered facade system when applied to the retrofit of an existing masonry wall. For this scenario, the pre-existing wall is assumed to consist of two layers of brick, each 100 mm thick, separated by a 50 mm air cavity. The mechanical fixings shown in the cross section can include expansion anchors, screw plugs, or mounting on a bracket or rail subframe, depending on the condition and evenness of the existing exterior wall surface.

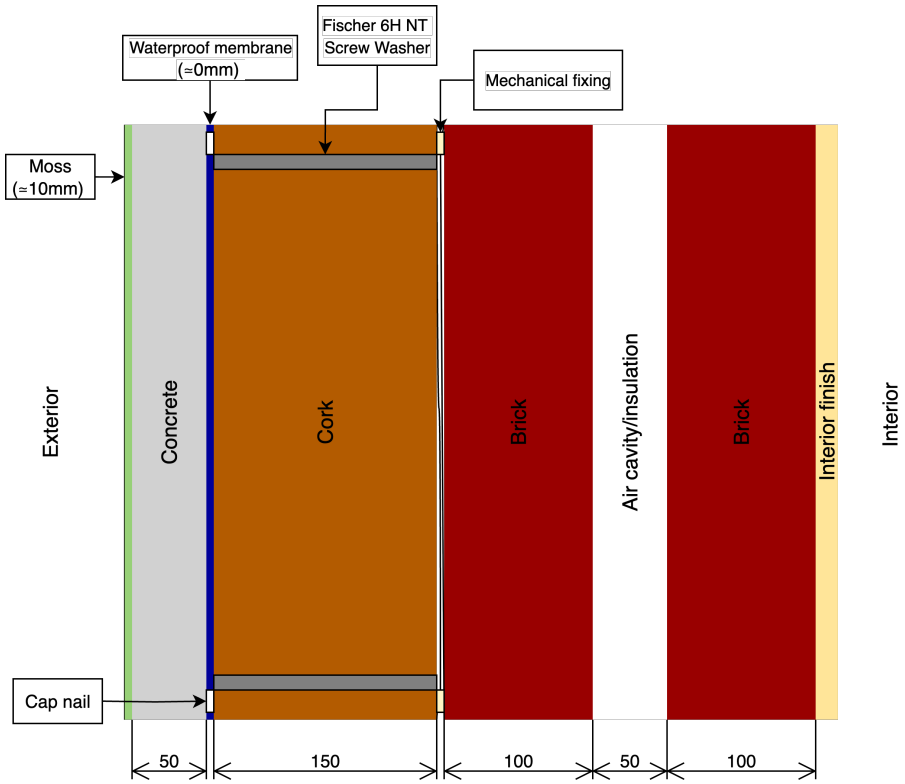

Figure 4.5: Multilayered facade system with concrete, cork insulation, and moss layer applied to an existing exterior brick wall as a retrofitting solution.

For the scenario, the pre-existing wall is assumed to consist of two layers of brick, each 100 mm thick, separated by a 50 mm air cavity. This air cavity can optionally be filled with insulation material. An example of this type of building envelope is shown in Figure 4.6.

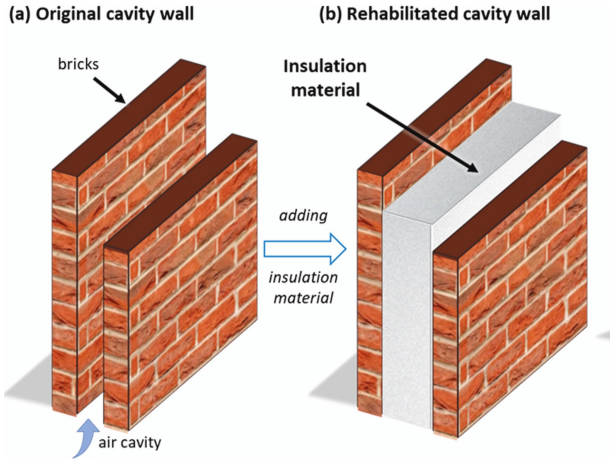

Figure 4.6: Example of a masonry cavity wall. Shown with (left Figure) and without (right Figure) the addition of an insulation material (Koh et al., 2022)

Installation methods can vary depending on project specific requirements and other influencing factors such as the condition of the wall or project constraints. Two possible assembly and installation options for the multilayered facade panel are presented here. Option 1 involves assembling and installing each layer sequentially directly on site, while Option 2 consists of pre-assembling the facade layers off site into modular units, which are then installed on the building.

Option 1: Full Assembly and Installation On-Site

In this approach, each layer of the facade is attached sequentially on site. The procedure can be implemented as follows:

1. Attach cork insulation to the exterior wall using mechanical fixings.
2. Fasten the waterproof membrane to the insulation layer with cap nails.
3. Install bioreceptive concrete panels on top using Fischer 6H NT screw washers.

Cork insulation boards can be anchored directly to solid masonry (brick or concrete block) using expansion anchors or screw plugs, or mounted on a bracket or rail subframe. See Chapter 3.5.2 for more information on materials and methods that can be used to achieve this. A limitation of this method is that the screw washers remain visible on the facade, which can potentially reduce moss growth.

Option 2: Pre-Assembled facade System and On-Site Installation

In this approach, the facade layers are assembled off-site into modular units, which are then installed on the building. The procedure can be implemented as follows:

1. Fasten the waterproof membrane to the insulation using cap nails (off-site).
2. Install bioreceptive concrete panels onto the membrane + cork using Fischer 6H NT screw washers (off-site).
3. Attach the pre-assembled facade system to the exterior wall using mechanical fixings(on-site).

This option can reduce on-site labor and construction time but requires careful handling during installation to ensure the expected functional performance.

Chapter 5

Methodology

5.1 Concrete panels

5.1.1 Aggregate properties

A few selected experiments were performed in order to evaluate the properties of the aggregates collected and used for the panels, which includes recycled sand and Argex 4/8. These tests include particle size distribution, water absorption testing and particle density and their methodology is described in detail in Appendix C.1.

5.1.2 Panel casting

A total of 12 concrete panels were made for this project with the purpose of testing thermal performance of the material. See Appendix C.2 for details on the concrete mixing process and panel casting.

5.2 Moss Layer

Due to time constraints, moss was glued onto the majority of the panels rather than allowing each species to grow naturally on individual panels. For final design purposes, one panel was dedicated to each specific colonizing moss species, which was grown in a growth chamber. While glueing allowed for a controlled and rapid establishment of moss cover, it is important to acknowledge that this method does not fully replicate a natural colonization processes of each moss species. In nature, moss growth is influenced by factors such as microclimatic conditions, surface porosity, moisture retention, light availability, and competition with other species. Glued moss does not fully address these ecological interactions, which may affect the structure, density, and water retention behavior of the moss layer. Therefore, the glued moss panels may not completely represent the thermal behavior of naturally colonized surfaces, which should be considered when interpreting heat flux measurements. Nevertheless, this approach ensured that each moss species was represented on the panels under consistent conditions.

The following sections describe the procedures for collecting and attaching the moss using glue, as well as the controlled moss growth process in the growth chamber.

5.2.1 Procedure for glueing the moss to the concrete panels

Glueing the moss onto the concrete panels involved two separate stages: collection and application. The procedures are described in detail here below.

Collection

Moss was collected from stone surfaces in shaded outdoor environments, such as bridges, parking lots, and sidewalks. The collection procedure included the following steps:

1. Identify a patch of the desired moss species.
2. Confirm that the moss is fully grown and provides sufficient coverage.
3. Carefully detach the moss using a suitable tool.
4. Place the moss in a labeled plastic bag for transport.

Application

A cyanoacrylate-based adhesive, commonly used in aquarium setups, was applied to attach the moss to the concrete panels. This type of glue was chosen for its relatively low thermal resistance, minimizing potential interference with heat flux measurements. The procedure was as follows:

1. Dry the collected moss thoroughly.
2. Moisten the concrete panel with water to enhance glue adhesion.
3. Apply a thin layer of glue to the base of the moss patch and press it onto the panel.
4. Allow the glue to set briefly to secure bonding.
5. Repeat the process with additional patches until the panel is fully covered.

Care was taken to avoid excessive use of glue, as this could introduce additional thermal resistance and affect heat flux readings. Any attached soil was removed from the moss to further minimize measurement interference.

Figure 5.1 demonstrates the procedure, where Figure 5.1a shows the dried moss, glue, and panel setup, and Figure 5.1b shows the panel once a layer of *Ptychostomum capillare* was glued.

(a) Setup for glueing moss to the panels

(b) Panel including glued moss

Figure 5.1: Example of the moss glueing procedure

5.2.2 Procedure for moss growth on panels

For the panels intended for moss growth rather than glueing, a controlled growth procedure was implemented:

1. Wash the moss with water.
2. Fully dry the moss.
3. Pulverise the moss into a powder using a blender.
4. Moisten the concrete surface with a water and nutrient mixture (3 g/L NPK fertilizer).
5. Sprinkle the pulverised moss evenly onto the surface.
6. Hydrate the surface again with the water and nutrient mixture.
7. Place the panels in a growth cabinet, providing water twice daily for approximately two months.

This approach allowed each moss species to establish itself naturally on the panel surface, providing the possibility of a comparison to the glued moss method and a more ecologically representative growth pattern. Unfortunately, due to time constraints, it was not possible to perform heat-flux measurements on the moss grown panels.

5.3 Hot-box method

The hot-box method was selected to estimate the R-value of the panels, both with and without the glued moss layer. The following subsections describe the experimental setup for the heat flux testing, the procedure followed, and the data processing method.

5.3.1 Set up

The following items were used to perform thermal conductivity testing with the hot-box method. The numbers included in partenthesis indicate the number of items needed to conduct the experiment.

- Hot box made out of styrofoam
- Lightbulb (2)
- Eltek Squirrel SRV250 (1)
- Hukseflux sensors (2)
- Temperature sensor (4)
- Eltek GENII transmitter (type GS44HA)
- Tape
- Additional styrofoam (3)
- Windows computer with Eltec Darca Software
- Lightbulbs (2)
- Power outlet
- Toothpaste
- Thermal putty/paste

For more information on the sensors and equipment used, refer to Appendixes C.3 (HFPO1 sensor), C.4 (SRV250 Receiver Logger) , and C.5 (GenII transmitter).

Figure 5.2 shows a schematic diagram of the experimental hot-box setup as viewed from the outside. The setup includes the Styrofoam hot-box, the test concrete panel, a Hukseflux heat flux sensor on the outer surface of the panel, a temperature sensor on the exterior of the panel, a temperature sensor for ambient room conditions, and a total of three GenII Eltek transmitters.

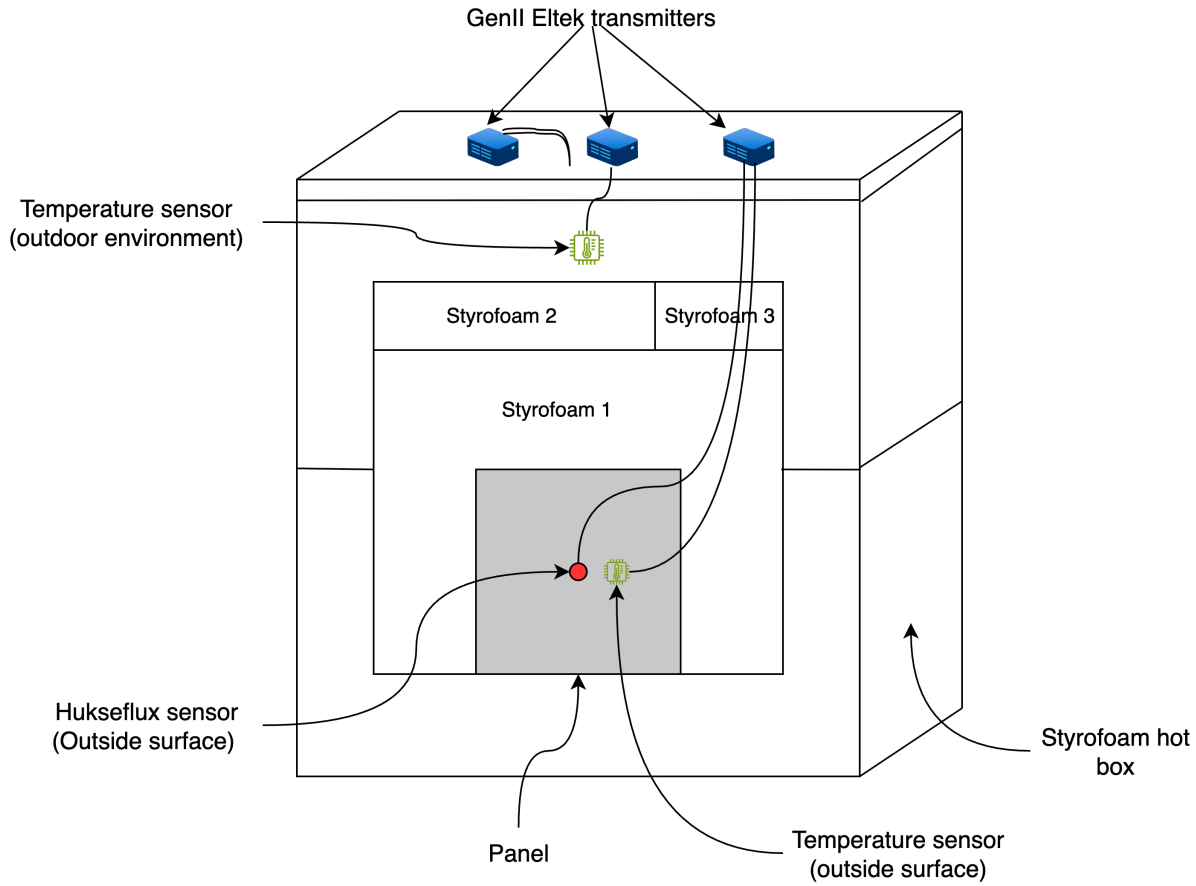

Figure 5.2: Schematic diagram of the experimental hot box setup as viewed from the outside. The diagram illustrates the placement of temperature and heat flux sensors, along with the the data transmission system.

As shown in Figure 5.2, three additional Styrofoam components were added to accommodate the size of the panel. One piece surrounds the panel itself, while the other two are placed at the top. Once these components are in place, the opening of the hot box is sealed, and testing can begin.

Figure 5.3 presents a cross-sectional schematic diagram of the experimental hot-box setup. The diagram shows two light bulbs, along with Hukseflux and temperature sensors placed on the interior surface of the test panel. Additionally, two Styrofoam components are placed inside the hot box to reduce direct radiation from the lightbulbs onto the concrete panel itself. Lightbulb 1 is partially covered with aluminum foil to further minimize direct heat flux toward the panel.

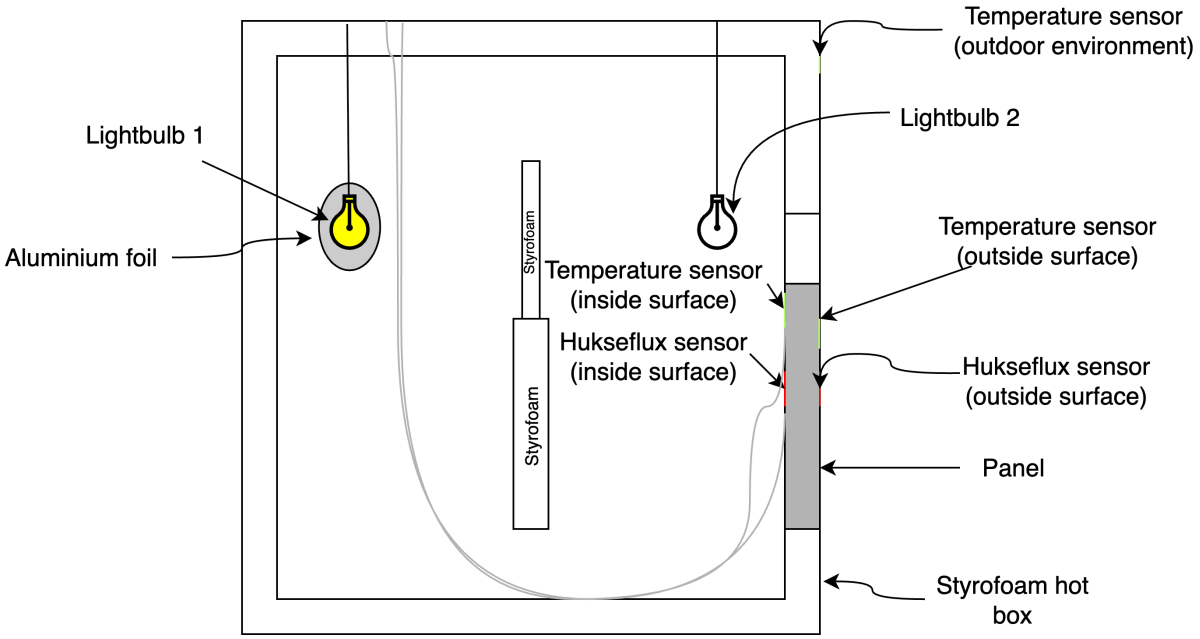

Figure 5.3: Cross-sectional schematic diagram of the experimental hot box setup. This view of the hot box highlights the positioning of lightbulb (heat source), addtional insulation layers, and sensors.

Two light bulbs are included in the hot-box to facilitate additional heat flux if needed. Lightbulb 2 was not used for the experiments conducted for this project, because additional time was accounted for to reach the intended temperature inside the hotbox.

Finally, Figure 5.4 includes a cross-sectional schematic diagram of the experimental hot box setup and further summarizes what has been included in 5.2 and 5.3.

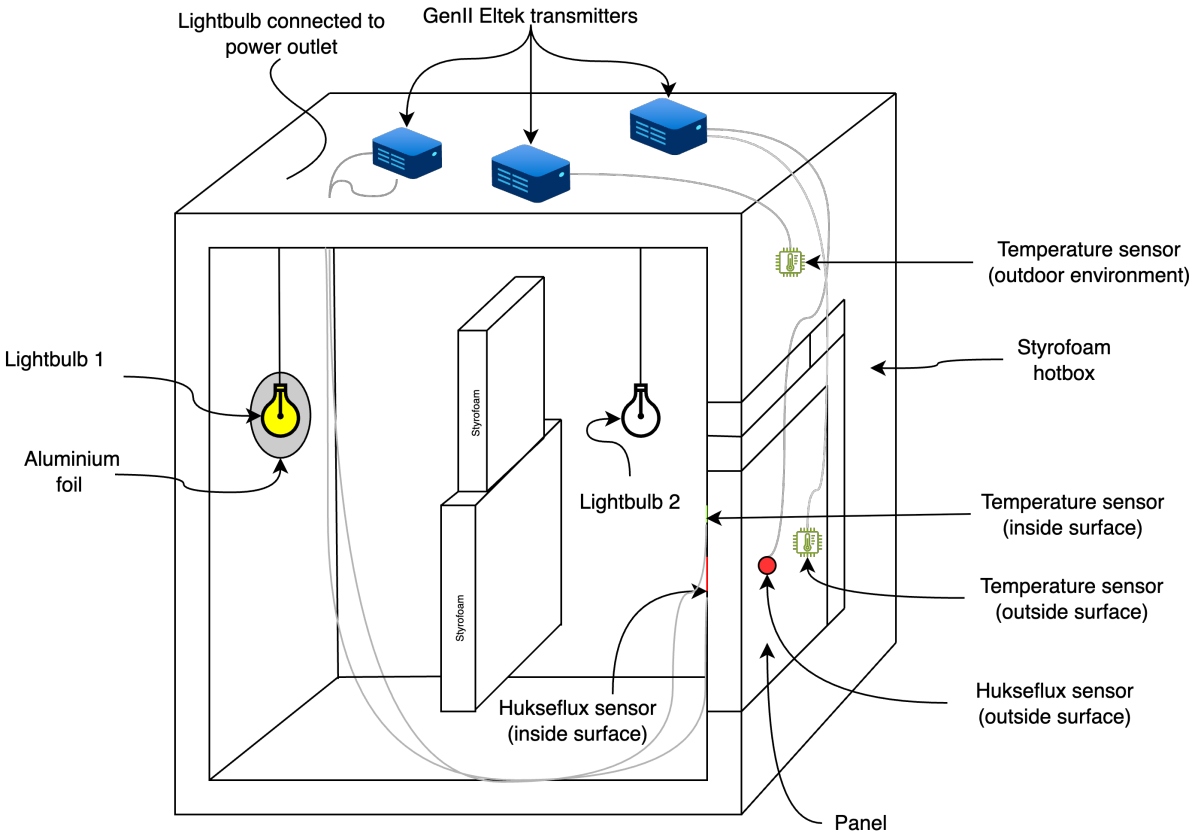

Figure 5.4: Experimental hot box setup showing the arrangement of lightbulbs (heat sources), insulation, sensors, and data transmitters.

Figure 5.5 includes the additional equipment needed to perform the hot-box experiment. This includes a power outlet, which supplies electricity to the lightbulb, Eltek squirrel SRV250 and a Windows computer. The Eltek Squirrel SRV250 is then connected to the computer, and transmits data to the Eltec Darca Software.

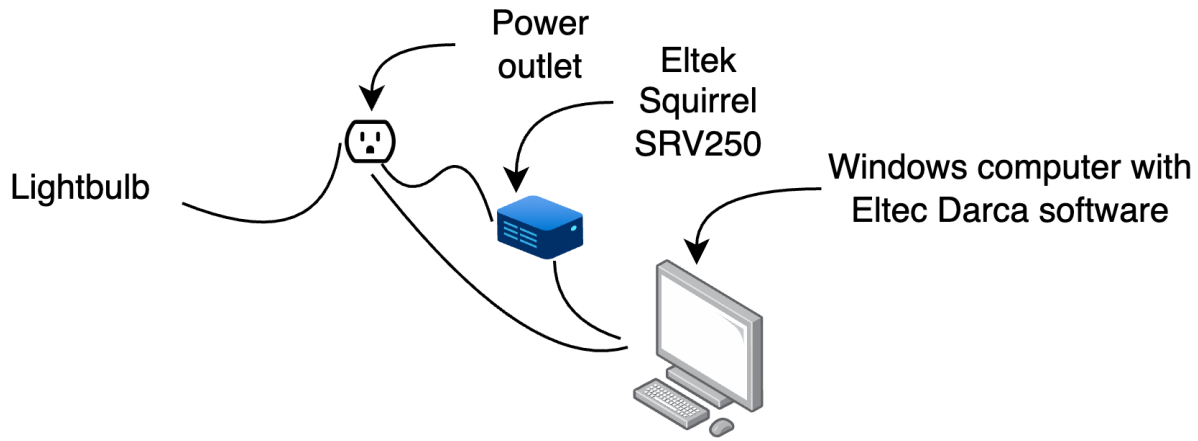

Figure 5.5: Additional equipment required for the hot-box experiment. The setup includes a power outlet for supplying electricity to the lightbulbs, Eltek Squirrel SRV250 data logger, and a Windows computer. The data logger is connected to the computer and transmits measurements to the Eltek Darca software, which enables continuous monitoring and recording of the experimental data.

-

As can be seen in Figure 5.5, the Eltek Darca Software is used for the heat flux measurements. This software can be used for configuring, monitoring, and retrieving data from Eltek data loggers and transmitters, such as the Squirrel SRV20 and GenII Eltek transmitters. In the context of heat flux measurements, the software allows users to set logging intervals, monitor real time sensor values, and export recorded data for analysis. Its interface supports reliable data retrival from multiple sensors, ensuring accurate data of temperatures and heat flux over time (Ltd., n.d.).

5.3.2 Procedure

The following procedure was followed to test the heat flux and temperatures of the panels. For moss covered panels, an additional step was included to saturate the moss layer before sensor attachment, simulating realistic moisture conditions. Sensor attachment methods were adapted depending on whether the surface was smooth, rough, or moss covered.

1. Prepare the materials needed for the hot-box setup. This includes the panel, tape, scissors, the two heatflux and temperature sensors, three additional styrofoam components and toothpaste.
2. **Saturate panel (for moss covered panels only):** Completely saturate the panel by pouring water over it or using a spray bottle until the moss layer is visibly moist. This step was performed to enable a comparison between dry and saturated moss conditions, allowing analysis of how moisture content affects thermal behavior and sensor readings, while still reflecting realistic outdoor conditions where moss retains water after rainfall or irrigation.
3. **Attach exterior sensors:** Attach one temperature sensor and one Hukseflux heat flux sensor to the exterior surface of the panel (the side facing the outdoor environment) using Pro Clima Tescon Vana tape.
4. **Attach interior sensors:** Attach the remaining temperature and Hukseflux sensors to the interior surface of the panel (the side facing the hot-box environment).
5. **Special considerations for sensor attachment:**
   - For **smooth surfaces**, place the sensor directly on the panel surface and secure it with tape.
   - For **rough surfaces**, apply a thin, even layer of toothpaste (or thermal putty, when available) across the diameter of the sensor before taping to improve thermal contact.
   - For **moss covered surfaces**, prepare two long strips of tape that span the full width of the panel. Remove only the center section of the backing from the first strip, spanning the width of the heat flux sensor itself. Secure the sensor on the portion of the tape that has no backing tape. Place the sensor on the moss surface by securing the tape ends to the panel sides. Add the second strip in the same way, fixing the opposite ends so that the sensor is held firmly against both the moss and the panel.
6. Insert the panel into the opening of the hot-box and surround it with three additional Styrofoam components. First, place the component that covers the panel, followed by the two top components. Add duct tape at the joints between the Styrofoam and the panel to minimize heat loss.
7. Ensure the GenII Eltek transmitters are powered on. If not, use a screwdriver to switch them on.
8. Switch on the light bulb to initialize heat flux inside the hot-box. A smart plug with timer functionality may also be used to automate heating (e.g., switching on at 6:00 AM and off at 8:00 PM).

9. Power on the Eltek Squirrel SRV250 data logger and ensure it is connected to the computer.
10. Open the Eltek Darca software on the computer, connect to the wizard, and click "Start" to begin data collection.
11. Continue measurements until both Hukseflux sensors have stabilized and display consistent values. At this point, the test can be stopped and the collected data analyzed.

Additional steps and limitations

The following steps and limitiations outline the specific procedures and considerations that were implemented in this experiment to ensure accurate and reliable measurements of heat flux and temperature through the panels. These steps include methods for sealing the hotbox, attaching sensors to uneven or rough surfaces, filling gaps to improve sensor contact, automating heating, and addressing environmental influences.

- To ensure the hotbox was sufficiently sealed, three additional styrofoam components were added around the panel. Where gaps were observed between the hotbox and the surrounding environment, tape was applied to further seal the assembly and minimize thermal leakage.
- When attaching a sensor to an uneven surface, applying toothpaste to the corners of the Hukseflux sensor significantly improved the sensor output. This method helped eliminate gaps between the sensor and the panel surface, ensuring better contact and more accurate readings. Thermal paste or putty can also be used to reduce air gaps between the sensor and the surface.
- On rough surfaces, using double-sided tape as recommended in the sensor manual (Hukseflux Thermal Sensors B.V., 2023) proved difficult. The rough texture prevented the sensor from being placed securely and could result in inaccurate values. In this experiment, Pro Clima Tescon Vana, a multipurpose airtight adhesive tape, was used instead to secure both heat flux and temperature sensors effectively.
- A smart plug with a built-in power meter was used to automate the lightbulb inside the hotbox. The plug was programmed to switch on at 6:00 AM and turn off at 8:00 PM, providing a 14-hour heating period. This ensured that the hotbox consistently reached temperatures above 40°C, allowing the heat flux through the panel to stabilize before measurements.
- To fill the space between the heat flux sensors and the concrete panels, either toothpaste or thermal putty/paste was used. Toothpaste was applied in the majority of the experiments performed. This was done to maintain consistency in t4esting, as thermal putty became available later in the experimental process. Thermal putty remains a promising alternative for future experiments, especially for replication or extended testing.
- No formal calibration was carried out prior to testing. Guidance from the heat flux specialist at TU Delft indicated that calibration was not required for this setup, but this could have also been overlooked. But to ensure testing reliability, the first tests were performed to optimize sensor placement. This led to the development of filling gaps with toothpaste and orienting the panels rough side inward to reduce environmental influences.
- The temperature outside the hotbox was not actively controlled. Experiments were conducted in an office space within the TU Delft architecture faculty, where occasional human activity (students

and staff entering or moving through the room) could influence ambient conditions. To mitigate these effects, an extra styrofoam component was positioned around the panel.

5.3.3 Data analysis

Before the sensor data could be analyzed, it first had to be corrected using the individual sensitivity values provided by the manufacturer for each Hukseflux sensor. Once the heat flux measurements were corrected, the thermal resistance and thermal conductivity of the test panels could be calculated from the measured heat flux and surface temperature differences. To check the reliability of the results, the data was then processed and visualized using Jupyter Lab. The following subsections shortly describe the steps of sensitivity correction, calculation of thermal resistance and thermal conductivity, and visualization of the results.

Heat-flux sensitivity correction

Before the data could be analyzed and visualized, the heat flux sensor readings were corrected using their respective sensitivity values.

The HFP01 sensor measures heat flux through the material it is either embedded in or mounted on. Heat flux is expressed in watts per square meter (W/m^2). To correct the readings from the sensor, the heat flux, ϕ [W/m^2], is calculated by dividing the sensor's voltage output, U, by its sensitivity, S, as shown in Equation C.5 (Hukseflux Thermal Sensors B.V., 2023):

$$\Phi = \frac{U}{S} \tag{5.1}$$

The sensitivity value S is specific to each sensor and is provided by the manufacturer along with the sensor.

Thermal resistance (R)

Thermal resistance (R) measures the thermal resistance of building materials to heat flow. A higher R-value indicates better insulating performance, i.e. the material is more effective at resisting the transfer of heat and cold (Boswell, 2013). In this study, R is measured from surface to surface by conduction using the HUKSEFLUX HFP01 sensor, calculated from the heat flux and the surface temperature difference. Its inverse, the Λ-value (thermal conductance), can also be used (Hukseflux Thermal Sensors B.V., 2023).

The wall's thermal conductance can be calculated from the surface temperatures of the reference wall, as shown in Equation 5.2 (Hukseflux Thermal Sensors B.V., 2023):

$$\Lambda = 1/R_{thermal,A} = \Phi/(T_{surface,indoor} - T_{surfaceoutdoor}) \tag{5.2}$$

Thermal conductivity (λ)

When the thermal resistance R of a wall or homogeneous layer is know, calculating the thermal conductivity λ is quite straightforward. Thermal conductivity can therefore be calculated by using equation 5.3

$$R = \frac{d}{\lambda} \quad \Longrightarrow \quad \lambda = \frac{d}{R} \tag{5.3}$$

where:

- R = thermal resistance of the layer ($m^2 \cdot K/W$)
- d = thickness of the layer (m)
- λ = thermal conductivity (W/m·K)

Visualization of data

The program Jupyter Lab was used to visualize the data obtained from the temperature and heat-flux sensors. A code was made to generate the following graphs:

- A graph showing the data from the two temperature sensors, along with the average temperature difference between them during the final two hours of data collection.
- A graph showing the data from the two heat flux sensors, including the average heat flux during the final two hours.
- A combined graph displaying the data from all four sensors, with the final two hours highlighted and the average $\triangle T$ and heat flux for the period indicated.

In addition, the following calculations were performed using the same code:

- Average temperature difference $\triangle T$ between the two sensors
- Average heat flux of the two sensors
- R-value calculated with by using Equation 5.2

The final **two hours** of data were used to calculate average heat flux and $\triangle T$, as the sensors typically reach a steady state about two hours before the end of data collection. It is essential to confirm that steady state is maintained for at least this duration before stopping measurements and analyzing the data.

5.4 Life Cycle Assessment (LCA)

Life cycle assessment (LCA) is a standardized technique developed to evaluate and address the environmental impacts associated with the production and consumption of products (International Organization

for Standardization, 2006). In the building industry, LCA serves as a valuable tool for comparing different design alternatives and making informed decisions to improve environmental performance. It provides a rational, quantifiable approach to assess specific environmental impacts across the entire life cycle of a product or system (Kunič, 2017).

LCA evaluates impacts across several environmental indicators, including acidification, eutrophication, ozone depletion, various forms of ecotoxicity, air pollution, resource depletion, and greenhouse gas emissions. Among these, the most significant is greenhouse gas emissions, commonly measured as a carbon footprint. LCA helps identify opportunities to reduce environmental impacts at different stages of a product's life cycle, from raw material extraction and production to use, end-of-life treatment, and final disposal. It also supports decision-making processes in industry, government, and non-governmental organizations (International Organization for Standardization, 2006).

5.4.1 Scope

The product system assessed is the designed multilayered facade panel, including the concrete substrate, selected insulation material, the membrane layer, and potential additional environmental benefits associated with the system.

Functional Unit

The functional unit is defined as 1 m^2 of the facade panel system over a 30-year reference study period, reflecting the limited service life of the water permeable membrane. The panel function includes the combined performance of the concrete mixture, insulation material, and membrane, as well as expected environmental benefits.

Excluded from the assessment are the fastening system, due to lack of reliable data, and minor contributions of bone ash and tap water in the concrete mixture. Table 5.1 presents the expected service life for each layer of the facade system.

Facade layer	**Expected service life [years]**
Moss	30+
Concrete	50+
water permeable membrane	30 (pro clima, 2025b)
Insulation layer	75 (Pro Suber, 2023)

Table 5.1: Expected service life of individual layers of the facade system

The system's expected service life is 30 years, primarily determined by the shortest lived critical layer, the water permeable membrane.

System boundary

Figure 5.6 illustrates the system boundary for this LCA study. Included are the product stage (A1–A3), the end-of-life stage (C1–C4), and supplementary Module D. Excluded stages are the construction process (A4–A5) and the use stage (B1–B7).

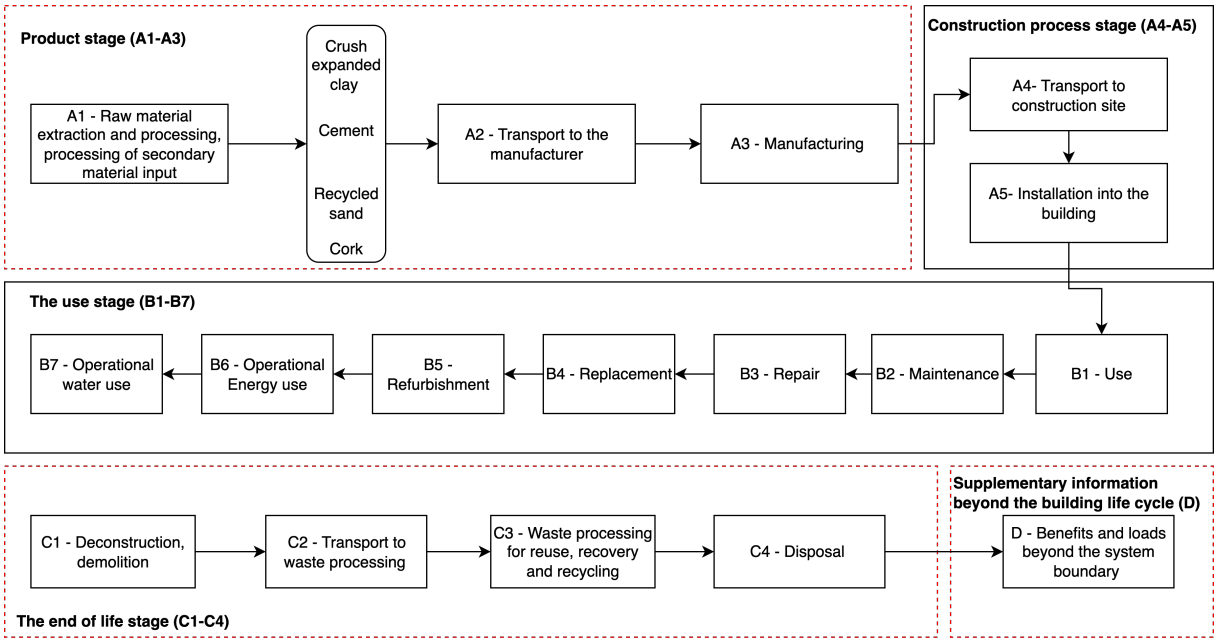

Figure 5.6: Defined system boundary for the LCA of the multilayered facade system. Life cycle stages included in the assessment are marked with a dashed red line, while excluded stages are shown within a black frame.

The product stage comprises:

1. A1 – Raw material supply
2. A2 – Transport to production site
3. A3 – Manufacturing

The construction process (A4–A5) and use stage (B1–B7) are excluded. The end-of-life stage includes:

1. C1 – Deconstruction/demolition
2. C2 – Transport to waste processing
3. C3 – Waste processing for reuse, recovery, or recycling
4. C4 – Final disposal

Figure 5.7 shows possible end-of-life scenarios for each layer of the facade system, including Module D.

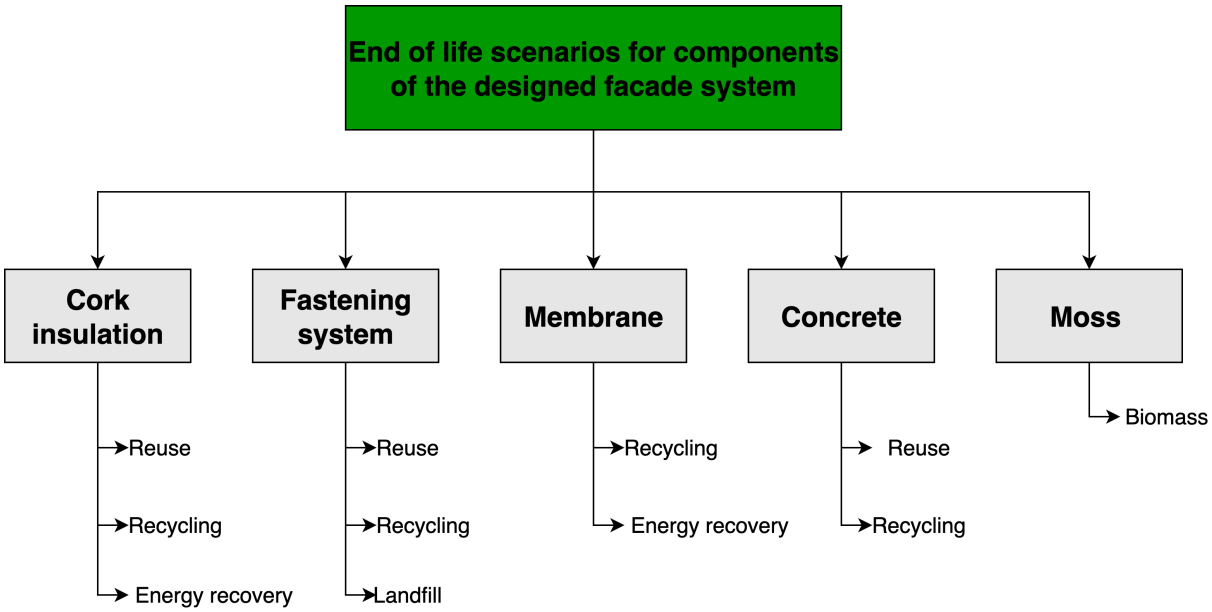

Figure 5.7: Possible end-of-life scenarios for components of the designed facade system, including cork, fastening system, membrane, concrete, and moss layer.

Allocation procedures

Allocation is based entirely on the procedures applied in the Environmental Product Declarations (EPDs) used as data sources, following EN 15804:2019+A2.

Assumptions and limitations

The fastening system, bone ash, and tap water in the concrete mix were excluded due to lack of reliable data or negligible influence. The cork insulation EPD (140 mm) was linearly scaled to 150 mm to reflect system requirements.

5.4.2 Life Cycle Inventory

Inventory analysis quantifies the relevant inputs and outputs of the defined product system (International Organization for Standardization, 2006). Table 5.2 summarizes the material inventory of the multilayered facade system.

Facade layer	Material	Notes/assumptions
Insulation material	Cork insulation boards by PRO SUBRA	Scaled by a factor 1.07
Membrane	SOLITEX FRONTA HUMIDA membrane	
Concrete	CEMIII/B 42.5 N-LH/SR cement	Scaled according to mix design
	Recycled concrete	-
	Argex 4/8	-
Moss	*Grimmia pulvinata*, *Ptyschostomum cappilare*, or *Brachythecium rutabulum*	

Table 5.2: Material inventory of the multilayered facade system, categorized by facade layer

All material inventory data were retrieved from their respective EPDs. Transport in the product stage (A2) is taken directly from the EPDs.

5.4.3 Impact assessment method

Environmental impact indicators follow EN 15804+A2:2019. Table 5.3 lists the selected indicators and shadow prices used to calculate the Environmental Cost Indicator (ECI) for comparison.

Environmental indicator:	Unit:	Shadow price (€/ unit indicator)
GWP - total	kg CO2-eq	0.116
GWP - fossil	kg CO2-eq	0.116
GWP - biogenic	kg CO2-eq	0.116
GWP - luluc	kg CO2-eq	0.116
ODP	kg CFK11-eq	32
AP	Mol H^+-eq.	0.39
EP - freshwater	kg P-eq	1.96
EP - marine	kg N-eq	3.28
EP - terrestrial	Mol N-eq.	0.36
POCP	kg NMVOC-eq.	1.22
ADP - minerals & metals	kg Sb-eq	0.3
ADP - fossil	MJ, net cal. val.	0.00033
WDP	m^3 water, world eq. deprived	0.00506
Additional parameters:		
PM Particulate Matter emissions	kg disease incidence	138 (de Vries et al., 2024)
Ionising Radiation	kg kBq U235-eq	0.049
Ecotoxicity (freshwater)	CTUe	0.00013
Human toxicity, cancer effects	CTUh	1096368
Human toxicity, non-cancer effects	CTUh	147588
Landuse related impacts / Soil quality potential	Pt/m^2.jaar	0.000178

Table 5.3: Environmental impact categories based on EN 15804+A2:2019 and their representative shadow prices

5.4.4 Evaluation of additional environmental benefits

The following additional benefits were considered:

- Carbon sequestration of the moss species
- Air purification (PM2.5) of the moss species
- Energy demand reduction of the system

Carbon sequestration

Carbon sequestration of the moss layer is calculated using Equation 5.4.

$$\text{Total GWP - biogenic} = \text{carbon sequestration rate/year} \cdot \text{service life [years]} \tag{5.4}$$

In order to estimate the carbon sequestration uptake of the facades moss layer, a general value for a thin layer of moss was used. This value was retrieved from Ji et al. (2024), where the reported carbon sequestration is around 95.14 g C/m^2yr, which results in approximately 0.35 kg CO_2/m^2 year. This value provides an estimate of CO_2 fluxes of subtropical moss dominated biocrusts at diurnal and seasonal scales in subtropical China (Ji et al., 2024). Since this represents a thin layer of moss and exposed to the urban environment, this value was used to represent the moss layer in the multilayered facade system.

PM2.5 sequestration

PM2.5 capture is calculated using Equation 5.5.

$$\text{Total PM2.5 capture [g]} = \text{PM2.5 deposition rate} \cdot \text{service life} \cdot \text{functional unit} \tag{5.5}$$

The PM2.5 deposition rate chosen for the moss is retrieved from (Speak et al., 2012), where the rate for PM2.5 is approximately 0.20 g/m^2/year.It was decided to focus solely on PM2.5 capture which explains why the carbon sequestration rate of PM10 is therefore not included in the evaulation of total PM capture for the LCA. This decision is based on the fact that PM2.5 is more harmful to the environment.

Energy reduction of the system

Energy saved by the facade is calculated using Equations 5.6–5.9, based on the size of the reference wall (A), the difference in U-value between a reference wall and the insulated wall (ΔU), heating degree days (HDD), and local carbon intensity (Scarlat et al., 2022).

$$\Delta U = U_{ref} - U_{new} \tag{5.6}$$

$$Q\ (J) = A \cdot \Delta U \cdot HDD \tag{5.7}$$

Where the reference wall area is 1 m^2, which corresponds to the functional unit of the LCA study. A U value used is 1.1 W/m^2K (Yu et al., 2024), which is representative of a reference wall which is uninsulated

and consists of either concrete or brick. The number of heating Degree days in Delft, Netherlands, is around 4.676 K · days/year (CEIC Data (World Bank WDI), 2020) and will be used for the calculations.

$$Q_{\text{kWh}} = Q_J/(3.6 \cdot 10^6) \tag{5.8}$$

$$CO_2 \textit{ saved } (CO_2/\text{year}/m^2) = Q_{\text{kWh}} \cdot \text{carbon intensity}(kgCO2/kWh) \tag{5.9}$$

It was decided to use local grid density of Delft, Netherlands, representing a standard sized city in the Netherlands. For the Dutch electricity grid, the carbon intensity is approximately 0.440 kg CO_2/kWh (Scarlat et al., 2022). This calculated value will then be included in the impact category *Climate Change Fossil (kg CO_2 eq* as an avoided impact.

Chapter 6

Results

6.1 Aggregate properties

In order to prepare for the casting of the concrete panels, the particle size distribution of Argex 4/8 and recycled sand was investigated. Additonally, the water absorption of Argex 4/8 was determined and the particle density.

6.1.1 Particle size distribution

The following table includes the collected data and results for the sieve analysis of Argex 4/8, which acts as the coarse aggregate fraction of the concrete mixture design. Table 6.1 includes the total mass retained by the sieves, % retained, cumulative % retained and passing %.

The following tables present the collected data from the sieve analyses conducted on the granular materials used in the concrete mixture design. Table 6.1 shows the sieve analysis results for Argex 4/8, which serves as the coarse aggregate fraction in the concrete mix. The table includes the total mass retained on each sieve, the percentage retained, cumulative percentage retained, and the percentage passing through the sieves.

Sieve size	**Weight [g]**	**Retained [%]**	**Cumulative retained [%]**	**Passing [%]**
M(8mm)	301	6.0	6.0	94.0
M(4mm)	3670	73.4	79.4	20.6
M(2mm)	117	2.3	81.8	18.2
M(1mm)	6	0.1	81.9	18.1
Passing	306	6.1	88.0	12.0
TOTAL	4400	88.0		

Table 6.1: Sieve analysis results for Argex 4/8 aggregate (initial mass: 5000 g)

Figure 6.1 presents the particle size distribution for Argex 4/8. The initial aggregate mass was 5 kg and the cumulative sieved weight recorded was 4.4 kg. This weight discrepancy may be due to material loss during drying (48 hours) or handling losses when transferring the material from the sieve to the scale.

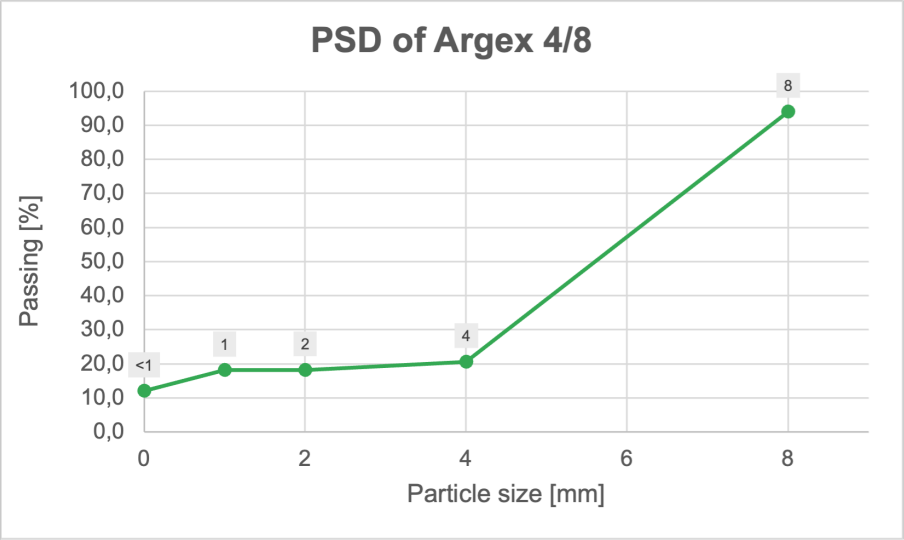

Figure 6.1: PSD of Argex 4/8

According to Figure 6.1 above and Table 6.2 below, Argex 4/8 contains a high proportion of particles in the 4–8 mm range, accounting for approximately 94% of the total mass. The final passing percentage is also 94%, which suggests a total moisture content of about 6%, assuming that the observed mass loss during drying was primarily due to water evaporation.

Sieve size	Passing [%]
<1	12
1	18.1
2	18.2
4	20.6
8	94

Table 6.2: Passing % for Argex 4/8

Table 6.3 contains the results for the recycled sand, which is the fine aggregate fraction of the concrete mixture. Similar to Table 6.1, the data includes the weight retained per sieve, the percentage retained, cumulative retained percentage, and the percentage of material passing each sieve.

Sieve size	**Weight [g]**	**Retained [%]**	**Cumulative retained [%]**	**Passing [%]**
M(4mm)	54.8	1.1	1.1	98.9
M(2mm)	898.5	18.0	19.1	80.9
M(1mm)	869.5	17.4	36.5	63.5
M(500µm)	941.8	18.8	55.3	44.7
M(250µm)	978.5	19.6	74.9	25.1
M(125µm)	454.5	9.1	84.0	16.0
M(63µm)	283.2	5.7	89.6	10.4
Passing	309.3	6.2	95.8	4.2
TOTAL	4790.1	95.8		

Table 6.3: Sieve analysis results for recycled sand (initial weight: 5000 g)

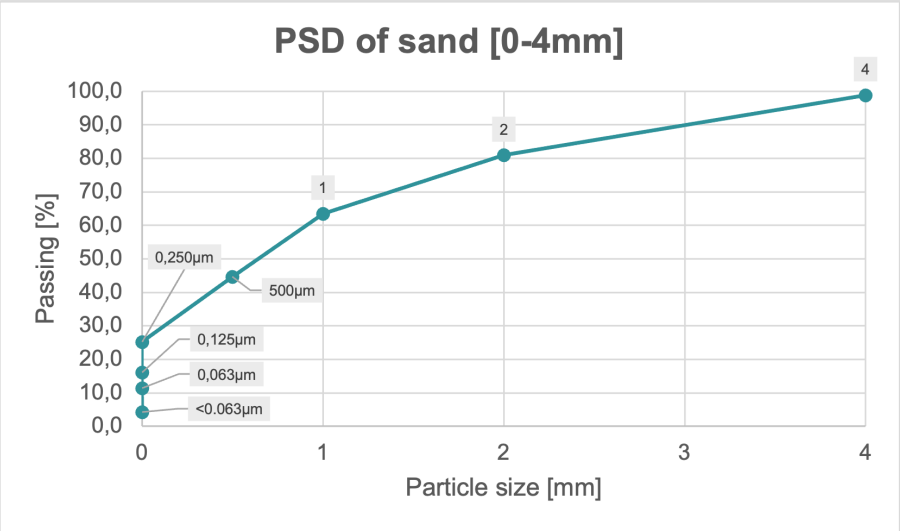

Figure 6.2: Passing % for recycled sand (0-4mm)

Figure 6.2 above and Table 6.4 below includes PSD results for recycled sand (0-4mm). The majority of recycled sand particles fall below 1 mm, with 71.4% passing through the 1 mm sieve. The final passing percentage is 98.9%, indicating a moisture content of approximately 1.1%.

Sieve size	Passing [%]
<0,063µm	4.2
0,063µm	10.4
0.125µm	16.0
0.250µm	25.1
0.550µm	44.7
1mm	63.5
2mm	80.9
4mm	98.9

Table 6.4: Passing % for sand (0-4mm)

6.1.2 Water absorption

Table 6.5 includes the calculated water absorption of Argex 4/8. The calculated water absorption is 75.93%. The value is calculated by using the method described in section C.1.

Dry aggregates (M_a) [g]	1000
Saturated mass (M_w) [g]	1696
Dry mass (M_d) [g]	964
Water absorption [%]	75.93

Table 6.5: Water absorption of Argex 4/8

6.1.3 Particle density

Table 6.6 includes the results of the estimated particle density of the collected Argex 4/8.

	Test 1	Test 2	Average
Empty pycnometer [grams]	709.1	708.8	709.0
Pycnometer+water [grams]	2035.8	2035.2	2035.5
Volume pycnometer [mL]	306.2	270.9	288.6
Weight aggregates [grams]	299.4	300.0	299.7
Aggregates + pycnometer [grams]	1008.5	1008.5	1008.5
Aggregates+water+pycnometer [grams]	2029.0	2064.3	2046.7
Density [g/mL]	1.0	1.1	1.0

Table 6.6: Calculated particle density of Argex 4/8

As shown in Table 6.6, the test was conducted twice, and the average was calculated from the two results. Test 1 yielded an aggregate density of 1.0 g/mL, while Test 2 gave a slightly higher value of 1.1 g/mL. The resulting average density is 1.0 g/mL.

6.2 Life cycle analysis (LCA)

This chapter presents the results of the life cycle analysis of the multilayered facade system. First, the environmental impact of each material, insulation, membrane, additional environmental benefits, and concrete, is shown individually across the chosen indicators. Finally, the results are combined to give the total environmental impact and shadow cost of the complete facade system.

6.2.1 Cork (insulation material)

Figure 6.3 shows the environmental impact of the chosen cork insulation material across thirteen indicators. The data can be found in Table D.11 in Appendix D.3.1.

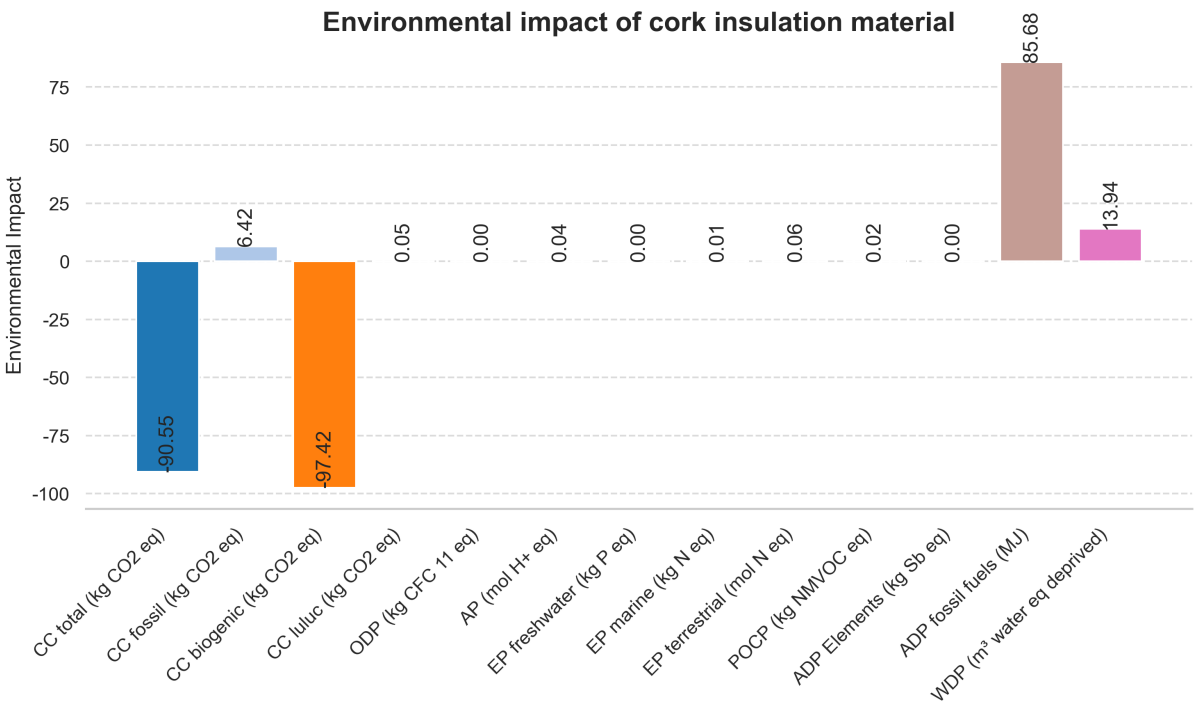

Figure 6.3: Environmental impact of the chosen cork insulation material

The estimated environmental impact of the chosen cork insulation material has been translated to monetary terms in Table 6.7.

Impact Category	A1-A3	C1-C4	TOTAL	%
CC total (kg CO2 eq)	-10,50	1,69	-8,81	-
CC fossil (kg CO2 eq)	0,74	-0,25	0,49	-6%
CC biogenic (kg CO2 eq)	-11,30	1,95	-9,35	106%
CC luluc (kg CO2 eq)	0,01	0,00	0,00	0%
ODP (kg CFC 11 eq)	0,00	0,00	0,00	0%
AP (mol H+ eq)	0,02	-0,01	0,00	0%
EP freshwater (kg P eq)	0,00	0,00	0,00	0%
EP marine (kg N eq)	0,02	-0,03	-0,01	0%
EP terrestrial (mol N eq)	0,02	-0,06	-0,03	0%
POCP (kg NMVOC eq)	0,03	-0,03	-0,01	0%
ADP Elements (kg Sb eq)	0,00	0,00	0,00	0%
ADP fossil fuels (MJ)	0,03	-0,01	0,02	0%
WDP (m^3 water eq deprived)	0,07	-0,01	0,06	-1%
TOTAL	-10,36	1,54	**-8,82**	100%
%	117%	-17%	100%	

Table 6.7: Total shadow cost of Pro Suber cork insulation material

The total shadow cost of the chosen insulation material, at 150 mm thickness, amounts to –€8.82. Most impact categories are negligible, each contributing only 0–1% to the total. End-of-life processes (C1–C4) add €1.54, but the overall shadow cost remains negative due to the dominant effect of biogenic carbon

uptake during the production stage (A1–A3), reducing the shadow cost by €10.36.

6.2.2 Concrete

Figure 6.4 illustrates the environmental impact of the concrete substrate across thirteen specific indicators. The results shown represent the combined impact of cement, Argex 4/8, and recycled sand. Data is provided in Table D.13 in Appendix D.4. Figure 6.4 illustrates that the categories with the highest contribution are CC fossil (kg CO_2-eq) and ADP fossil fuels (MJ), with cement as the highest contributing material to the total environmental impact.

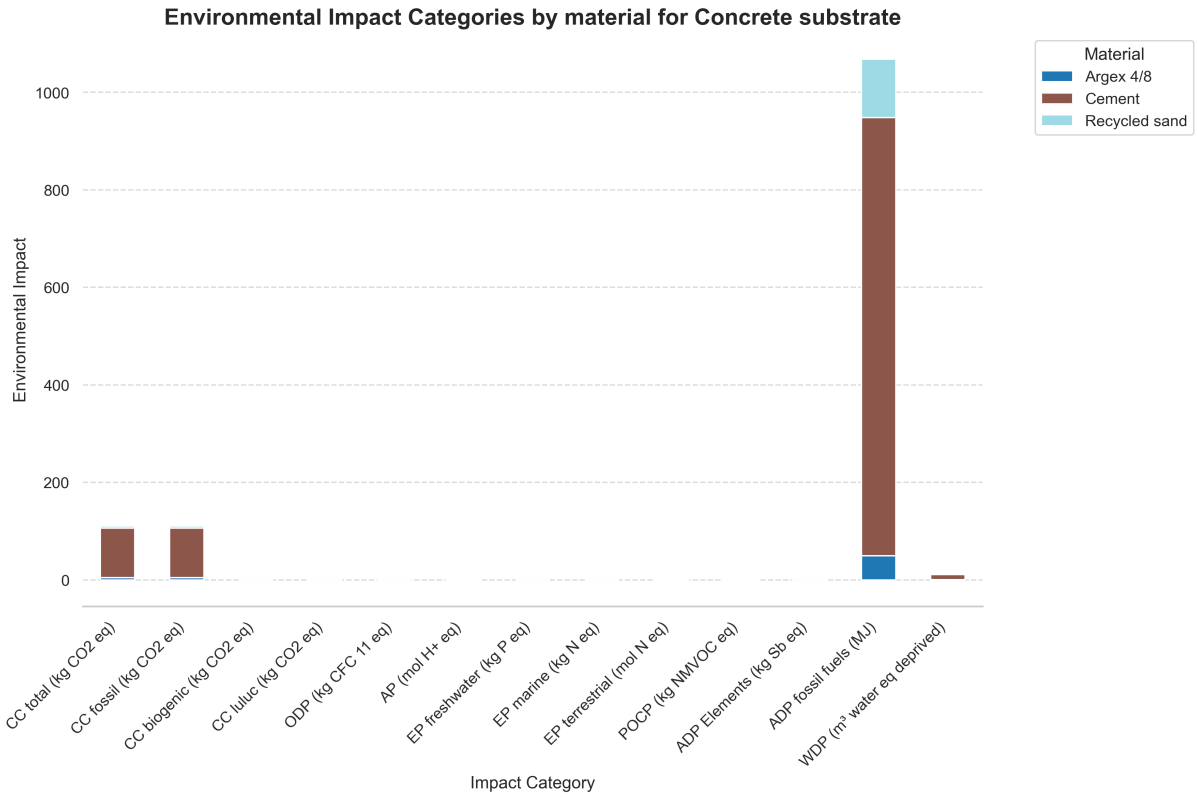

Figure 6.4: Environmental impact of the concrete mixture

The estimated environmental impact of concrete has been translated to monetary terms in Table 6.8.

Impact Category	A1–A3	C1-C4	D	Total	%
CC total (kg CO2 eq)	20,4	0,7	-8,3	12,8	-
CC fossil (kg CO2 eq)	20,4	0,7	-8,3	12,8	88%
CC biogenic (kg CO2 eq)	0,0	0,0	0,0	0,0	0%
CC luluc (kg CO2 eq)	0,0	0,0	0,0	0,0	0%
ODP (kg CFC 11 eq)	0,0	0,0	0,0	0,0	0%
AP (mol H+ eq)	1,2	0,0	-1,0	0,2	1%
EP freshwater (kg P eq)	0,0	0,0	0,0	0,0	0%
EP marine (kg N eq)	0,6	0,0	-0,3	0,4	2%
EP terrestrial (mol N eq)	0,7	0,0	-0,3	0,5	3%
POCP (kg NMVOC eq)	0,8	0,0	-0,5	0,4	3%
ADP Elements (kg Sb eq)	0,0	0,0	0,0	0,0	0%
ADP fossil fuels (MJ)	0,5	0,0	-0,1	0,4	2%
WDP (m^3 water eq deprived)	0,1	0,0	0,0	0,1	0%
TOTAL	24,3	0,9	-10,5	**14,6**	100%
%	166%	6%	-72%	100%	

Table 6.8: Total shadow cost of the concrete layer

The total shadow cost of the concrete mixture is €14.6. The stage with the highest contribution is the production stage (A1–A3), with a shadow cost of €24.3. However, the end-of-life stage offsets this impact by –€10.5, reducing the overall total. Among the impact categories, the largest contributor to the shadow cost is Climate Change fossil) (kg CO_2-eq) while the production stage (A1–A3) is the dominant life cycle stage.

6.2.3 Waterproof membrane

Figure 6.3 illustrates the environmental impact of the chosen waterproof membrane, considering the thirteen specific indicators. See Tables D.12 in Appendix D.3.2 for more information on the data plotted in the graph shown here below.

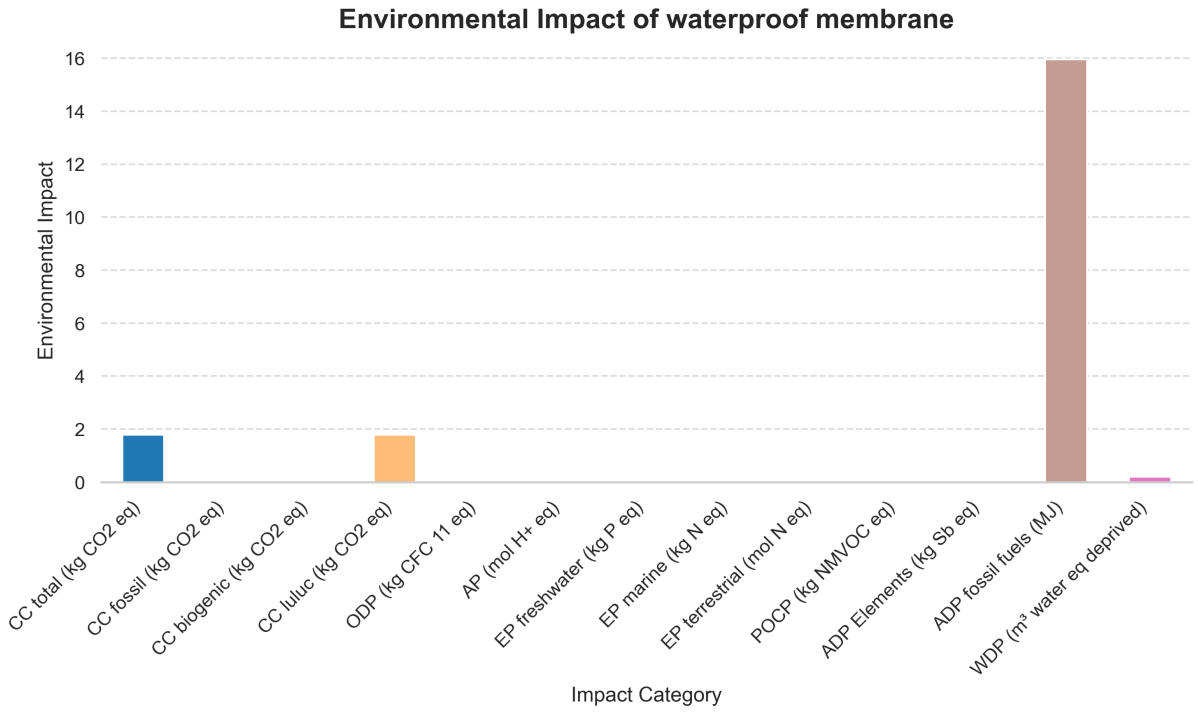

Figure 6.5: Environmental impact of SOLITEX FRONTA HUMIDA waterproof membrane

The estimated environmental impact of concrete has been translated to monetary terms and the results are summarized in Table 6.9.

Impact Category	A1–A3	C1-C4	D	Total	%
CC total (kg CO2 eq)	0,09	0,08	-0,03	0,13	-
CC fossil (kg CO2 eq)	0,00	0,00	0,00	0,00	0%
CC biogenic (kg CO2 eq)	0,00	0,00	0,00	0,00	0%
CC luluc (kg CO2 eq)	0,09	0,08	-0,03	0,13	7%
ODP (kg CFC 11 eq)	0,00	0,00	0,00	0,00	0%
AP (mol H+ eq)	0,00	0,00	0,00	0,00	0%
EP freshwater (kg P eq)	0,00	0,00	0,00	0,00	0%
EP marine (kg N eq)	0,00	0,00	0,00	0,00	0%
EP terrestrial (mol N eq)	0,00	0,00	0,00	0,00	0%
POCP (kg NMVOC eq)	0,00	0,00	0,00	0,00	0%
ADP Elements (kg Sb eq)	0,00	0,00	0,00	0,00	0%
ADP fossil fuels (MJ)	2,41	0,02	-0,60	1,83	93%
WDP (m^3 water eq deprived)	0,01	0,00	0,00	0,01	1%
TOTAL	2,60	0,18	-0,67	**1,97**	100%
%	132%	9%	-34%	100%	

Table 6.9: Shadow cost of Solitex Fronta Humida waterproof membrane

The total shadow cost of the Solitex Fronta Humida waterproof membrane is €1.97. The highest contribution comes from the production stage (A1–A3) with 2.60, while the end-of-life stage (C1–C4) slightly offsets this impact with –0.67. Among the impact categories, the largest contributor to the shadow cost

is ADP fossil fuels (MJ), accounting for 93% of the total.

6.2.4 Estimated additional environmental benefits of the multilayered facade system

The multilayered facade system provides additional environmental contributions beyond thermal insulation, including carbon sequestration, energy reduction, and PM2.5 filtration.

Carbon sequestration The service life of the facade panel as a whole is assumed to be 30 years, which results in a total carbon sequestration of approximately:

$$\begin{aligned}\text{Total GWP} &= \text{Carbon sequestration rate/year} \cdot \text{Service life [years]} \cdot \text{Functional unit } [\text{m}^2] \\ &= 0.35 \text{ kg } \text{CO}_2/\text{m}^2/\text{yr} \cdot 30 \text{ years} \cdot 1 \text{ m}^2 \\ &= 10.5 \text{ kg } \text{CO}_2\end{aligned}$$

This value is negative, as it refers to carbon sequestration by the colonizing moss species. It corresponds to a total negative shadow cost of -0.040 €/year and -1.218 €/30 years.

Energy reduction Energy savings were assessed for three scenarios: (1) addition of the moss layer, (2) addition of the bioreceptive concrete panel, and (3) the complete multilayered facade system including cork insulation and bioreceptive concrete.

1. **Moss layer**

$$\begin{aligned}\Delta U &= 1.1050 - 0.7874 = 0.318 \text{ W/m}^2\text{K} \\ Q_{\text{annual}} &= \Delta U \cdot A \cdot \text{HDD} \\ &= 0.318 \text{ W/m}^2\text{K} \cdot 1 \text{ m}^2 \cdot 4767 \text{ K·days/year} \\ &= 4.82 \cdot 10^7 \text{ J/year} = 22.9 \text{ kWh/year} \\ \text{CO}_2\text{\_saved} &= 4.56 \text{ kg } \text{CO}_2/\text{year} = 233.2 \text{ kg } \text{CO}_2/30 \text{ years} \\ \text{Shadow cost avoided} &= 0.90 \text{ €/year} = 27 \text{ €/30 years}\end{aligned}$$

2. **Bioreceptive concrete**

$$\begin{aligned}\Delta U &= 1.050 - 0.7042 = 0.401 \text{ W/m}^2\text{K} \\ Q_{\text{annual}} &= 1.04 \cdot 10^8 \text{ J/year} = 28.9 \text{ kWh/year} \\ \text{CO}_2\text{\_saved} &= 9.81 \text{ kg } \text{CO}_2/\text{year} = 294.3 \text{ kg } \text{CO}_2/30 \text{ years} \\ \text{Shadow cost avoided} &= 1.14 \text{ €/year} = 34.1 \text{ €/30 years}\end{aligned}$$

3. **Multilayered facade system**

$$\begin{aligned}
\Delta U &= 1.1050 - 0.1953 = 0.910 \text{ W/m}^2\text{K} \\
Q_{\text{annual}} &= 2.17 \cdot 10^7 \text{ J/year} = 60.3 \text{ kWh/year} \\
\text{CO}_2\text{_saved} &= 20.5 \text{ kg CO}_2\text{/year} = 616 \text{ kg CO}_2\text{/30 years} \\
\text{Shadow cost avoided} &= 2.58 \text{ €/year} = 77.5 \text{ €/30 years}
\end{aligned}$$

PM2.5 sequestration In addition to energy reduction, the facade system contributes to air quality improvement through PM2.5 sequestration. This was estimated based on deposition rates from the literature:

$$\begin{aligned}
\text{Total PM2.5 capture [g]} &= \text{Deposition rate} \cdot \text{Service life} \cdot \text{Functional unit} \\
&= 20 \text{ g/m}^2\text{/year} \cdot 30 \text{ years} \cdot 1 \text{ m}^2 \\
&= 600 \text{ g PM2.5/panel} \\
&= 0.6 \text{ kg PM2.5/panel}
\end{aligned}$$

This corresponds to a total of **2.8 €/year** or **82.9 €/30 years** in avoided shadow costs for particulate matter emissions.

Summary of the estimated additional environmental benefits of the multilayered facade system

Table 6.10 summarizes the estimated additional environmental contributions of the moss layer and the multilayered facade system over time. These include energy reductions for the three scenarios, carbon sequestration, and PM2.5 filtration.

Performance indicator	**Shadow cost (€/year)**	**Shadow cost (€/30 years)**
Carbon sequestration	0.035	1.218
Energy reduction (moss layer)	0.90	27.06
Energy reduction (bioreceptive concrete)	1.14	34.14
Energy reduction (multilayered facade system)	2.58	77.50
PM2.5 sequestration	2.80	82.9

Table 6.10: Estimated additional environmental benefits of moss and the multilayered facade system over time.

Figure 6.6 visualizes these benefits for easier comparison. The analysis shows that PM2.5 sequestration provides the largest additional environmental contribution, followed by energy savings from the moss layer and the bioreceptive concrete. Carbon sequestration contributes the least among the three assessed categories.

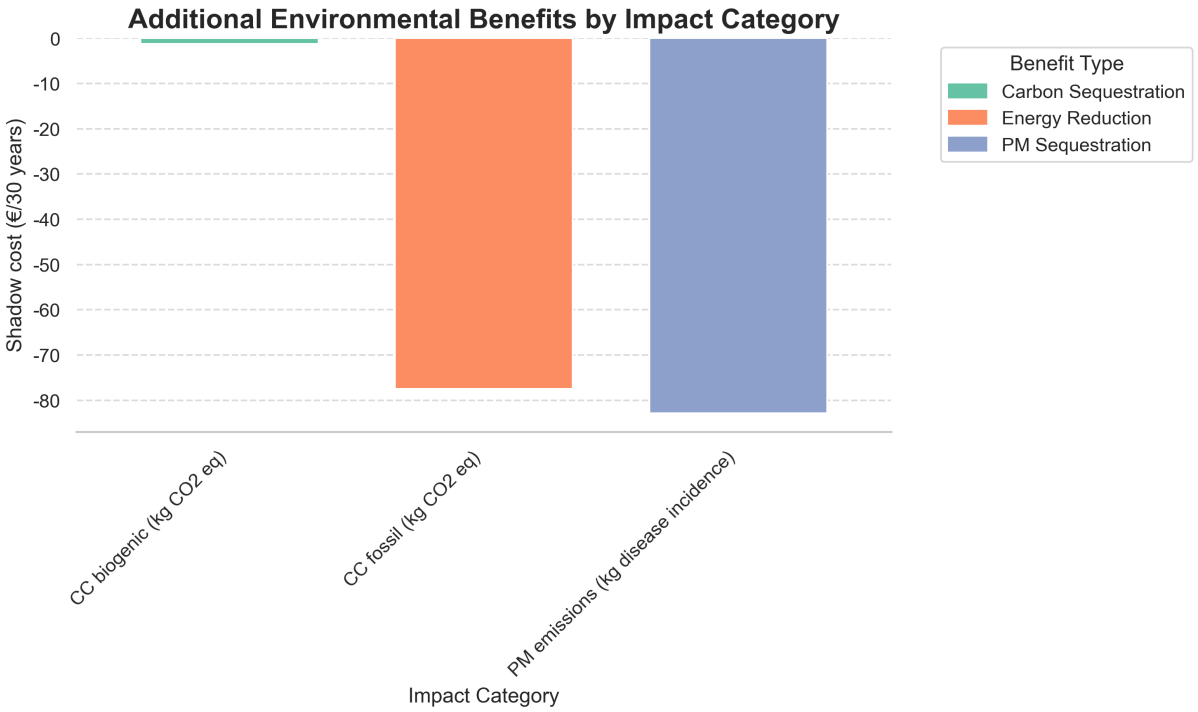

Figure 6.6: Additional environmental benefits of the facade system over a 30-year lifespan.

6.2.5 Total environmental impact of the facade system

Table 6.11 includes the results of the total environmental impact of the multilayered facade system. The layers included in the total environmental impact include concrete, and the chosen membrane and insulation material.

Impact Category	Concrete	Membrane	Insulation	TOTAL
CC total (kg CO2 eq)	170,4	0,6	-120,7	50,3
CC fossil (kg CO2 eq)	170,6	0,0	8,6	179,2
CC biogenic (kg CO2 eq)	-0,4	0,0	-129,9	-130,3
CC luluc (kg CO2 eq)	0,1	0,6	0,1	0,7
ODP (kg CFC 11 eq)	0,0	0,0	0,0	0,0
AP (mol H+ eq)	2,1	0,0	0,1	2,1
EP freshwater (kg P eq)	0,0	0,0	0,0	0,0
EP marine (kg N eq)	0,0	0,0	0,0	0,0
EP terrestrial (mol N eq)	1,8	0,0	0,1	1,8
POCP (kg NMVOC eq)	0,3	0,0	0,0	0,3
ADP Elements (kg Sb eq)	0,0	0,0	0,0	0,0
ADP fossil fuels (MJ)	1475,5	7,9	114,2	1597,7
WDP (m^3 water eq deprived)	16,5	0,1	18,6	35,2

Table 6.11: Total environmental impact per unit indicator of the multilayered facade system

Figure 6.7 shows the total shadow cost distributed over the LCA stage included within the scope of the LCA, see Table 6.12 for related data.

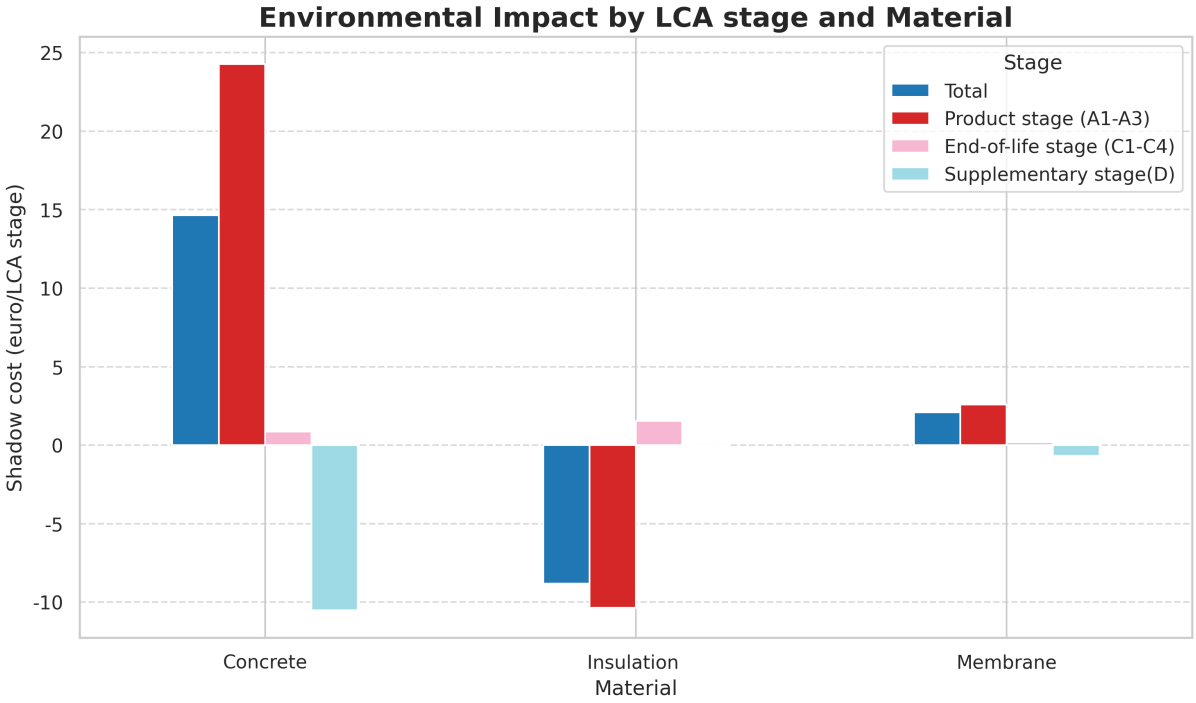

Figure 6.7: Environmental impact by LCA stage and material

The data shown in Table 6.11 is shown in Figure 6.8. The graph includes the environmental impact of each layer (concrete, membrane and insulation) for each of the 13 impact categories.

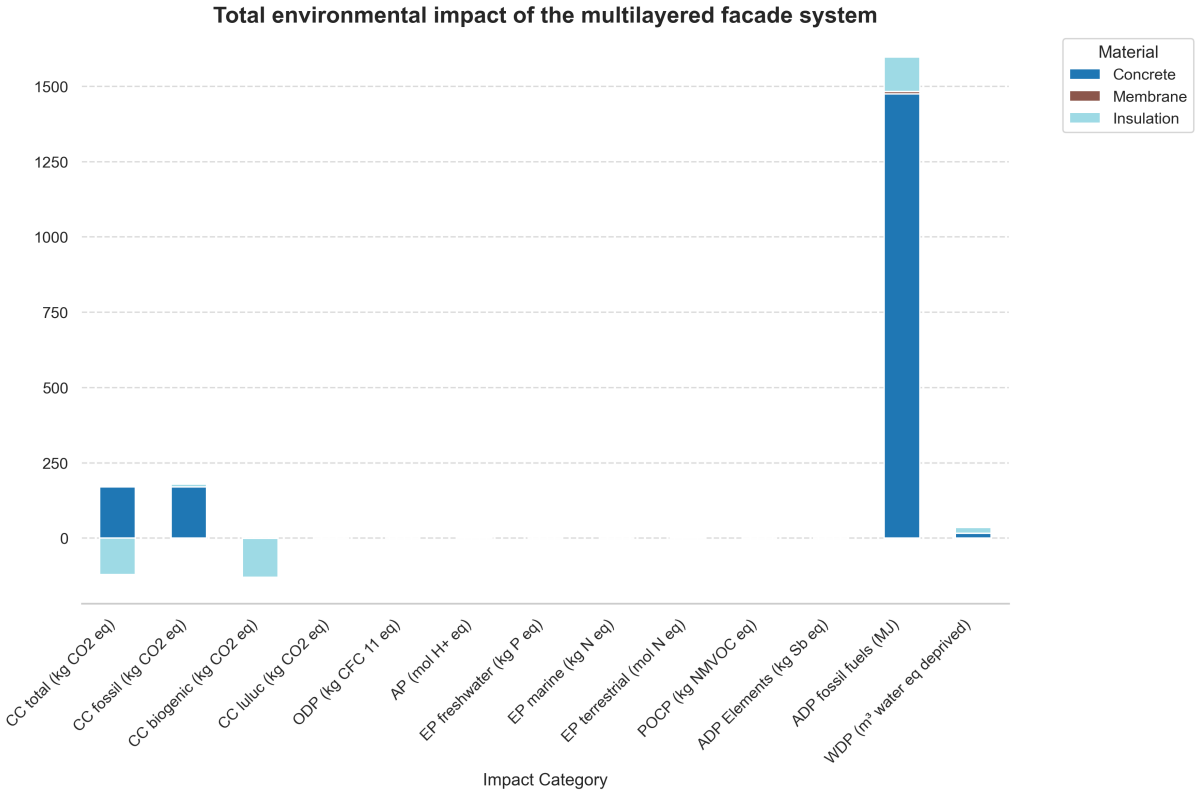

Figure 6.8: Total environmental impact of the multilayered facade system

The additional environmental benefits, presented in Chapter 6.2.4, aren't included in the total environmental impact of the facade system. The reasoning for this is that they represent an estimation of avoided impacts, not direct impacts from the materials themselves. Including them could skew the results, and unlike the other data, they are not based on comparable sources such as EPDs. Reporting them separately allows the LCA results to remain consistent and comparable across all materials.

The environmental impacts summarized in Table 6.11 and Figure 6.8 are expressed in monetary terms in Table 6.12. Detailed results for each material are provided in Appendix D.3. The specific results for cork, the waterproof membrane, and the concrete mixture are shown in Tables 6.7, 6.9, and 6.8, respectively.

Impact Category	**Concrete**	**Membrane**	**Insulation**	**Total**	**%**
CC total (kg CO2 eq)	12,8	0,1	-8,8	4,1	
CC fossil (kg CO2 eq)	12,8	0,0	0,5	13,3	171%
CC biogenic (kg CO2 eq)	0,0	0,0	-9,3	-9,4	-120%
CC luluc (kg CO2 eq)	0,0	0,1	0,0	0,1	2%
ODP (kg CFC 11 eq)	0,0	0,0	0,0	0,0	0%
AP (mol H+ eq)	0,2	0,0	0,0	0,2	3%
EP freshwater (kg P eq)	0,0	0,0	0,0	0,0	0%
EP marine (kg N eq)	0,4	0,0	0,0	0,3	4%
EP terrestrial (mol N eq)	0,5	0,0	0,0	0,4	5%
POCP (kg NMVOC eq)	0,4	0,0	0,0	0,4	5%
ADP Elements (kg Sb eq)	0,0	0,0	0,0	0,0	0%
ADP fossil fuels (MJ)	0,4	1,8	0,0	2,2	28%
WDP (m^3 water eq deprived)	0,1	0,0	0,1	0,1	2%
TOTAL	14,64	1,97	-8,82	7,79	100%
%	188%	25%	-113%	100%	

Table 6.12: Total shadow cost per unit indicator of the multilayered facade system

The total shadow cost of the multilayered facade system is €4.85. The largest contributors to this cost are two impact categories: CC fossil (kg CO_2 eq) and ADP fossil fuels (MJ). Among the layers, the concrete contributes the most, with a shadow cost of €14.33, followed by the waterproof membrane at €8.52. The inclusion of cork insulation reduces the total shadow cost by €11.76, due to its high positive effect on CC total (kg CO_2 eq).

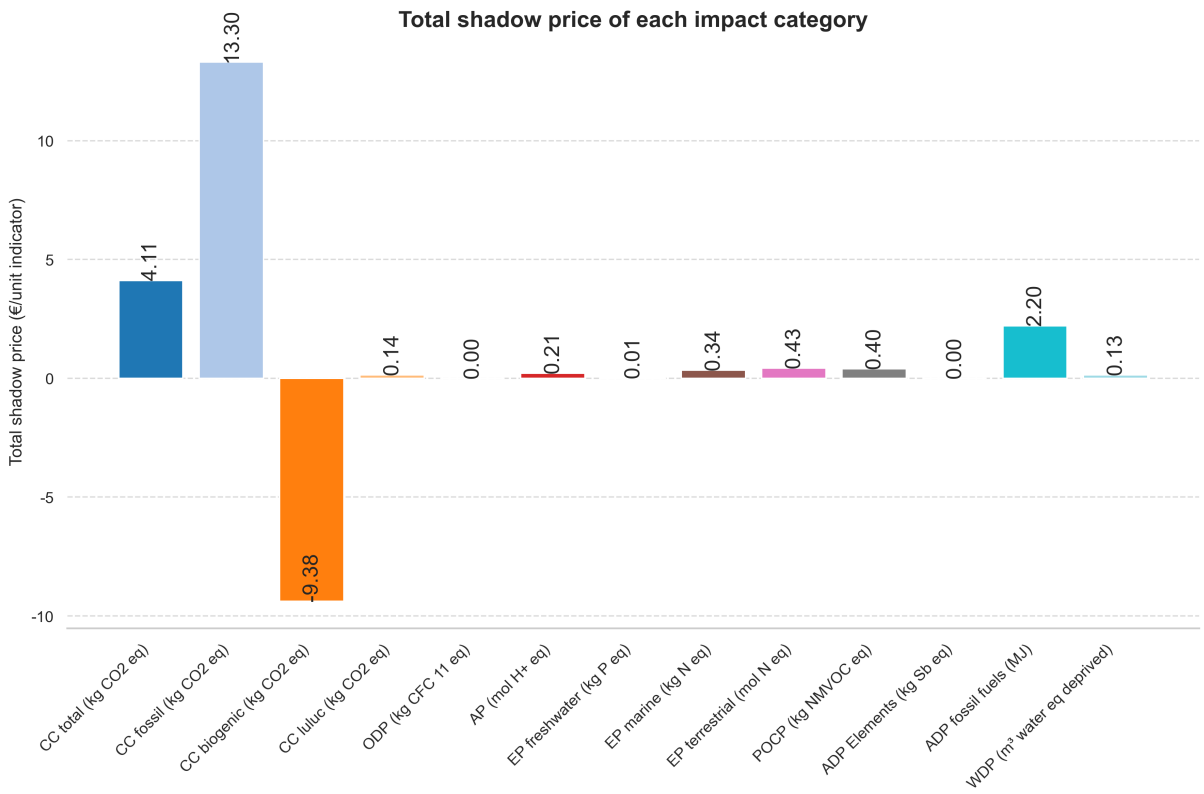

Figure 6.9: Total shadow cost of the multilayered facade system

6.3 Heat flux and thermal conductivity results

As described in Section 5.3, the heat flux of the panels was measured using a Hukseflux HFP01 sensor in combination with a temperature sensor. The following chapters present the heat flux and temperature results for the bare concrete panel as well as for the panels featuring the three moss species. Additionally, the R-value and thermal conductivity for each panel configuration, including the moss covered variants, has been calculated.,

6.3.1 Bare concrete

Table 6.13 presents the results of the heat flux measurements for the bare concrete panels. Three panels were tested to evaluate the thermal performance of the bare concrete panels.

Panel	**Average** $\boldsymbol{\Delta T}$ [°C]	**Average** HF [W/m^2]	**Average** R [m^{2}K/W]	$\boldsymbol{\lambda}$ [W/mK]
Bare concrete panel 1	6.02	33.16	0.18	0.27
Bare concrete panel 2	5.21	35.80	0.15	0.34
Bare concrete panel 3	6.09	37.71	0.16	0.31
Average	**5.77**	**35.56**	**0.16**	**0.31**

Table 6.13: Results of average temperature difference, average heat flux, average thermal resistance and thermal conductivity of the bare concrete panels

The measured temperature differences across the panel surfaces ranged from 5.21 °C to 6.09 °C, resulting in average heat flux values between 33.16 W/m^2 and 37.71 W/m^2. The corresponding R-values varied from 0.15 to 0.18 m^{2}K/W, resulting in an overall average R-value of 0.16 m^{2}K/W. The calculated thermal conductivity (λ) of the panels, using the panels thickness of 50mm, ranged from 0.27 to 0.34 W/mK, with an average of 0.31 W/mK. Figure 6.10 illustrates the calculated R-value for each bare concrete panel, along with the average R-value of the three panels tested.

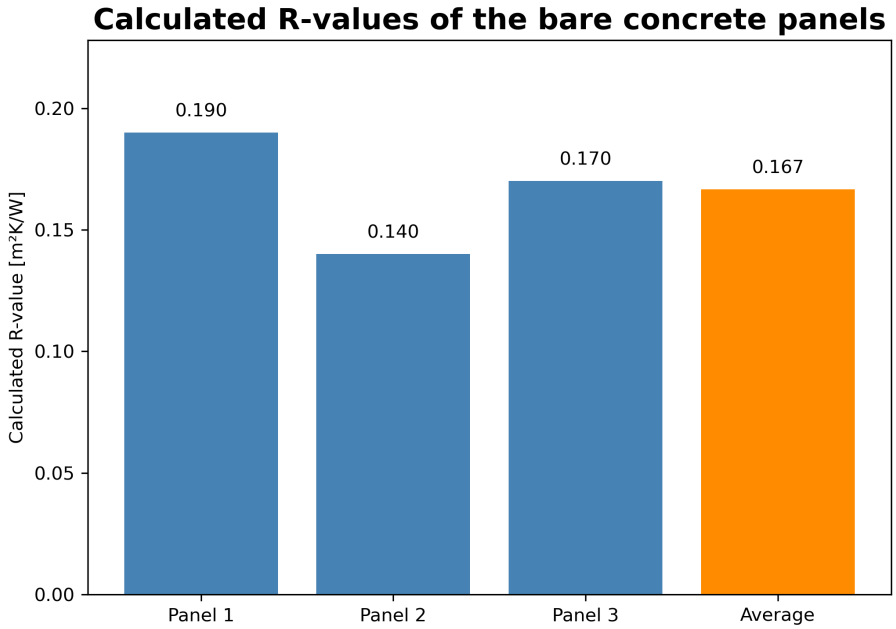

Figure 6.10: Calculated R-value of the bare concrete panels.

6.3.2 Bioreceptive concrete

Three variations of the bioreceptive concrete were tested with the hot-box. Each variation uses the same concrete substrate but differs in the moss species applied to the panel surface. The species tested were *Brachythecium rutabulum*, *Ptycstomum capillare*, and *Grimmia pulvinata*. The results for each variation are presented in the following subchapters.

It is important to highlight that the results presented in this chapter all include the concrete panel as well as the moss species, presenting the results for the bioreceptive concrete.

Moss species	**Saturation state**	**Average thickness** [cm]
Grimmia pulvinata	Dry	6.33
Grimmia pulvinata	Saturated	7.33
Brachythecium rutabulum	Dry	10
Brachythecium rutabulum	Saturated	12.66
Ptychostomum cappilare	Dry	9.33
Ptychostomum cappilare	Saturated	11.66

Table 6.14: Average moss layer thickness for different species and saturation states.

Brachythecium rutabulum

The following section presents the results of the hot-box experiments for panels covered with the moss species *Brachythecium rutabulum*. Three panels were tested, and for each panel, two saturation states were examined: fully dry and saturated. The results for each panel are summarized in Tables 6.15, 6.16, and 6.17.

Saturation state	**Average** $\boldsymbol{\Delta T}$ [°C]	**Average** HF [W/m^2]	**Average** R [m^{2}K/W]	$\boldsymbol{\lambda}$ [W/mK]
Fully dry	7.09	25.79	0.27	0.22
Saturated	6.67	24.91	0.27	0.23

Table 6.15: Measured heat flux and thermal properties of panel 1 covered with *Brachythecium rutabulum*

Saturation state	**Average** $\boldsymbol{\Delta T}$ [°C]	**Average** HF [W/m^2]	**Average** R [m^{2}K/W]	$\boldsymbol{\lambda}$ [W/mK]
Fully dry	7.94	22.24	0.36	0.17
Saturated	8.93	26.35	0.34	0.18

Table 6.16: Measured heat flux and thermal properties of panel 2 covered with *Brachythecium rutabulum*.

Saturation state	**Average** $\boldsymbol{\Delta T}$ [°C]	**Average** HF [W/m^2]	**Average** R [m^{2}K/W]	$\boldsymbol{\lambda}$ [W/mK]
Fully dry	6.96	27.37	0.25	0.24
Saturated	6.46	28.82	0.22	0.28

Table 6.17: Measured heat flux and thermal properties of panel 3 covered with *Brachythecium rutabulum*.

The measured temperature differences across the panel surfaces ranged from 6.46 °C to 8.93 °C, resulting in average heat flux values between 22.24 W/m^2 and 28.82 W/m^2. The corresponding R-values varied from 0.22 to 0.36 m^{2}K/W, yielding an overall average R-value of 0.28 m^{2}K/W. The calculated thermal conductivity (λ) ranged from 0.17 to 0.28 W/mK.

Figure 6.11 provides a visual summary of the calculated R-values for all three panels under both saturation states, including the average R-value across the panels.

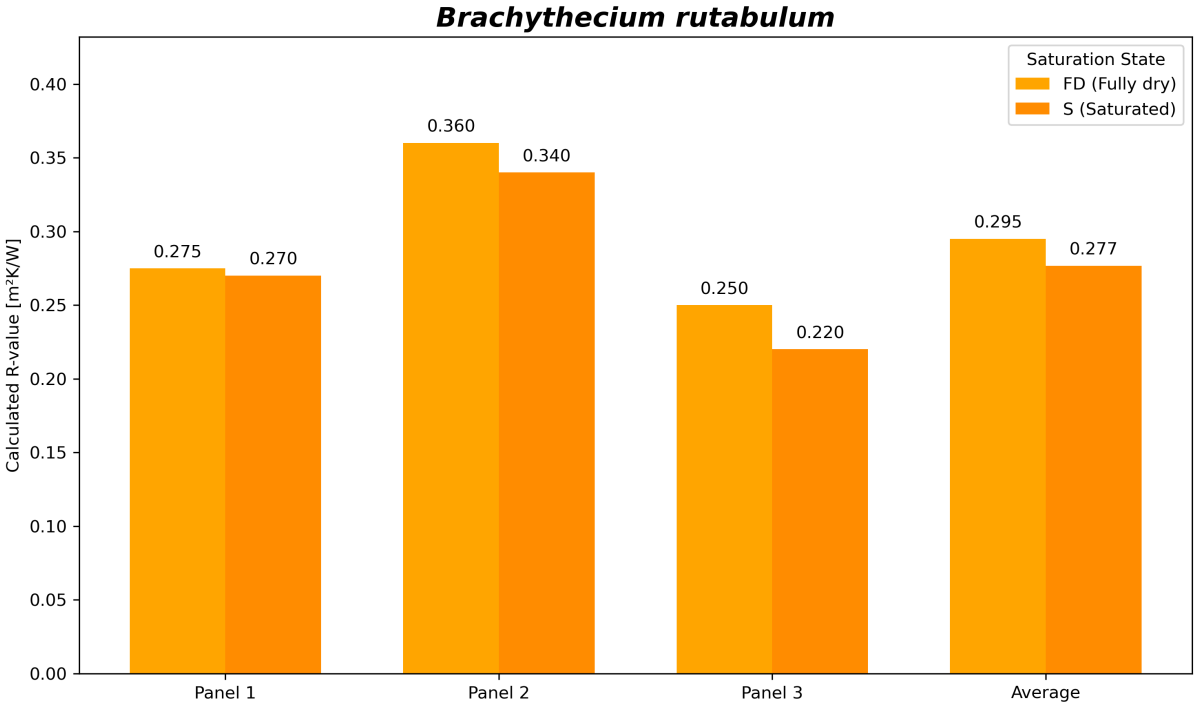

Figure 6.11: Calculated R-values for panels covered with *Brachythecium rutabulum*, showing both fully dry and saturated conditions.

Ptychostomum cappilare

The following section presents the results of the hot-box experiments for panels covered with the moss species *Ptychostomum cappilare*. The results for each panel are summarized in Tables 6.18, 6.19, and 6.20.

Saturation state	**Average ΔT** [°C]	**Average** HF [W/m^2]	**Average** R [m^{2}K/W]	**λ** [W/mK]
Fully dry	10.18	27.86	0.37	0.16
Saturated	9.16	27.09	0.34	0.18

Table 6.18: Measured heat flux and thermal properties of panel 1 covered with *Ptychostomum cappilare*.

Saturation state	**Average ΔT** [°C]	**Average** HF [W/m^2]	**Average** R [m^{2}K/W]	**λ** [W/mK]
Fully dry	7.88	26.2	0.3	0.2
Saturated	6.93	27.35	0.25	0.25

Table 6.19: Measured heat flux and thermal properties of panel 2 covered with *Ptychostomum cappilare*.

Saturation state	**Average ΔT** [°C]	**Average** HF [W/m^2]	**Average** R [m^{2}K/W]	**λ** [W/mK]
Fully dry	6.9	20.25	0.34	0.17
Saturated	9.64	24.82	0.39	0.16

Table 6.20: Measured heat flux and thermal properties of panel 3 covered with *Ptychostomum cappilare*.

The measured temperature differences across the panel surfaces ranged from 6.90 °C to 10.18 °C, resulting in average heat flux values between 20.25 W/m^2 and 27.86 W/m^2. The corresponding R-values varied from 0.25 to 0.39 m^{2}K/W, yielding an overall average R-value of 0.32 m^{2}K/W. The calculated thermal conductivity (λ) ranged from 0.16 to 0.25 W/mK.

Figure 6.12 provides a visual summary of the calculated R-values for all three panels under both saturation states, including the average R-value across the panels. The results indicate that saturation generally decreases the thermal resistance slightly, reflecting the influence of moisture on the insulating properties of the moss layer.

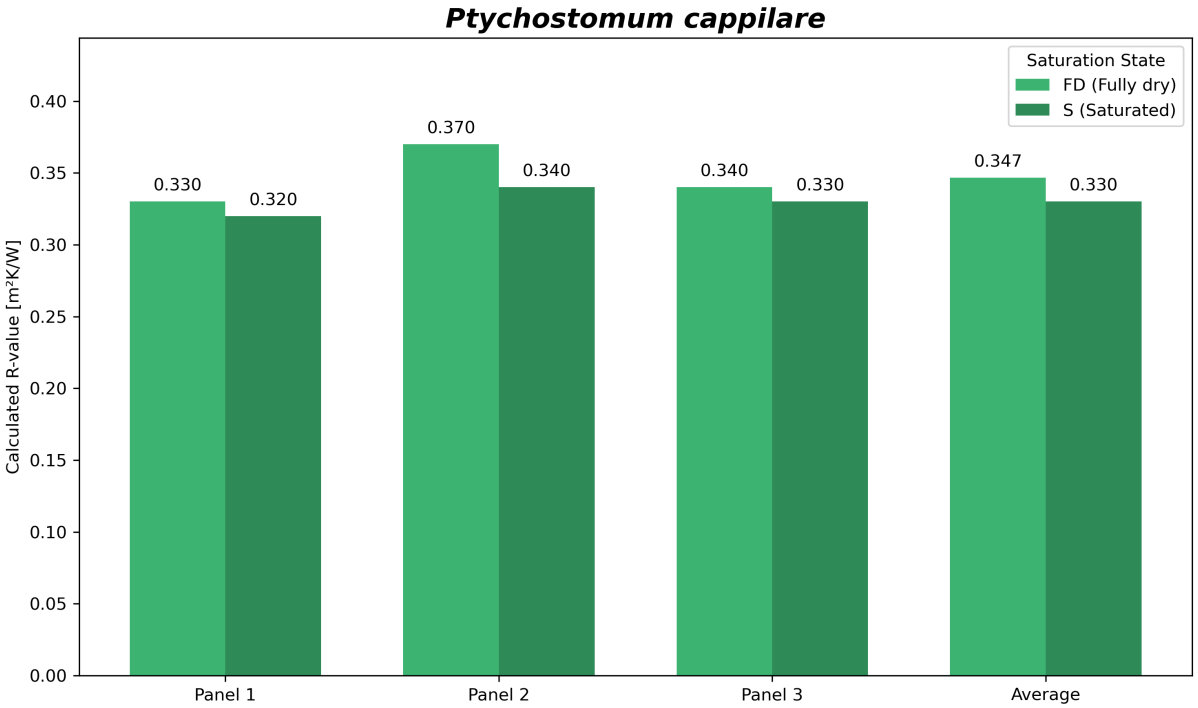

Figure 6.12: Calculated R-values of panels with *Ptychostomum cappilare*, showing fully dry and saturated conditions.

Grimmia pulvinata

The following section presents the results of the hot-box experiments for panels covered with the moss species *Grimmia pulvinata*. Three panels were tested, and for each panel, two saturation states were examined: fully dry and saturated. The results for each panel are summarized in Tables 6.21, 6.22, and 6.23.

Saturation state	**Average ΔT** [°C]	**Average** HF [W/m^2]	**Average** R [m^{2}K/W]	**λ** [W/mK]
Fully dry	8.34	29.76	0.28	0.20
Saturated	8.23	30.67	0.27	0.21

Table 6.21: Measured heat flux and thermal properties of panel 1 covered with *Grimmia Pulvinata*.

Saturation state	**Average ΔT** [°C]	**Average** HF [W/m^2]	**Average** R [m^{2}K/W]	**λ** [W/mK]
Fully dry	8.04	24.60	0.33	0.17
Saturated	7.69	23.87	0.32	0.18

Table 6.22: Measured heat flux and thermal properties of panel 2 covered with *Grimmia Pulvinata*

Saturation state	**Average ΔT** [°C]	**Average** HF [W/m^2]	**Average** R [m^{2}K/W]	**λ** [W/mK]
Fully dry	8.49	25.79	0.33	0.17
Saturated	7.02	20.58	0.34	0.17

Table 6.23: Measured heat flux and thermal properties of panel 3 covered with *Grimmia Pulvinata*

The measured temperature differences across the panel surfaces ranged from 7.02 °C to 8.49 °C, resulting in average heat flux values between 20.58 W/m^2 and 30.67 W/m^2. The corresponding R-values varied from 0.27 to 0.34 m^{2}K/W, yielding an overall average R-value of approximately 0.31 m^{2}K/W. The calculated thermal conductivity (λ) ranged from 0.27 to 0.34 W/mK.

Figure 6.13 provides a visual summary of the calculated R-values for all panels under both saturation states, including the average R-value across the panels.

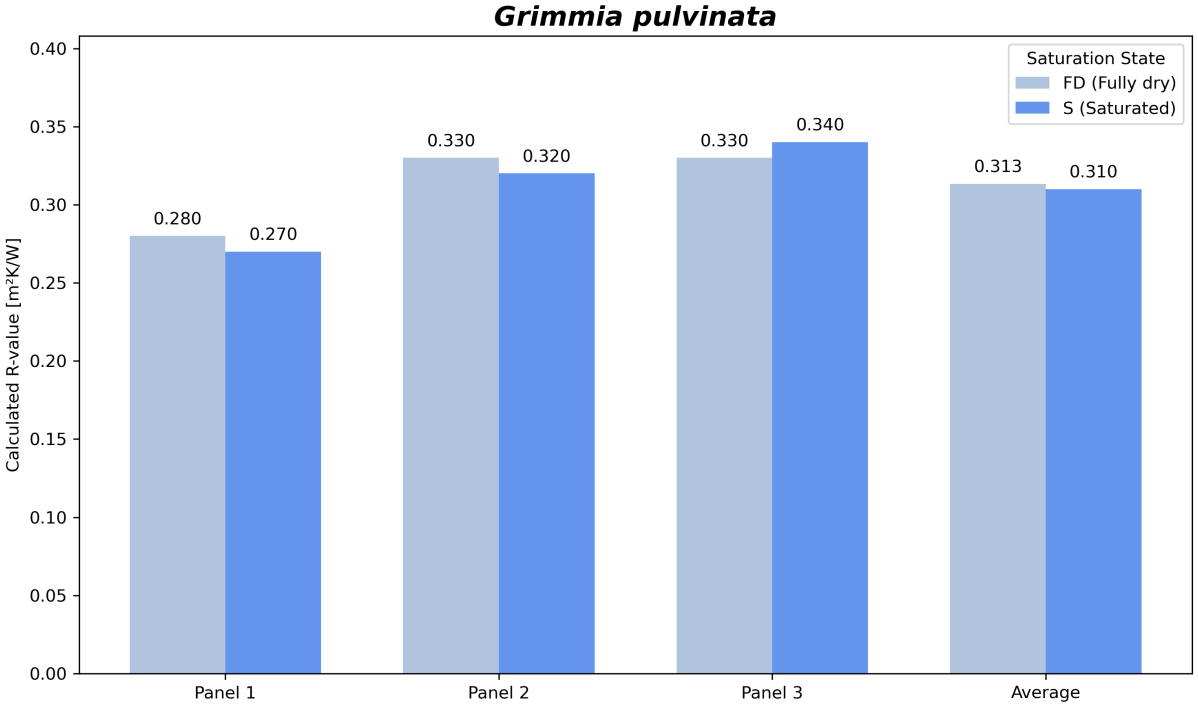

Figure 6.13: Calculated R-values of panels with *Grimmia pulvinata*, showing fully dry and saturated conditions

6.3.3 Thermal Performance of *Brachythecium rutabulum*, *Ptycstomum capillare*, and *Grimmia pulvinata*

By subtracting the average R-value of the bare concrete panel, presented in Chapter 6.3.1, with the average R-value of each moss species, the estimated R-value and thermal conductivity of each moss species can be estimated. The results are presented in Table 6.24, where the estimated R- and λ value is shown for both saturation states, fully dry and saturated.

Moss species	**Saturation state**	**Average** R [m^2K/W]	**λ** [W/mK]
Brachythecium rutabulum	Fully dry	0.132	0.453
Grimmia pulvinata	Fully dry	0.151	0.373
Ptychostomum cappilare	Fully dry	0.174	0.341
Brachythecium rutabulum	Saturated	0.114	0.549
Grimmia pulvinata	Saturated	0.148	0.389
Ptychostomum cappilare	Saturated	0.164	0.376

Table 6.24: Average R-value and thermal conductivity of *Brachythecium rutabulum*, *Grimmia pulvinata* and *Ptychostomum cappilare*

The Table shows that the the Average thermal conductivity value for a saturated state is between 0.376 to 0.549 W/mK, while for a fully dry state it is between 0.341 and 0.453 W/mK.

6.3.4 Thermal performance of moss covered panels under dry and saturated conditions

The impact of moisture on the thermal performance of panels covered with different moss species can be clearly seen in Table 6.25. The table presents average temperature differences (ΔT), heat flux (HF), calculated thermal resistance (R-value), and thermal conductivity (λ) for each moss species under both fully dry and saturated conditions.

Moss species	**Saturation state**	**Average** ΔT [°C]	**Average** HF [W/m^2]	**Average** R [m^2K/W]	**λ [W/mK]**
Brachythecium rutabulum	Fully dry	7.52	24.02	0.29	0.203
Grimmia pulvinata	Fully dry	8.19	27.18	0.31	0.179
Ptychostomum cappilare	Fully dry	6.02	18.02	0.34	0.176
Brachythecium rutabulum	Saturated	7.80	25.63	0.28	0.226
Grimmia pulvinata	Saturated	7.96	27.27	0.31	0.185
Ptychostomum cappilare	Saturated	5.36	18.15	0.33	0.188

Table 6.25: Average temperature difference, heat flux, R-value, and thermal conductivity for panels covered with various moss species under two saturation states

Figure 6.14 visualizes the average thermal conductivity (λ) of the bioreceptive panels for each moss species and saturation state, providing a clear comparison of the insulating effect of different moss covers.

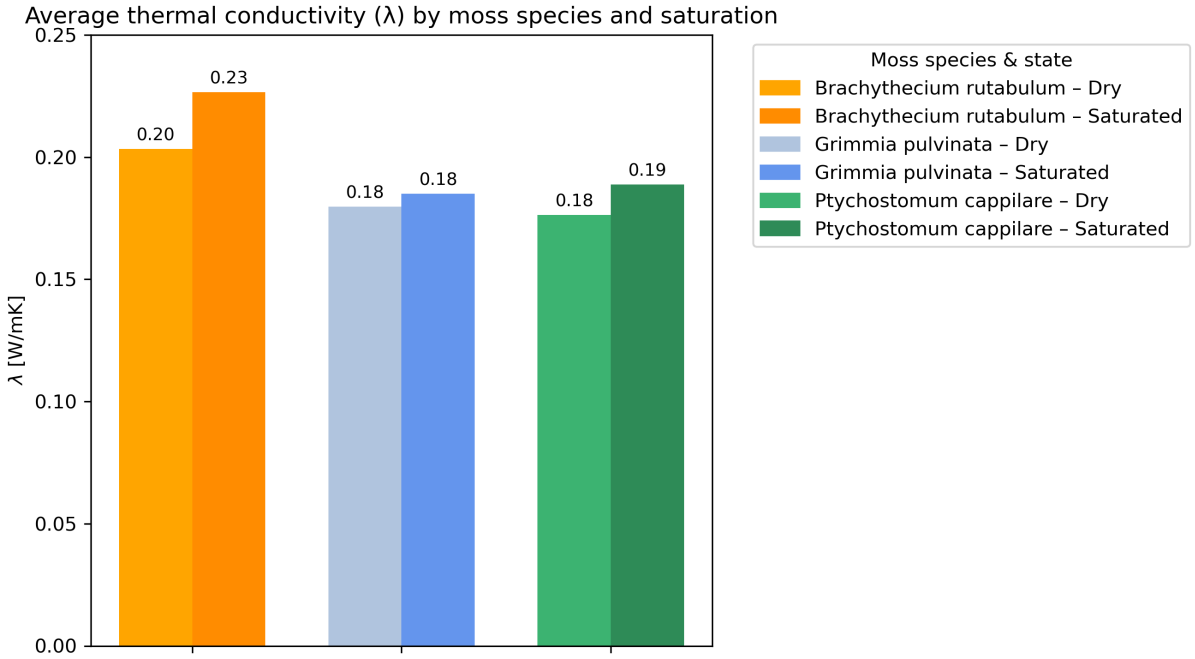

Figure 6.14: Average thermal conductivity (λ) of the bioreceptive panels, grouped by moss species and saturation state

To further assess the impact of moisture content on thermal performance, the difference in R-value between the dry and saturated states was calculated for each moss species. Table 6.26 summarizes the estimated reduction in R-value due to saturation.

Moss species	**Estimated impact of saturation on R-value**
Brachythecium rutabulum	6%
Grimmia pulvinata	1%
Ptychostomum cappilare	3%

Table 6.26: Estimated reduction in R-value due to saturation for different moss species

These results indicate that the saturation state has a minor effect on the thermal performance of the panels, with *Brachythecium rutabulum* showing the highest reduction in R-value (6%) and *Grimmia pulvinata* the lowest (1%).

Chapter 7

Discussion

7.1 Material selection

Selecting materials for the facade system requires balancing technical performance, environmental sustainability, and circularity. The multi-criteria analysis (MCA) highlights the trade-offs inherent in **insulation selection**. Rock wool scored highest overall due to excellent thermal conductivity, fire resistance, and water vapor diffusion performance, which are critical for exterior facades. However, when circularity, material composition, and environmental impact are prioritized, cork becomes more favorable despite a lower MCA score, illustrating the tension between conventional performance metrics and sustainability goals.

Cork excels in circularity, environmental impact, material composition, and carbon sequestration. Its slightly lower thermal performance and Euroclass E fire rating are trade-offs for substantial ecological benefits, making it a strong candidate for sustainable facade systems. This aligns with the thesis goal of integrating technical requirements with environmental objectives. Representative products, *Pro Suber cork boards* and *Rockwool stone wool*, reflect these trends, where rock wool offers better thermal and fire performance, while cork provides longer service life, lower embodied carbon, and circularity advantages.

While cork is naturally water resistant, a **waterproof membrane** was added to compensate for the absence of an air gap between the concrete and insulation layers. This decision minimized the overall thickness of the system while maintaining long-term durability. Although the membrane introduces additional considerations such as replacement after 30 years and implications for assembly, it was deemed essential. The SFH membrane was selected for its technical suitability, alignment with circularity criteria, and compatibility with cork.

For the **concrete panels**, a previously developed bioreceptive concrete mixture was used instead of creating a new mix optimized for thermal performance. While enhancing thermal behavior could have improved overall thermal performance of the system, it risked compromising bioreceptivity, which is a central goal of the facade. Using an established mix therefore prioritizes ecological functions while providing a reliable baseline for evaluating thermal performance in future experiments of the developed mixture. Adjustments to aggregates or binder ratios could later be explored to enhance thermal properties without comprimising bioreceptivity.

The decision to test three **moss species,** *Grimmia pulvinata*, *Ptychostomum capillare*, and *Brachythecium*

rutabulum, was made with practical feasibility in mind, as these species are most likely to establish and survive outdoors on the panels. Comparing them also enables the assessment of their thermal properties, with R-value measurements indicating which species contributes most to the overall thermal performance of the system. This selection should demonstrate how biological selection directly influences multifunctional facade performance.

Finally, the proposed **assembly methods** for the three layers remain preliminary but emphasize disassembly and circularity. Cap nails and Fischer 6H NT screw washers were identified as promising solutions, consistent with manufacturer recommendations for both cork boards and the waterproof membrane. Further research, including long-term mechanical and durability testing, is needed to confirm their suitability. Nonetheless, these methods provide a practical foundation for integrating circularity, thermal performance, and experimental feasibility into the facade system.

The proposed clip-and-rail **installation method** once again supports the broader circularity goals of the facade system. By allowing individual panels and layers to be removed, repaired, or replaced without damaging surrounding materials, the system reduces waste and extends the service life of components. Mechanical fasteners maintain structural stability, weatherproofing, and thermal performance while avoiding irreversible bonding methods. Although initial installation may require greater precision and attention to thermal bridging at attachment points, the approach offers flexibility for future maintenance, upgrades, or material recovery, reinforcing the system's experimental yet sustainable design ethos.

7.2 Facade design

Balancing multiple layers with distinct functional requirements presents a significant challenge in the design of the proposed facade system. The inclusion of functionally diverse layers raises questions regarding their compatibility. For example, direct contact between cork insulation and bioreceptive concrete can enhance compactness and overall thermal performance, but it restricts vapor diffusion and complicates moisture management. To mitigate this, a waterproof membrane was introduced to protect the cork from moisture damage. However, membrane failure could compromise the long-term performance and durability of the system due to cork's sensitivity to water. Consequently, successful integration of both bioreceptive and thermal functions relies on waterproofing solutions that are both effective and reversible.

The decision to prioritize mechanical fastenings over adhesives reflects the project's commitment to circularity, enabling clean disassembly and reuse. This approach, however, introduces new challenges:

- **Aesthetic trade-offs:** Mechanical fasteners may be visible on the building exterior, potentially affecting moss colonization and the visual appearance of the facade.
- **Installation complexity:** Reversible fixings require high installation precision, increasing on-site assembly time compared to adhesive systems. Maintaining continuity of the waterproof membrane and insulation across pre-assembled panels further complicates installation, as gaps or misalignments could reduce thermal performance and compromise moisture protection.
- **Layer continuity:** Achieving uninterrupted insulation and membrane coverage across pre-assembled panels necessitates careful coordination with mechanical fixings, as any discontinuity could undermine both moisture protection and thermal performance.

These trade-offs highlight that circular assembly methods cannot simply replicate conventional construction practices. Workflows must be adapted to balance disassembly potential with practical performance. It is also important to note that only a limited set of assembly options were analyzed, based on design-stage assumptions rather than long-term field data. In practice, durability, maintenance requirements, and workmanship quality may significantly affect the performance of these circular methods.

The service life of each layer also varies considerably, ranging from approximately 30 years for the membrane to 75 years for cork insulation. This variation necessitates a maintenance strategy that allows selective replacement without compromising system integrity. While the modular design facilitates such an approach, practical considerations remain: responsibility for component replacement and ensuring selective disassembly and recycling must be clearly defined. Without supportive policies, even carefully designed circular systems risk being treated as conventional waste at the end of their service life.

For full-scale implementation, several risks must be evaluated. Moisture ingress remains critical, even with the waterproof membrane, and fire safety considerations are heightened for larger projects. Euroclass E insulation, such as the cork chosen, may not meet regulatory requirements in high-rise or dense urban contexts without additional fire-resistant requirements. Supply chain and cost considerations could also affect scalability, as cork is primarily produced in Southern Europe, potentially increasing embodied transport impacts. Alternative design scenarios could mitigate some of these risks. For instance, combining a thin outer layer of rock wool with cork could balance fire safety, thermal performance, and environmental benefits while reducing overall thickness. A drained and ventilated cavity could replace the membrane in this scenario, improving moisture management and reducing replacement needs.

The proposed design demonstrates the potential for integrating bioreceptivity with circular insulation strategies. However, further work is needed, particularly in:

- Testing the long-term durability of multilayer facade systems under different climatic conditions.
- Developing standardized reversible fastening systems tailored for bioreceptive panel and multilayered facade systems
- Assessing at full scale the possible risks caused by the implementation of the facade system.

Addressing these challenges will bring multifunctional facades closer to practical implementation, bridging the gap between environmental ambition and technical feasibility.

7.3 Life-cycle analysis

The total shadow cost of the multilayered facade system is €4.85 per m^2 over a 30-year lifespan. Concrete contributes the largest share of environmental impacts, with a shadow cost of €14.64, primarily due to fossil-based CO_2 emissions and fossil fuel consumption during production. In contrast, cork insulation demonstrates a net negative shadow cost of –€8.82, largely due to its biogenic carbon uptake during production offsets a substantial portion of other emissions. The waterproof membrane contributes €1.97, representing a relatively minor impact compared to the concrete layer.

Although not directly included in the LCA result, it is estimated that the moss layer provides additional environmental benefits through PM2.5 filtration, energy reduction, and carbon sequestration. These

estimated benefits suggest that including such contributions in future LCAs could further improve the environmental performance of facade systems that do incorporate a green layer.

Stage-specific analysis shows that most environmental impacts occur during the product stage (A1–A3), with the concrete layer contributing the most, consistent with literature that identifies cement production as a major source of CO_2 emissions in construction (Hanifa et al., 2023). The supplementary stage (D) partially offsets the product stage impacts, reducing the total shadow cost of concrete by approximately 35% due to the potential for recycling and material recovery.

The LCA results support several design recommendations for multifunctional, bioreceptive facade systems:

- **Material selection:** Prioritize renewable, biogenic, or recycled materials. The positive impact of cork insulation and recycled aggregates shows that these measures can significantly reduce overall environmental impact.
- **Concrete mixture design:** Reducing cement content through supplementary cementitious materials or increasing recycled content can further lower fossil-based CO_2 emissions and fossil fuel consumption.
- **End-of-life scenarios:** Designing for disassembly and circularity of each facade layer ensures that potential environmental benefits are realized in real-life scenarios
- **Green layer:** Including moss or other bioreceptive materials adds environmental services such as PM2.5 filtration, enhanced thermal performance, and carbon sequestration. Quantitative studies are desperately needed to incorporate these benefits accurately into LCA models.

Several limitations of the study should be noted. These include data gaps, assumptions in scaling, estimated environmental impact of the moss layer, and reliance on generic EPD data:

- **Data gaps:** Data for the fastening system and bone ash in the concrete were unavailable. Their overall impact is assumed to be minor but may affect detailed results.
- **Assumptions in scaling:** The cork insulation EPD was scaled from 140 mm to 150 mm thickness, assuming linear proportionality in environmental impact. Actual production processes may yield different results.
- **Moss impact estimation:** Environmental benefits of moss are based on literature values and may not fully represent the species selected for this project. Benefits may vary depending on climate, exposure, and maintenance.
- **Use of EPDs:** Material data were derived from Environmental Product Declarations, which may not reflect site-specific or project-specific conditions, potentially creating differences between modeled and actual impacts.

Other types of green wall systems often have higher embodied impacts due to irrigation, steel supports, and maintenance (Ottele et al., 2011). By comparison, the cork–moss panel studied here offers low or negative shadow cost due to biogenic carbon uptake of the insulation material, alongside ecological benefits, without the need for resource intensive irrigation measures. This positions the designed system

as a promising solution compared to conventional insulation and other green wall typologies, although technical trade-offs remain.

Future LCAs should focus on refining moss-related data, including growth patterns, carbon sequestration potential, and PM2.5 filtration. Incorporating field measurements will improve accuracy and reduce uncertainty. Sensitivity analyses on variables such as concrete mix design, insulation thickness, and membrane lifespans would further strengthen LCA robustness. Integrating operational phases and long-term maintenance into future studies would provide a more holistic assessment.

Overall, these results highlight that combining cork insulation with moss-covered concrete panels can reduce lifecycle impacts, support circular design, and add ecological value, making such hybrid systems a promising strategy for sustainable building envelopes.

7.4 Heat flux and thermal conductivity results

The heat flux measurements and calculated thermal performance indicate that adding moss layers to concrete panels moderately enhances their thermal resistance. The bare concrete panels exhibited an average R-value of 0.16 m^2K/W and a thermal conductivity of 0.31 W/mK, consistent with values reported by Duran-Herrera et al. (2016) for concrete comprising portland cement-fly ash mortar with lightweight aggregates.

Applying moss layers increased the overall thermal resistance, with estimated R-values for the moss ranging from 0.132 to 0.174 m^2K/W, depending on species and saturation state.

- ***Ptychostomum cappilare*** achieved the lowest λ value (0.341 and showed moderate sensitivity to saturation.
- ***Grimmia pulvinata*** resulted in a slightly higher λ value (0.373 W/mK) and displayed minor sensitivity to moisture.
- ***Brachythecium rutabulum*** had the highest λ value (0.454 W/mK) and the greatest increase when saturated

These differences are likely due to structural traits, where both *Ptychostomum cappilare* and *Grimmia pulvinata* form a more dense cushion-like structure that reduces heat transfer more effectively than the looser structure *Brachythecium rutabulum*. Moisture content had a minor but noticeable effect on thermal performance. Saturation reduced the R-value of the moss layers by 1–6%, with *Brachythecium rutabulum* being the most affected and *Grimmia pulvinata* the least. This indicates that while water retention slightly decreases insulating efficiency, moss-covered panels retain most of their thermal benefit even when saturated. Thermal conductivity trends reflect this behavior, showing modest increases under saturated conditions.

Several limitations affect these thermal performance results presented in the report, they include the following:

- **Laboratory conditions:** Hot-box experiments cannot fully replicate outdoor conditions such as wind, solar radiation, precipitation, and seasonal temperature fluctuations. These factors can

substantially influence the heat transfer, moisture content, and overall thermal performance of moss layers in real-world applications.

- **Moss application method:** In this study, moss was manually collected and glued to panels. Naturally colonized moss may differ in density, growth pattern, adhesion, moisture retention, and microstructure, which will likely alter the thermal behavior.
- **Moisture dynamics:** Moisture content was controlled under laboratory conditions, but in situ moss experiences wetting and drying cycles, evapotranspiration, and water absorption from rain or dew, which may change insulation properties of the moss species
- **Panel variability:** Variations in concrete casting, surface roughness, and moss coverage introduce variations in heat flux measurements, contributing to uncertainty in R-values and thermal conductivity values.
- **Measurement limitations:** Hot-box equipment, including sensor placement on uneven moss and panel surfaces, may cause minor measurement errors. Heat leakage around panel edges or imperfect insulation in the test setup could slightly overestimate or underestimate thermal resistance.
- **Scale effects:** Small-scale panels may behave differently than full-scale facade panels due to edge effects, thermal bridging, and differences in heat flow paths. Scaling up the results may require correction factors or further validation.
- **Temporal changes:** Moss thermal properties may change as the moss mat matures, dries, or experiences seasonal variations, which were not captured in the short-term laboratory tests.
- **Species selection and diversity:** Only three moss species were tested. Other species or mixed-species mats may exhibit different thermal characteristics, potentially affecting the generalizability of results.

In summary, moss layers enhance the thermal performance of concrete panels, with effectiveness influenced by species and moisture content. *Ptychostomum cappilare* provides the highest insulation in dry conditions, while *Grimmia pulvinata* remains the mot stable when wet. Results indicate potential performance of the selected moss species, though naturally colonized moss may behave differently. The results further validate that moss serves as a multifunctional addition to the built environment, with modestly increasing thermal resistance while improving ecological quality and bioreceptivity.

Chapter 8

Conclusions

This thesis explored the design and performance of a multifunctional bioreceptive facade panel that combines recycled concrete, cork insulation, and three different moss species. The aim was to evaluate the thermal performance, environmental impact, and bioreceptive potential of such a system, while addressing the main research question: How can a concrete facade panel be optimized for **bioreceptivity** and **thermal insulation** by selecting the best-performing moss species and suitable insulation material?

The results demonstrate that integrating biobased insulation with bioreceptive surfaces is a promising approach for exterior facades and can meet Dutch thermal performance standards. The addition of the cork-baed insulation was essential to achieve the required R-value of 4.7 $(m^2 \cdot K)/W)$, while also partially offsetting the concrete related emissions. The three moss species contributed to additional insulation and ecological benefits, although their thermal influence was moderate. However, the design is subject to several limitations, including moisture sensitivity of certain moss species, the embodied impact of concrete, and questions of long-term durability and lare-scale project scalability.

The proposed prototype highlights several design lessons and trade-offs that are important for future facade systems and their design.Moss species selection is quite crucial, where findings suggest that *Ptychostomum capillare* provides the highest insulation under dry conditions, whereas *Grimmia pulvinata* appears to be more resilient under moisture conditions. This indicates that species choice should be climate specific, and a combination of species may be used to balance insulation and ecological resilience. Similarly, cork insulation aligns with circularity and goals of low environmental impact. But this comes at a cost of a slightly lower thermal resistance than some synthetic alternatives. Concrete is a suitable substrate for moss but has high embodied emissions. The ecological benefits of moss layers, including carbon sequestration and biodiversity support, partially offset these impacts, highlighting the need to carefully balance technical, ecological, and sustainability objectives in the design.

This project was limited by laboratory scale testing and a short timeframe. Moss layers were glued onto concrete panels rather than grown naturally, introducing uncertainty regarding establishment, growth, and long-term resilience. Heat flux measurements were performed in a styrofoam hot box under unstable conditions, which may have affected the accuracy and reproducibility of thermal performance results. Future research should focus on real world testing of moss covered panels, improved experimental setups for thermal measurements, and quantification of additional ecosystem services such as carbon sequestration and air pollution mitigation.

In conclusion, this research demonstrates that multifunctional bioreceptive facade panels offer a promis-

ing route toward more sustainable and circular building envelopes. The combination of cork insulation and moss covered recycled concrete can reduce life-cycle impacts while delivering ecological benefits. By explicitly considering trade-offs between bioreceptivity, thermal insulation, and material sustainability, designers can create facade systems that achieve multiple objectives simultaneously. With further refinement and validation in real-world scenarios, bioreceptive facades have the potential to become an important component of future urban building design.

Bibliography

AFT Fasteners. (2025). Cap nails - plastic & metal cap nails [Accessed: 2025-08-19]. https://www.aftfasteners.com/round-cap-nails/

Aguayo, M., Das, S., Castro, C., Kabay, N., Sant, G., & Neithalath, N. (2017). Porous inclusions as hosts for phase change materials in cementitious composites: Characterization, thermal performance, and analytical models. *Construction and Building Materials*, *134*, 574–584.

Ahmed, A., & Kamau, J. (2017). Properties of different mortars and their effect on the flexural strength of low density block walls. *European Journal of Engineering and Technology Research*, *2*(5), 31–35.

Ali, A., Issa, A., & Elshaer, A. (2024). A comprehensive review and recent trends in thermal insulation materials for energy conservation in buildings. *Sustainability*, *16*, 8782.

Anderson, B., & Kosmina, L. (2019). *Conventions for u-value calculations* (tech. rep.) (Accessed: 2025-09-05). CIBSE. https://www.cibse.org/media/wzrjrf3l/conventions-for-u-value-calculations.pdf

Asadi, I., Shafigh, P., Hassan, Z. F. B. A., & Mahyuddin, N. B. (2018). Thermal conductivity of concrete: A review. *Journal of Building Engineering*, *20*, 81–93.

Asdrubali, F., D'Alessandro, F., & Schiavoni, S. (2015). A review of unconventional sustainable building insulation materials. *Sustainable Materials and Technologies*, *4*, 1–17. https://doi.org/10.1016/j.susmat.2015.05.002

Azariy, L., Fakhratov, M., Sinenko, S., et al. (2023). Organizational and design requirements for facade systems works in structures and buildings. *E3S Web of Conferences*, *431*, 06037. https://doi.org/10.1051/e3sconf/202343106037

Bessenouci, M., Bibi-Triki, N., Bendimerad, S., Nakoul, Z., Khelladi, S., & Hakem, A. (2014). Influence of humidity on the apparent thermal conductivity of concrete pozzolan. *Phys. Procedia*, *55*, 150–156.

Bianchi, S., Andriotis, C., Klein, T., & Overend, M. (2024). Multi-criteria design methods in façade engineering: State-of-the-art and future trends. *Building and Environment*, *250*, 111184.

Bienert, S. (2023). Embodied carbon of retrofits [Accessed: 2025-09-06]. https://www.crrem.eu/wp-content/uploads/2023/09/Report-Embodied-carbon-vs-operational-savings_Sep23.pdf

Bossche, N. V. D., Staljanssens, J., Mangé, S., & Moens, J. (2015). Façade retrofit strategies: Case study of the building complex k12 of the university hospital ghent. *Energy Procedia*, *78*, 961–966. https://doi.org/10.1016/j.egypro.2015.11.032

Boswell, K. (2013). *Exterior building enclosures: Design process and composition for innovative facades*. John Wiley & Sons.

Bouw, M. (2025a). Polytex® fassade eco [Accessed: 2025-08-19]. https://www.mg-bouw.com/en/polytex-fassade-eco

Bouw, M. (2025b). Polytex® fassade fr [Accessed: 2025-08-19]. https://www.mg-bouw.com/en/polytex-fassade-fr

Bouw, M. (2025c). Taftex® ex 150 [Accessed: 2025-08-19]. https://www.mg-bouw.com/en/taftex-ex-150

British Bryological Society. (2025). Common mosses on walls [Accessed 22 May 2025].

British Standards Institution. (2019). Bs en 13501-1:2018: Fire classification of construction products and building elements – classification using data from reaction to fire tests [Standard No. BS EN 13501-1:2018]. https://doi.org/10.3403/30348263

CEIC Data (World Bank WDI). (2020). Netherlands heating degree days, 1970–2020 [Accessed 2025-08-19].

de Vries, J., de Bruyn, S., Boerdijk, S., Juijn, D., Bijleveld, M., van der Giesen, C., Korteland, M., Odenhoven, N., van Santen, W., & Pápai, S. (2024, November). *Environmental prices handbook 2024: Eu27 version – methodical justification of key indicators used for the valuation of emissions and the environmental impact* (Technical Report No. 24.230107.151). CE Delft. Delft, Netherlands. https://cedelft.eu/wp-content/uploads/sites/2/2024/12/CE_Delft_230107_Environmental-Prices-Handbook-2024-EU-version_def_V1.1.pdf Commissioned by the Ministry of Infrastructure and Water Management.

De Isolatieshop. (2025). Miofol 125 g damp-open folie 1.5x50m1 (=75 m^2) [Geraadpleegd op 19 augustus 2025]. https://www.isolatiemateriaal.nl/folie/damp-open-folie/miofol-125-g-damp-open-folie-15x50m1-75-m2

Dickson, T., & Pavía, S. (2021). Energy performance, environmental impact and cost of a range of insulation materials. *Renewable and Sustainable Energy Reviews*, *140*, 110752.

Duran-Herrera, A., Campos-Dimas, J. K., Valdez-Tamez, P., & Bentz, D. P. (2016). Effect of a micro-copolymer addition on the thermal conductivity of fly ash mortars. *Journal of building physics*, *40*(1), 3–16.

Eltek Ltd. (2025). Genii srv250 receiver logger [Accessed 27 June 2025]. https://eltekdataloggers.co.uk/gen2_srv250.php

Erzen, B., Karataş, M., Orhan, R., & Aydoğmuş, E. (2025). Innovative insulation materials: A comprehensive review of current trends, challenges, and future directions in sustainable building technologies. *Polymer-Plastics Technology and Materials*, 1–24.

Feng, L., Zhang, Y., Xi, J., Zhu, Y., Wang, N., Xia, F., & Jiang, L. (2008). Petal effect: A superhydrophobic state with high adhesive force. *Langmuir*, *24*(8), 4114–4119.

Fernando, D., Navaratnam, S., Rajeev, P., & Sanjayan, J. (2023). Study of technological advancement and challenges of façade system for sustainable building: Current design practice. *Sustainability*, *15*, 14319.

Fischer. (n.d.). Termofix 6h-nt – insulation screw and washer [Accessed: 2025-08-19].

Floral Images. (2025). Brachythecium rutabulum, picture 1 of 1 [Accessed 22 May 2025].

GBIF. (2025). Occurrence detail 5006886785 [Accessed 22 May 2025].

Glime, J. M. (2017a). Chapter 3 - sexual strategies. In J. M. Glime (Ed.), *Bryophyte ecology, volume 1: Physiological ecology* (Vol. 1). Michigan Technological University. https://digitalcommons.mtu.edu/bryophyte-ecology1/3/

Glime, J. M. (2017b). Chapter 7 - water relations. In J. M. Glime (Ed.), *Bryophyte ecology, volume 1: Physiological ecology* (Vol. 1). Michigan Technological University. https://digitalcommons.mtu.edu/bryophyte-ecology1/6/

Glime, J. M. (2017c). Chapter 8 - nutrients. In J. M. Glime (Ed.), *Bryophyte ecology, volume 1: Physiological ecology* (Vol. 1). Michigan Technological University. https://digitalcommons.mtu.edu/bryophyte-ecology1/7/

Guillitte, O. (1995). Bioreceptivity: A new concept for building ecology studies. *Science of the total environment*, *167*(1-3), 215–220.

Hanifa, M., Agarwal, R., Sharma, U., Thapliyal, P., & Singh, L. (2023). A review on co2 capture and sequestration in the construction industry: Emerging approaches and commercialised technologies. *Journal of CO2 Utilization*, *67*, 102292.

Hartwell, R., Macmillan, S., & Overend, M. (2021). Circular economy of façades: Real-world challenges and opportunities. *Resources, Conservation and Recycling*, *175*, 105827.

Häubner, N., Schumann, R., & Karsten, U. (2006). Aeroterrestrial microalgae growing in biofilms on facades—response to temperature and water stress. *Microbial ecology*, *51*(3), 285–293.

Hueck, H. (1965). The biodeterioration of materials as a part of hylobiology [Reprinted from Centraal Laboratorium TNO, P.O. Box 217, Delft, The Netherlands]. *Material und Organismen*, *1*(1), 5–34. https://publications.tno.nl/publication/34619961/jAoI1w/hueck-1965-hylobiology.pdf

Hukseflux Thermal Sensors B.V. (2023, May). *Hfp01 and hfp03 user manual* [Version 2527]. https://www.hukseflux.com/uploads/product-documents/HFP01_HFP03_manual_v2527.pdf

Institute), N. (S. (2012). *Tests for geometrical properties of aggregates – part 1: Determination of particle size distribution – sieving method*. https://www.nen.nl/en/nen-en-933-1-2012-en-167446

Institute), N. (S. (2022). *Beproevingsmethoden voor de bepaling van mechanische en fysische eigenschappen van toeslagmaterialen – deel 6: Bepaling van de deeltjesdichtheid en de wateropname*. https://www.nen.nl/en/nen-en-1097-6-2022-en-293453

International Organization for Standardization. (2006). Nen-en-iso 14040:2006 environmental management – life cycle assessment – principles and framework [Accessed 6 June 2025]. *NEN, Delft*.

Intini, F., & Kühtz, S. (2011). Recycling in buildings: An lca case study of a thermal insulation panel made of polyester fiber, recycled from post-consumer pet bottles. *The international journal of life cycle assessment*, *16*(4), 306–315.

Iwuanyanwu, O., Gil-Ozoudeh, I., Okwandu, A. C., & P., I. (2025). Retrofitting existing buildings for enhanced sustainability: A literature review on energy efficiency and building performance. *Engineering Science & Technology Journal*, *5*(8), 2616–2631. https://doi.org/10.5334/bc.37

Jamilu, G., Abdou, A., & Asif, M. (2024). Dynamic facades for sustainable buildings: A review of classification, applications, prospects and challenges. *Energy Reports*, *11*, 5999–6014.

Jelle, B. P. (2011). Traditional, state-of-the-art and future thermal building insulation materials and solutions: Properties, requirements and possibilities. *Energy and Buildings*, *43*, 2549–2563.

Ji, Y., Su, X., Lin, T. C., Liu, X., Xiong, D., Xu, C., Chen, S., Yang, Z., & Yang, Y. (2024). Diurnal and seasonal carbon budget of subtropical moss-dominated biocrusts. *Plant and Soil*, *505*(1), 513–526. https://doi.org/10.1007/s11104-024-06693-9

Katarzyna, L., Sai, G., & Singh, O. A. (2015). Non-enclosure methods for non-suspended microalgae cultivation: Literature review and research needs. *Renewable and sustainable energy reviews*, *42*, 1418–1427.

Knaack, U., Klein, T., Bilow, M., & Auer, T. (2014). *Façades: Principles of construction* (2nd revised edition) [Includes new case studies chapter "Future Façades"]. Birkhäuser Verlag.

Koh, C., Schollbach, K., Gauvin, F., & Brouwers, H. (2022). Aerogel composite for cavity wall rehabilitation in the netherlands: Material characterization and thermal comfort assessment. *Building and Environment*, *224*, 109535.

Kunič, R. (2017). Carbon footprint of thermal insulation materials in building envelopes. *Energy Efficiency*, *10*, 1511–1528.

Kvande, T., Bakken, N., Bergheim, E., & Thue, J. V. (2018). Durability of etics with rendering in norway—experimental and field investigations. *Buildings*, *8*(7), 93.

Li, L. G., Feng, J.-J., Xiao, B.-F., Chu, S.-H., & Kwan, A. K. H. (2021). Roles of mortar volume in porosity, permeability and strength of pervious concrete. *Journal of Infrastructure Preservation and Resilience*, *2*(1), 19.

Ltd., E. (n.d.). Heat flux transmitters [Accessed 22 July 2025].

Manso, M., & Castro-Gomes, J. (2015). Green wall systems: A review of their characteristics. *Renewable and sustainable energy reviews*, *41*, 863–871.

Manso, M., Teotónio, I., Silva, C. M., & Cruz, C. O. (2021). Green roof and green wall benefits and costs: A review of the quantitative evidence. *Renewable and Sustainable Energy Reviews*, *135*, 110111.

Manso, S., Mestres, G., Ginebra, M. P., De Belie, N., Segura, I., & Aguado, A. (2014). Development of a low ph cementitious material to enlarge bioreceptivity. *Construction and Building Materials*, *54*, 485–495.

MaterialDistrict. (2025). *Cork façade*. Retrieved May 21, 2025, from https://materialdistrict.com/material/cork-facade/

Ministerie van Binnenlandse Zaken en Koninkrijksrelaties. (2022). *Bouwbesluit – minimale rc-waarde gevels (nieuwbouw)*. Retrieved August 19, 2025, from https://www.bouwbesluitonline.nl/

Moghtadernejad, S. (2013). *Design, inspection, maintenance, life cycle performance and integrity of building facades* [Doctoral dissertation, McGill University Libraries].

Mustafa, K. F., Prieto, A., & Ottele, M. (2021). The role of geometry on a self-sustaining bio-receptive concrete panel for facade application. *Sustainability*, *13*(13), 7453.

Natanzi, A. S., Thompson, B. J., Brooks, P. R., Crowe, T. P., & McNally, C. (2021). Influence of concrete properties on the initial biological colonisation of marine artificial structures. *Ecological Engineering*, *159*, 106104.

Nikaido, H., & Vaara, M. (1985). Molecular basis of bacterial outer membrane permeability. *Microbiological reviews*, *49*(1), 1–32.

Ostapska, K., Rüther, P., Loli, A., & Gradeci, K. (2024). Design for disassembly: A systematic scoping review and analysis of built structures designed for disassembly. *Sustainable Production and Consumption*, *48*, 377–395.

Ottele, M., Perini, K., Fraaij, A., Haas, E., & Raiteri, R. (2011). Comparative life cycle analysis for green façades and living walls. *Energy and Buildings*, *43*(12), 3419–3429. https://doi.org/10.1016/j.enbuild.2011.09.010

pro clima. (2025a). Solitex® fronta penta [Accessed: 2025-08-19]. https://proclima.com/products/external-sealing/solitex-fronta-penta

pro clima. (2025b). Environmental product declaration (epd) data [Accessed via Environdec API]. https://api.environdec.com/api/v1/EPDLibrary/Files/d3243ad3-cd23-468d-fbef-08dd7d0d76b5/Data

Pro Suber. (2023). Environmental product declaration (epd) – expanded cork insulation (icb) [Accessed 31 July 2025]. https://www.prosuber.com/wp-content/uploads/231216_EPD_geexpandeerde-kurkisolatie_PSQ1_Pro-Suber%C2%AE_ICB_expanded-cork-insulation_insulation-cork-board_ISOKURK_isolatiekurk.pdf

Proctor, M. C., Oliver, M. J., Wood, A. J., Alpert, P., Stark, L. R., Cleavitt, N. L., & Mishler, B. D. (2007). Desiccation-tolerance in bryophytes: A review. *The bryologist*, *110*(4), 595–621.

RDH Building Science Inc. (2018). Cladding attachment solutions for exterior insulation [Accessed: 2025-09-06].

Real, S., Gomes, M. G., Rodrigues, A. M., & Bogas, J. A. (2016). Contribution of structural lightweight aggregate concrete to the reduction of thermal bridging effect in buildings. *Construction and Building Materials*, *121*, 460–470.

Rijksoverheid. (2024). Besluit bouwwerken leefomgeving [Dutch Building Decree under the Environment and Planning Act (Omgevingswet)].

ROCKWOOL Polska Sp. z o.o. (2025, March). *Environmental product declaration: Rockwool cce – stone wool thermal insulation for buildings* (tech. rep.). ROCKWOOL A.S. (CZ), Rockwool Hungary Kft., Rockwool Polska Sp. z o.o. Cigacice, Poland. https://www.rockwool.com/syssiteassets/rw-cz/dokumenty/environmentalni-prohlaeni-o-produktu/epd.pdf

Rotondi, C., Gironi, C., Ciufo, D., Diana, M., & Lucibello, S. (2024). Bioreceptive ceramic surfaces: Material experimentations for responsible research and design innovation in circular economy transition and "ecological augmentation". *Sustainability*, *16*(8), 3208.

Sá, A. V., Azenha, M., De Sousa, H., & Samagaio, A. (2012). Thermal enhancement of plastering mortars with phase change materials: Experimental and numerical approach. *Energy and Buildings*, *49*, 16–27.

Sanmartín, P., Miller, A., Prieto, B., & Viles, H. A. (2021). Revisiting and reanalysing the concept of bioreceptivity 25 years on. *Science of the total environment*, *770*, 145314.

Scarlat, N., Prussi, M., & Padella, M. (2022). Quantification of the carbon intensity of electricity produced and used in europe. *Applied Energy*, *305*, 117901.

Schiavoni, S., Bianchi, F., Asdrubali, F., et al. (2016). Insulation materials for the building sector: A review and comparative analysis. *Renewable and Sustainable Energy Reviews*, *62*, 988–1011.

Sengul, O., Azizi, S., Karaosmanoglu, F., & Tasdemir, M. A. (2011). Effect of expanded perlite on the mechanical properties and thermal conductivity of lightweight concrete. *Energy and Buildings*, *43*(2-3), 671–676.

Shin, A. H.-C., & Kodide, U. (2012). Thermal conductivity of ternary mixtures for concrete pavements. *Cement and Concrete Composites*, *34*(4), 575–582.

Solga, A., Cerman, Z., Striffler, B. F., Spaeth, M., & Barthlott, W. (2007). The dream of staying clean: Lotus and biomimetic surfaces. *Bioinspiration & biomimetics*, *2*(4), S126.

Speak, A. F., Rothwell, J. J., Lindley, S. J., & Smith, C. L. (2012). Urban particulate pollution reduction by four species of green roof vegetation in a uk city. *Atmospheric Environment*, *61*, 283–293.

Stichting MRPI and Hollandse Cement Maatschappij B.V. (2025). Mrpi® epd hoogovencement cem iii/b 42,5 n lh sr [Accessed 2025-08-11]. https://www.mrpi.nl/epd-files/epd/1.1.00758.2025%20MRPI%20EPD%20Hoogovencement.pdf

Stirbet, A., Lazár, D., Guo, Y., & Govindjee, G. (2020). Photosynthesis: Basics, history and modelling. *Annals of botany*, *126*(4), 511–537.

Stohl, L., Manninger, T., von Werder, J., Dehn, F., Gorbushina, A., & Meng, B. (2023). Bioreceptivity of concrete: A review. *Journal of Building Engineering*, *76*, 107201.

Suber, P. (2022). Productblad psq4: Geëxpandeerde kurkgranulaat [Geraadpleegd op 26 augustus 2025]. https://www.groenebouwsystemen.nl/wp-content/uploads/2022/02/220214_PSQ4_datasheet-informatie-productblad-Pro-Suber-geexpandeerde-kurk.pdf

Sung, D. (2016). A new look at building facades as infrastructure. *Engineering*, *2*(1), 63–68.

Transport- en Aannemingsbedrijf Van der Waal B.V. (2025). *Argex – van der waal b.v.* Retrieved March 25, 2025, from https://www.vanderwaalbv.nl/producten-en-diensten/argex

United Nations. (2014). *World urbanization prospects: The 2014 revision, highlights*. Population Division, United Nations.

Urban Mine. (2025). Urbanmine – gerecycled beton met de stad als bron [Accessed 2025-08-11]. https://urbanmine.nl/

Valore, R. C. (1980). Calculations of u-values of hollow concrete masonry. *Concrete International*, *2*(2), 40–63.

Veeger, M., Nabbe, A., Jonkers, H., & Ottele, M. (2023). Bioreceptive concrete: State of the art and potential benefits. *Heron*, *68*(1), 47–76.

Veeger, M., Veenendaal, E., Limpens, J., Ottelé, M., & Jonkers, H. (2025). Moss species for bioreceptive concrete: A survey of epilithic urban moss communities and their dynamics. *Ecological Engineering*, *212*, 107502.

von Werder, J., Venzmer, H., & Černỳ, R. (2015). Application of fluorometric and numerical analysis for assessing the algal resistance of external thermal insulation composite systems. *Journal of building physics*, *38*(4), 290–316.

Wang, W., Lu, C., Li, Y., & Li, Q. (2017). An investigation on thermal conductivity of fly ash concrete after elevated temperature exposure. *Construction and Building Materials*, *148*, 148–154.

Yu, J., Dong, Y., Wang, T., Chang, W.-S., & Park, J. (2024). U-values for building envelopes of different materials: A review. *Buildings*, *14*(8), 2434.

Zhang, Z., Shi, G., Wang, S., Fang, X., & Liu, X. (2013). Thermal energy storage cement mortar containing n-octadecane/expanded graphite composite phase change material. *Renewable energy*, *50*, 670–675.

Appendix A

Literature review

A.1 Definitions

A.1.1 Water vapor resistance factor μ

Water vapor resistance factor (μ) is used to evaluate the vapor permeability of building materials. It is a dimensionless parameter where the higher the value is, the lower the permeability is. The μ-value for insulation materials can be determined by either EN12086 and EN 12088 standards. These standards define the procedure to quantify the long-term water absorbed by diffusion (Schiavoni et al., 2016).

A.1.2 Thermal conductivity

Thermal conductivity (λ) represents the steady-state heat flow passing through a unit area of a homogeneous material with a thickness of 1 meter, induced by a 1K temperature difference across its surfaces. This parameter is expressed in W/m $\cdot$ K and measured in compliance with EN12664 (low thermal resistance), EN 12667 (high thermal resistance, EN 12939 (thick products of high and medium thermal resistance (Asdrubali et al., 2015).

Total overall thermal conductivity λ_{tot} is made up from several contributions

$$\lambda_{tot} = \lambda_{solid} + \lambda_{gas} + \lambda_{rad} + \lambda_{conv} + \lambda_{coupling} + \lambda_{leak} \tag{A.1}$$

Where λ_{solid} is the solid state thermal conductivity, λ_{gas} is the gas thermal conductivity, λ_{rad} is the radiation thermal conductivity, λ_{gconv} is the convection thermal condcuctivity, $\lambda_{coupling}$ is the thermal conductivity term accounting for second order effets between the various thermal conductivities, and λ_{leak} is the leakage thermal conductivity. Usually, λ_{leak}, representing air and moisture leakage, is not considered for insulation materials as they are supposed to be without any houles and thus enabling such thermal leakage transport. Additonally, $\lambda_{coupling}$ is rather complex, as it accounts for second order effects between various thermal conductivities, shown in Equation A.1, and will therefore be neglected for this

project. When all of these specific contributions are minimized, the lowest possible thermal conductivity can be achieved (Jelle, 2011).

A.1.3 Thermal transmittance (U-value/factor)

Thermal transmittance (U-Value) quantifies the steady-state heat flow through a unit surface area under a 1K temperature difference. Unlike thermal conductivity, the U-value also accounts for convective and radiative heat transfer. The unit of measurement for the U-value is $W/m^2 \cdot K$, and it is determined using the hot-box method (Asdrubali et al., 2015).The U-value is the inverse of the R-value, i.e. U=1/R, and defines how well a building material acts as a conductor.

A.1.4 Fire classification standards

The EN 13501-1 standard provides a unified European system for classifying the reaction to fire of construction products and building elements. It is designed to support fire safety in the built environment through standardized testing and evaluation (British Standards Institution, 2019).

Materials are classified using a combination of letters and numbers that indicate whether the material is combustible or can contribute to a fire. The fire classification system is summarized briefly here below:

- A1: Non-combustible; no contribution to fire.
- A2: Limited combustibility.
- B, C, D: Increasing contribution to fire (B being the best among these).
- E: Acceptable only for brief exposure.
- F: No performance determined.

A.1.5 Design for disassembly (DfD)

Design for disassembly (DfD) is a design approach that has the goal to eliminate waste and thus contribute to a circular economy. A recent standards, ISO 20887:2020 has further defined DfD, in the context of Architecture, Engineering, and Construction (AEC) as:

> approach to the design of a product or constructed asset [...] that facilitates disassembly [...] at the end of its useful life, in such a way that enables components [...] and parts to be reused, recycled, recovered for energy or, in some other way, diverted from the waste stream

A rise in popularity for DfD has been noted in recent years, mostly due to waste minimization policies and the beginning of the circular economy transition in many countries (Ostapska et al., 2024).

A.2 Facade layers

As outlined by Knaack et al. (2014), a facade system can be divided into three constructional layers:

1. Primary structure
2. Secondary structure
3. Infill elements

The primary structure is the building's main loadbearing frame. It usually consists of concrete, and transfers all loads of the building itself to the foundation. The *secondary structure*, supports the facade and connects it to the primary structure. It has to accommodate structural movement and differences in manufacturing tolerances. *Infill elements*, such as panels, glazing, or ventilation components, enclose the space and must meet specific environmental performance requirements such as airtightness, water resistance, and thermal bridging prevention (Knaack et al., 2014).

This layered construction allows each part to fulfill specific functions, improving assembly flexibility and performance. The secondary structure is a quite critical component, as it serves as the interface between the building's loadbearing shell and the exterior envelope. It balances movement, supports infill elements, and has to meet high precision standards (Knaack et al., 2014)..

For some systems, the primary and secondary structures are integrated, which reduces interfaces but can complicate maintenance and tolerances. In such systems, the facade components are part of the load bearing structure (primary structure) and cannot be easily replaced (Knaack et al., 2014).

Appendix B

Material selection

B.1 Concrete layer

Argex 4/8

Argex is a lightweight granulate made from expanded Boom clay, baked in a rotary kiln at 1100°C. It has a reddish-brown microporous exterior and a black core with a cellular structure. Key properties include a draining effect, rot resistance, durability, and incombustibility (Transport- en Aannemingsbedrijf Van der Waal B.V., 2025).

It is possible to choose between 3 different types of Argex (Transport- en Aannemingsbedrijf Van der Waal B.V., 2025).,

1. Round materials: AR 8/16-340 and AR 4/10-430
2. Broken materials AG 4/8-370
3. Sand: AG 0/4-500

The chosen type of Argex for the concrete mixture is AG 4/8-370, the features of this type are the following (Transport- en Aannemingsbedrijf Van der Waal B.V., 2025):

- Weight (loose, not compacted and dry): 320 kg/m^3
- Weight (compacted and wet(in situ)): approx. 650 kg/m^3

Recycling of demolition rubble to recycled sand

Fine aggregates used in the concrete mixture is recycled sand that is acquired from demolition rubble. The process begins at the demoolition site, where it is determined whether demolition rubble is deemed to be suitable for further recycling, the rubble is transported to Urban Mine. High-tech machines are utilized there which process the rubble into new raw materials. The energy required and used for this process is generated by solar panels which are located on-site (Urban Mine, 2025)

B.2 Production process of PRO SUBRA Cork insulation material

The cork used for the boards is derived from falca cork, which is a unique type of cork that periodically harvested from the upper branches of the cork oak tree. After harvesting, the cork is stored in a factory yard before being processed. The production process does not include the use of any additives (Pro Suber, 2023).

The production process of the cork boards begins by grinding the cork into smaller granules. These granules are then placed in an autoclave and exposed to 350°C, a superheated steam. As a result, the cork granules expand and release suberin, which is a natural resinous binder found within cork itself. This suberin allows the granules to self bind, forming a solid block without the need for synthetic adhesives (Pro Suber, 2023).

After this initial processing step, the blocks go through a stabilization period before being sawn into expanded insulation cork boards (Pro Suber, 2023).

The process is highly resourceful, where 100% of the production waste is reusable, and over 90% of the energy used is sourced from biomass, which is the by-product of the board manufacturing process itself. This results in a product with very low embodied energy (Pro Suber, 2023).

B.3 Membrane selection

The following membranes shown in Table B.1 were researched and further evaluated for the use of the facade system. The purpose of the membrane is to ensure moisture control and durability of the facade system as whole. Additionally, it should ensure long term UV stability and circularity of the facade system.

Membrane	Type	UV Resistance	Key Features
Tyvek® UV facade (**TyvekUVfacade**)	Spunbonded breathable WRB	High (up to 4 months)	Very breathable, durable, UV-stable
Polytex® Fassade FR (Bouw, 2025b)	Breathable facade membrane	Moderate (2 months)	Fire class B-s1-d0, tear-resistant
Polytex® Fassade ECO (Bouw, 2025a)	Economical WRB	Good (open joints OK)	Lightweight, vapor-open, budget-friendly
TAFTEX® EX-150 / EX-210 (Bouw, 2025c)	PP/HDPE facade membrane	High	Tear-resistant, UV-stable, facade-optimized
Miofol® 125G / 210AG (De Isolatieshop, 2025)	Micro-perforated WRB	High	Reinforced, A2 fire-rated options
SOLITEX FRONTA HUMIDA (pro clima, 2025a)	Breathable facade WRB	Moderate (3 months)	High vapor permeability, suited to timber/mineral insulation
SOLITEX FRONTA PENTA (pro clima, 2025a)	Open-joint UV WRB	Very high (10,000 h)	UV-stable for large joint widths, weatherproof

Table B.1: Membrane selection for the facade system

Appendix C

Methodology

C.1 Aggregate properties

Particle size distribution

The methodology used to determine the particle size distribution (PSD) of the aggregates is in accordance with the NEN-EN 933-1:2012 (E) standard (Institute), 2012). The following procedure was followed:

1. A known mass of aggregate was weighed and then oven-dried before sieving
2. A Stack of sieves was then prepared, arranged in ascending order from the smallest mesh size at the bottom (pan, 0mm) to the largest at the top (16 mm).
3. The dried sample was placed on the top (largest) sieve.
4. The sieve stack was secured in a mechanical shaker, and the shaking duration and intensity were set according to the standard.
5. After sieving, each sieve was carefully removed and the mass of material retained on each sieve was recorded.

Water absorption

To determine the water absorption of the coarse aggregate fraction of the concrete, Argex 4/8, the NEN-EN 1097-6:2022 (E) standard (Institute), 2022) was followed. The procedure followed to do so has been summarized here below,

1. Weigh a specific amount of aggregates
2. Immerse aggregates in water for a total of 24 hours
3. Pad the surface of the saturated aggregates dry with a cloth
4. Weigh the saturated mass (Mw)

5. Dry aggregates in oven for a total of 24 hours at 75°C
6. Leave aggregates to cool down
7. Weigh dry mass of aggregates (Md)

Once the procedure described here above has been followed, equation C.1 can be used to calculate the water absorption of the aggregates.

$$WA = \frac{M_w M_d}{M_d} \cdot 100 \tag{C.1}$$

Particle density

Particle density of the coarse aggregates used for this project, Argex 4/8, was done to assess the influence of the fraction on the concretes mix proportions and the volume of aggregates in the concrete mix design. The procedure followed was based on the NEN-EN 1097-6:2022 (E) standard (Institute), 2022). The steps outlined below summarize the method used to determine the particle density in accordance with this standard.

Prior to testing, a specific amount of aggregates was weighed and dried in an oven at 75 °C for 24 hours. After drying, the aggregates need to be cooled to room temperature before starting the measurements.

The empty pycnometer was weighed and recorded as W_p. Afterwards, it was filled with water and weighed again, recorded as W_{p+w}. Using these two values, W_p and W_a, the volume of the water added to the pycnometer was found by using Equation C.2

$$V_w = (W_{p+w} W_p / p_w) \cdot 100 \tag{C.2}$$

A known mass of the previously dried and cooled aggregates was then added to the pycnometer, and the combined weight is recorded as W_{p+a}. Water was then added to the pycnometer containing the aggregates, ensuring all air bubbles were removed by shaking the pycnometer gently. Water was then added to ensure that the vessel is completely filled. The final weight, including pycnometer, aggregates and water was recorded as W_{p+a+w}. The volume of displaced water volume is calculated next by using Equation C.3.

$$V_w = (W_{p+w}(W_{p+a+w} - W_a) \cdot 100 \tag{C.3}$$

The density of the aggregates can then finally be calculated by using Equation C.4

$$Density = W_a / V_w \tag{C.4}$$

C.2 Concrete mixing

The following procedure was followed when casting the concrete panels.

1. Each material was weighed according to the mix design and placed in separate buckets.
2. The 40L concrete mixer was prepared and cleaned with water to remove any residual material.
3. Fine and coarse aggregates were added to the mixer first and mixed to ensure a consistent distribution.
4. Cement and bone ash were then added to the mixed fine and coarse aggregates. Mixing was continued until the materials are homogeneously combined.
5. Water was gradually added to the dry mixture while mixing continued until the desired consistency was achieved.
6. Once the mix reached the required workability, it was transferred into a clean barrel for transport to where the casting panels were located.
7. The barrel containing the concrete mixture was transported to the casting area where the molds were prepared.
8. Each mold was filled to the top with the concrete mixture.
9. Air bubbles were removed manually by gently lifting and tapping the molds against the table surface.
10. After filling, the surface of each mold was leveled to ensure an even finish.

C.3 HFP01 Heat flux sensor

The HFP01 is a widely used sensor for measuring heat flux in both soil and building envelopes. It is known for its robustness and stability, which makes it suitable for long-term monitoring or repeated installations (Hukseflux Thermal Sensors B.V., 2023).

C.3.1 Working principle

Figure C.1 illustrates the general working principle of a heat flux sensor. HFP01 is a thermopile sensor, meaning it includes multiple thermocouples that measure the temperature difference across its ceramic-plastic composite body. Each thermocouple consists of two metal alloys, labeled (1) and (2) in the Figure C.1, which are electrically connected in series. As a passive device, the sensor does not require an external power supply (Hukseflux Thermal Sensors B.V., 2023).

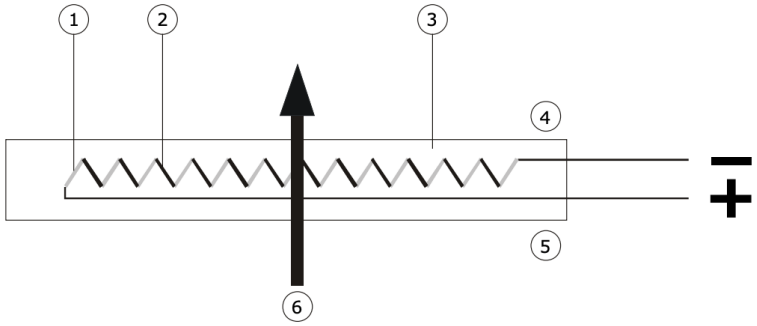

Figure C.1: General working principle of a heat flux sensor (Hukseflux Thermal Sensors B.V., 2023)

Thermocouples of the sensor generate a small voltage that is proportional to the temperature difference between its hot and cold junctions. Connecting multiple thermocouples in series amplifies this signal (Hukseflux Thermal Sensors B.V., 2023).

Once a thermal steady-state is reached within the system, the heat flux, shown as (6) in Figure C.1, becomes a linear function of the temperature difference across the sensor and the average thermal conductivity of the sensor body, shown as (3) in the figure. The resulting voltage output is directly proportional to the heat flux passing through the sensor (Hukseflux Thermal Sensors B.V., 2023).

The sensor measures heat flux through either the material in which it is embedded or mounted onto. Heat flux is expressed in watts per square meter (W/m^2). The heat flux Φ [W/m^2] is calculated by dividing the sensors voltage output U by its sensitivity S, as shown in Equation C.5 (Hukseflux Thermal Sensors B.V., 2023).

$$\phi = U/S \tag{C.5}$$

Typical applications of the HFP01 include (Hukseflux Thermal Sensors B.V., 2023):

- Heat flux measurements in buildings
- Determination of thermal transmittance (U-value) and thermal resistance (R-value)
- Soil heat flux measurements

Figure C.2 contains two illustrations: the HFP01 sensor (left) and its dimensions (right). In the right-hand image, three numbered elements are indicated(Hukseflux Thermal Sensors B.V., 2023) :

- The sensing area
- The passive guard made of a ceramic-plastic composite
- The cable, with a standard length of 5 meters

The dimensions shown on the right Figure are given in millimeters (x10^{-}3m) (Hukseflux Thermal Sensors B.V., 2023).

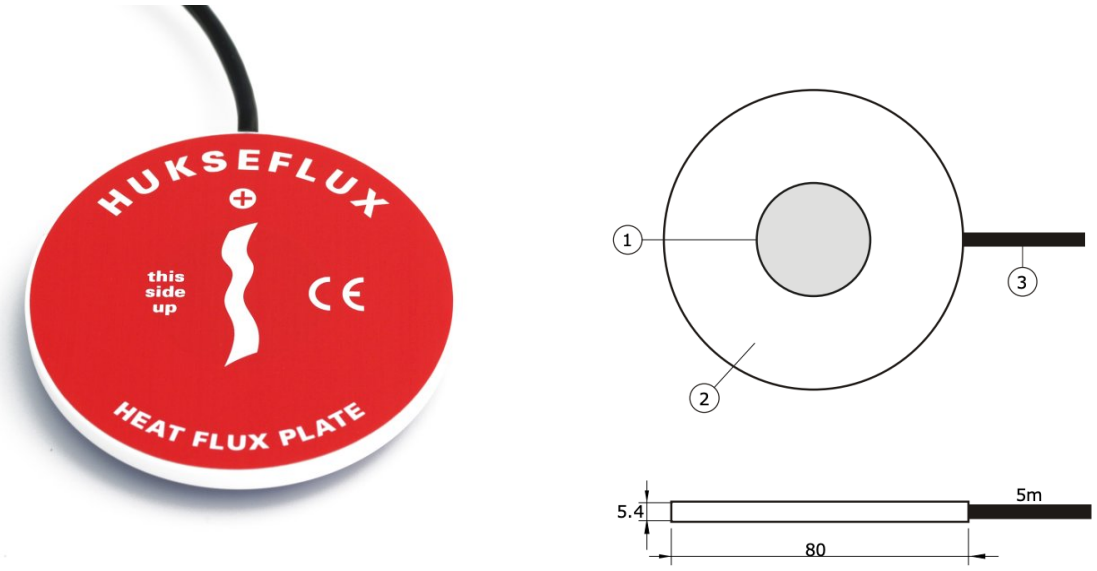

(a) Red side of the HFP01 sensor [source]

(b) HFP01 dimensions

Figure C.2: HFP01 sensor

C.3.2 Installation of HFP01

The following paragraphs include recommendations for site selection and installation in building physics, in the context of the measurements performed for this project. If the circumstances are different from what has been described in this report, it is recommended to look at Chapter 5 of the sensor user manual (Hukseflux Thermal Sensors B.V., 2023).

- Inside environment
- Large wall section
- Relatively homogenous material
- Avoid any air gaps between the sensor and wall. A 0.1x10^{-}3m air gap increases the thermal resistance of the sensor by 60 %.
- The use of double-sided "removable" carpet tape

C.3.3 Uncertainty of measurements with HFP01

There are some uncertainties that come with measuring with heat flux sensors, such as HFP01. The following list includes common uncertainties that may occur when using a HFP01 sensor (Hukseflux Thermal Sensors B.V., 2023):

- Calibration uncertainty
- Measurement and calibration measurement condition differences.
- Duration of sensor employment

- Application errors, which can include measurement conditions

It is recommended that a user of the sensor should make his own uncertainty evaluation (Hukseflux Thermal Sensors B.V., 2023).

C.4 SRV250 - Receiver Logger

SRV250 is a receiver logger from Eltek that is to be used with the extensive range of GenII transmitters, see Figure C.4. It offers real time data, multiple site access and advance analytical software (Eltek Ltd., 2025). The logger has a battery back-up, built-in 3G, and 250,000 readings fall back logging.

Figure C.3: SRV250 receiver logger (Eltek Ltd., 2025)

Figure C.4 includes the system connectivity of the SRV250 reciever logger. As can be seen, SRV250 is the hub of the system, where sensor values from transmitters are held in a register. These values are then continuously uploaded to the server (Eltek Ltd., 2025).

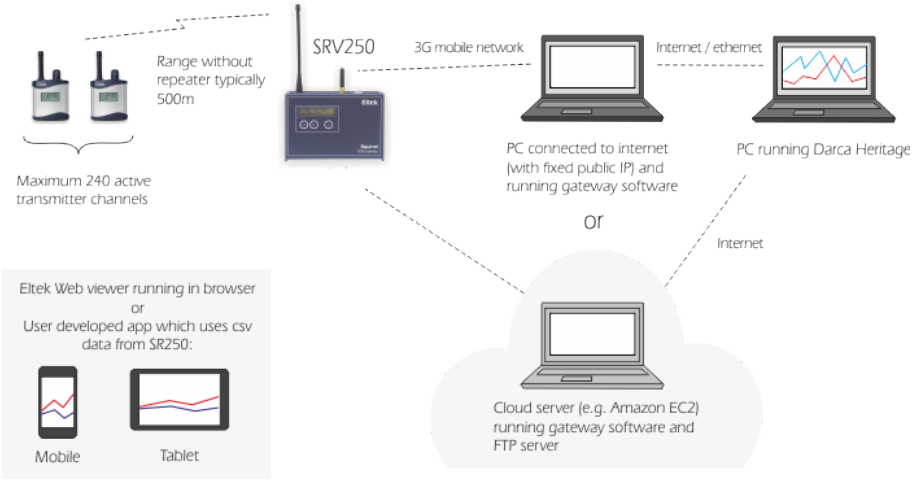

Figure C.4: System connectivity of the SRV250 receiver logger (Eltek Ltd., 2025)

C.5 GENII transmitters

Figure C.5 shows the GENII transmitter from Eltek. This general purpose bipolar range transmitter is specifically designed for use with the Hukseflux HFP01 heat flux plate (Ltd., n.d.).

Figure C.5: GENII transmitter (Ltd., n.d.)

The transmitter is available in two versions: the GS42H, which features two inputs, and the GS44H, which has four. All inputs share the same measurement range, which is hardware-configured during manufacturing (Ltd., n.d.).

Appendix D

Results

D.1 Aggregate properties

D.2 Multi-criteria analysis

Thermal conductivity

The first specific indicator evaluated was *thermal conductivity*. Gathered information, results before weights have been added and after weights have been added have been summarized in Table D.1.The highest score, 5 points are awarded for materials with low thermal conductivity, ranging from 0-10 $W/(m \cdot K)$). See Appendix A.1.2 for more information on thermal conductivity.

Thermal conductivity [W/(mK)]			
Insulation material	**Gathered information**	**Score**	**Score with specific weighing**
Glass wool	30–40 (Jelle, 2011)	2	0.4
Rock wool	30–40 (High) (Erzen et al., 2025), (Jelle, 2011)	2	0.4
Expanded polystyrene (EPS)	30–40 (Jelle, 2011)	2	0.4
Extruded polystyrene (EXS)	30–40 (Jelle, 2011)	2	0.4
Cellulose	40–50 (Jelle, 2011)	1	0.2
Cork	40–50 (Jelle, 2011)	1	0.2
Polyurethane	20–30 (Jelle, 2011)	3	0.6
Vacuum insulation panels	2–3 (Erzen et al., 2025), 3–4(Jelle, 2011) (fresh), 8 (after 25 years aging) (Jelle, 2011)	5	1
Gas insulated panels	0.010 (Schiavoni et al., 2016)	5	1
Aerogels	0.0131–0.0136 (Schiavoni et al., 2016)	5	1

Table D.1: MCA results for thermal conductivity with gathered reference data

Ideally, the material should have the lowest possible thermal conductivity, while at the same time, minimizing its thickness in order to save space, reduce costs, and lower its environmental impact. However, achieving this balance can be challenging, as some materials require increased thickness to attain lower thermal conductivity values (Jelle, 2011)

State-of-the-art thermal insulation materials, such as VIPs, GIPs, and aerogels, achieve the highest scores, followed by more conventional materials. In contrast, less traditional options like cellulose and cork receive the lowest scores due to their relatively high thermal conductivity, ranging from 40–50 $W/(m \cdot K)$.

Perforation vulnerability

Gathered information, results before weights have been added and after weights have been added have been summarized in Table D.2 for *perforation vulnerability*. Ideally, the chosen material should be robust and easily adaptable on-site. If the insulation material can be perforated, cut, and adjusted without compromising its thermal conductivity, it receives the highest score of five points. However, if puncturing or modifying the material leads to increased thermal conductivity, it receives only one point.

Perforation vulnerabilty			
Insulation material	**Gathered information**	**Score**	**Score with specific weighing**
Glass wool	Yes (Jelle, 2011)	5	0.25
Rock wool	Yes (Jelle, 2011)	5	0.25
Expanded polystyrene (EPS)	Yes (Jelle, 2011)	5	0.25
Extruded polystyrene (EXS)	Yes (Jelle, 2011)	5	0.25
Cellulose	Yes (Jelle, 2011)	5	0.25
Cork	Yes (Jelle, 2011)	5	0.25
Polyurethane	Yes (Jelle, 2011)	5	0.25
Vacuum insulation panels	No (Jelle, 2011)	1	0.05
Gas insulated panels	No (Jelle, 2011)	1	0.05
Aerogels	Yes (Jelle, 2011)	5	0.25

Table D.2: MCA results for perforation vulnerability with gathered reference data (Jelle, 2011)

As shown in Table D.2, only two materials, Vacuum Insulation Panels and Gas Insulated Panels, receive the lowest score of 1 point. All other evaluated materials receive the highest score of 5 points, as they can be perforated, cut, and adjusted on-site without a loss in thermal resistance.

Building site adaptability and cuttability

The gathered information, along with the scores before and after applying weights, is summarized in Table D.3 in Appendix D.2 for *building site adaptability*. A high score of 5 points is awarded when the material is flexible, lightweight, and easy for operators to handle on-site. If the material is fragile and susceptible to damage during handling, it receives a low score of 1 point.

Building site adaptability and cutability			
Insulation material	**Gathered information**	**Score**	**Score with specific weighing**
Glass wool	Yes (Jelle, 2011) Flexible structure (Erzen et al., 2025), lightweight (Erzen et al., 2025)	5	0.25
Rock wool	Yes (Jelle, 2011), easily handled by operators without losing thermal performance (Schiavoni et al., 2016)	5	0.25
Expanded polystyrene (EPS)	Yes (Jelle, 2011), Lightweight (Erzen et al., 2025)	5	0.25
Extruded polystyrene (EXS)	Yes (Jelle, 2011), Denser than EPS (Erzen et al., 2025)	5	0.25
Cellulose	Yes (Jelle, 2011)	5	0.25
Cork	Yes (Jelle, 2011), Lightweight structure (Erzen et al., 2025)	5	0.25
Polyurethane	Yes (Jelle, 2011)	5	0.25
Vacuum insulation panels	No (Jelle, 2011), very thin structure (Erzen et al., 2025)	1	0.05
Gas insulated panels	No (Jelle, 2011)	1	0.05
Aerogels	No, Lightweight (Erzen et al., 2025), thin structure (Erzen et al., 2025), very fragile (Jelle, 2011)	1	0.25

Table D.3: MCA results for building site adaptability with gathered reference data

Similar to the results of perforation vulnerability, there are three materials, Vacuum Insulation Panels, Gas Insulated Panels and aerogels, that receive the lowest score of 1 point for building site adaptability. These three materials all have a very thin structure and are quite fragile. All other evaluated materials receive the highest score of 5 points, as they can be easily handled by operators without the loss of thermal resistance.

Mechanical strength

The gathered information, along with the scores before and after applying weights, is summarized in Table D.4 for *mechanical strength*. The highest score is awarded to materials with load-bearing capacity, while materials without any load-bearing capacity receive a score of 1 point.

Mechanical strength			
Insulation material	**Gathered information**	**Score**	**Score with specific weighing**
Glass wool	No load bearing capabilities (NO) (Jelle, 2011)	1	0.05
Rock wool	No load bearing capabilities (NO)(Jelle, 2011)	1	0.05
Expanded polystyrene (EPS)	No load bearing capabilities (NO)(Jelle, 2011) Open pore structure (Jelle, 2011)	1	0.05
Extruded polystyrene (EXS)	No load bearing capabilities (NO)(Jelle, 2011)	1	0.05
Cellulose	No load bearing capabilities (NO) (Jelle, 2011)	1	0.05
Cork	No load bearing capabilities (NO) (Jelle, 2011) , High strength (Erzen et al., 2025)	1	0.05
Polyurethane	No load bearing capabilities (NO)(Jelle, 2011)	1	0.05
Vacuum insulation panels	No load bearing capabilities (NO) (Jelle, 2011)	1	0.05
Gas insulated panels	No load bearing capabilities (NO)(Jelle, 2011) , High compression strength (Jelle, 2011)	1	0.05
Aerogels	No load bearing capabilities (NO)(Jelle, 2011), High compression strength (Jelle, 2011)	1	0.05

Table D.4: MCA results for mechanical strength with gathered reference data

As shown in Table D.4, all evaluated insulation materials received the lowest score of 1 point, as none exhibit load-bearing capabilities. As can be seen in the table, some materials exhibit high compressive strength, but as this does not translate into structural load-bearing capacity, they still recieve the lowest score of 1 point.

Fire resistance

The gathered information, along with the scores before and after applying weights, is summarized in Table D.5 in Appendix D.2 for *fire resistance*. The scoring system is based on Euroclass rating, ranging from class A1 to F. The highest score is awarded if the insulation material is in Euroclass Rating A1 or A2, and the lowest score of 1 point is awarded for materials with a rating of F. See A.1.4 for more information on the European fire classification standard.

Fire resistance			
Insulation material	**Gathered information**	**Score**	**Score with specific weighing**
Glass wool	High (Erzen et al., 2025), fire resistant (class A2) (Erzen et al., 2025) A1-A2 (Schiavoni et al., 2016)	4	0.2
Rock wool	Very high (class A1) (Erzen et al., 2025) A1-A2-B (Schiavoni et al., 2016)	5	0.25
Expanded polystyrene (EPS)	E (Schiavoni et al., 2016)	2	0.1
Extruded polystyrene (EXS)	E	2	0.1
Cellulose	Medium (Erzen et al., 2025) B-C-E (Schiavoni et al., 2016)	2	0.1
Cork	E (Schiavoni et al., 2016)	2	0.1
Polyurethane	Medium (Erzen et al., 2025) E (Schiavoni et al., 2016)	2	0.1
Vacuum insulation panels	No information found	0.5	0.25
Gas insulated panels	No information found	0.5	0.025
Aerogels	Very high (Erzen et al., 2025) C (Schiavoni et al., 2016)	3	0.15

Table D.5: MCA results for fire resistance with gathered reference data

As can be seen in Table D.5, there is only one insulation material that receives the highest score of 5 points, the insulation material Rock Wool.

Water resistance

The gathered information, along with the scores before and after applying weights, is summarized in Table D.6 in Appendix D.2 for *water resistance*. Water resistance of an insulation material refers to the materials ability to repel water or resist moisture absorption when exposed to humidity, rain, or other sources of moisture.

Water resistance			
Insulation material	**Gathered information**	**Score**	**Score with specific weighing**
Glass wool	Medium (Erzen et al., 2025)	3	0.15
Rock wool	Medium (Erzen et al., 2025)	3	0.15
Expanded polystyrene (EPS)	Water resistant (Erzen et al., 2025), low water absorption rate (Erzen et al., 2025)	3	0.15
Extruded polystyrene (EXS)	Similar to EPS	3	0.15
Cellulose	High (Erzen et al., 2025)	4	0.2
Cork	Water resistant (Erzen et al., 2025)	3	0.15
Polyurethane	Low (Erzen et al., 2025)	2	0.1
Vacuum insulation panels	No information found	0.5	0.025
Gas insulated panels	No information found	0.5	0.025
Aerogels	High (Erzen et al., 2025)	4	0.2

Table D.6: MCA results for water resistance with gathered reference data

As can be seen in Table D.6, there is no insulation material that receives the highest score of 5 points. There are only two materials, cellulose and aerogels, that receive 4 points (High Water resistance).

Cost

The gathered information, along with the scores before and after applying weights, is summarized in Table D.7 in Appendix D.2 for the estimated *cost* of each insulation material.

Cost			
Insulation material	**Gathered information**	**Score**	**Score with specific weighing**
Glass wool	Medium (Erzen et al., 2025), cost effective (Erzen et al., 2025), relatively cheap (Schiavoni et al., 2016)	5	0.25
Rock wool	Low [1]	5	0.2
Expanded polystyrene (EPS)		4	0.2
Extruded polystyrene (EXS)	10-30 % higher than EPS(Schiavoni et al., 2016)	3	0.15
Cellulose	Low-medium (Erzen et al., 2025), Economical (Erzen et al., 2025)	3	0.15
Cork		3	0.15
Polyurethane	Medium-high (Erzen et al., 2025)	2	0.1
Vaccum insulation panels	Very high (Jelle, 2011)	1	0.05
Gas insulated panels	Very high (Jelle, 2011)	1	0.05
Aerogels	Very high (Erzen et al., 2025)	1	0.05

Table D.7: MCA results for costs with gathered reference data

As can be seen in Table D.7, there is only two insulation materials that receives the highest score of 5 points, rock and glass. This is followed by two other traditional insulation materials, Rock wool and expanded polystyrene.

Environmental impact (Global warming potential)

The gathered information, along with the scores before and after applying weights, is summarized in Table D.8 for Global Warming Potential (GWP). The values presented are expressed in kilograms of CO_2 per functional unit. Since a lower GWP indicates better environmental performance, materials with lower GWP values receive higher scores.

Environmental impact (Global warming potential (kg CO2 per functional unit)			
Insulation material	**Gathered information**	**Score**	**Score with specific weighing**
Glass wool	9.89 (Schiavoni et al., 2016)	3	0.25
Rock wool	1.45 (commercial Stone wool) (Schiavoni et al., 2016)	5	0.2
Expanded polystyrene (EPS)	5.05 or 8.25 (Schiavoni et al., 2016)	4	0.2
Extruded polystyrene (EXS)	13.22 (Schiavoni et al., 2016)	2	0.15
Cellulose	Environmentally friendly (Erzen et al., 2025), 3.66 (Schiavoni et al., 2016)	5	0.15
Cork	5.72 to 5.93 (Schiavoni et al., 2016)	4	0.15
Polyurethane	6.51 (Schiavoni et al., 2016)	4	0.15
Vacuum insulation panels	No information found	0.5	0.05
Gas insulated panels	No information found	0.5	0.05
Aerogels	Approx. 12.5 (Dickson & Pavía, 2021)	0.5	0.05

Table D.8: MCA results for global warming potential with gathered reference data

There are only two materials that receive a highest score of 4 points for Environmental impact , Rock Wool and Cellulose. Then, a total of three materials receive a score of 4, which are expanded polystyrene, cork and polyurethane.

Water vapor resistance factor

The gathered information, along with the scores before and after applying weights, is summarized in Table D.9 in Appendix D.2. See Appendix A.1.1 for more information on the concept of water vapor resistance factor.

Water vapor diffusion resistance factor			
Insulation material	**Gathered information**	**Score**	**Score with specific weighing**
Glass wool	1-1.1 (Schiavoni et al., 2016)	5	0.25
Rock wool	1-1.3 (Schiavoni et al., 2016)	5	0.25
Expanded polystyrene (EPS)	20-70 (Schiavoni et al., 2016)	4	0.2
Extruded polystyrene (EXS)	80-150 (Schiavoni et al., 2016)	3	0.15
Cellulose	1.7-3.0 (Schiavoni et al., 2016)	5	0.25
Cork	5-30 (Schiavoni et al., 2016)	5	0.25
Polyurethane	30-170 (Schiavoni et al., 2016)	1	0.05
Vacuum insulation panels	up to 340.000 (Schiavoni et al., 2016)	1	0.05
Gas insulated panels	Very high (Schiavoni et al., 2016)	1	0.05
Aerogels	5.0-5.5 (Schiavoni et al., 2016)	5	0.25

Table D.9: MCA results for water vapor resistance factor with gathered reference data

Circularity

Gathered information, results before weights have been added and after weights have been added have been summarized in Table D.10 in Appendix D.2 for the circularity of each specific insulation material.

Circularity			
Insulation material	**Gathered information**	**Score**	**Score with specific weighing**
Glass wool	Made from ligthweight recycled glass (Erzen et al., 2025), used glass wool can be recycled by the producing manufacturers (Schiavoni et al., 2016)	5	1.25
Rock wool	Stone wool can be recycled by the producing manufacturers or disposed into landfills (Schiavoni et al., 2016)	4	1
Expanded polystyrene (EPS)	Recycling process is performed by specialized industries (Schiavoni et al., 2016)	3	0.75
Extruded polystyrene (EXS)	Same recycling issues as for EPS - recycling process is performed by specialized industries (Schiavoni et al., 2016)	5	1.25
Cellulose	Made from renewable resources (recycled paper and modified with fire resistant chemicals) (Erzen et al., 2025), can be recycled but are not suitable for composting purposes due to the content of boron salts (Schiavoni et al., 2016)	4	1
Cork	High, no additional binders or chemical used in the production process [5]	4	1
Polyurethane	Same recycling issues as for EPS - recycling process is performed by specialized industries (Schiavoni et al., 2016)	3	0.75
Vacuum insulation panels	No information found	0.5	0.125
Gas insulated panels	No information found	0.5	0.125
Aerogels	No information found	0.5	0.125

Table D.10: MCA results for material circularity with gathered reference data

High emphasis has been put on the circularity of the chosen product. By choosing insulation materials with recycled content or materials that facilitate recycling, the reduction of waste and carbon footprint can be achieved. Bio-materials have been proven to have recyclable properties with minimal environmental impact in their production process (Kunič, 2017).

D.3 LCA

D.3.1 Cork insulation material

Table D.11 includes the results of the environmental impact of the the chosen cork insulation material which is produces by Pro Suber. As mentioned in the report itself, the data had to be adjusted to account for the chosen thickness of 200mm instead of the thickness of 140mm, which is specified in the chosen EPD. These results are then presented graphically in Figure 6.3.

Impact Category	A1-A3	C1-C4	TOTAL
CC total (kg CO2 eq)	-140,16	19,43	-120,73
CC fossil (kg CO2 eq)	11,44	-2,89	8,55
CC biogenic (kg CO2 eq)	-152,32	22,43	-129,89
CC luluc (kg CO2 eq)	0,09	-0,03	0,07
ODP (kg CFC 11 eq)	0,00	0,00	0,00
AP (mol H+ eq)	0,11	-0,05	0,06
EP freshwater (kg P eq)	0,00	0,00	0,00
EP marine (kg N eq)	0,02	-0,01	0,01
EP terrestrial (mol N eq)	0,28	-0,20	0,08
POCP (kg NMVOC eq)	0,07	-0,04	0,03
ADP Elements (kg Sb eq)	0,00	0,00	0,00
ADP fossil fuels (MJ)	154,24	-40,00	114,24
WDP (m^3 water eq deprived)	21,95	-3,37	18,58

Table D.11: Environmental impact of Pro Suber cork insulation material

D.3.2 Membrane

Table D.12 includes the results of the environmental impact of the membrane system. In the calculations, two membranes are accounted for as it is expected that the membrane must be replaced once over the facades service life. These results are then presented graphically in Figure 6.5.

Impact Category	A1-A3	C1-C4	D	TOTAL
CC total (kg CO2 eq)	0,37	0,33	-0,15	0,56
CC fossil (kg CO2 eq)	0,00	0,00	0,00	0,00
CC biogenic (kg CO2 eq)	0,00	0,00	0,00	0,00
CC luluc (kg CO2 eq)	0,37	0,33	-0,15	0,56
ODP (kg CFC 11 eq)	0,00	0,00	0,00	0,00
AP (mol H+ eq)	0,00	0,00	0,00	0,00
EP freshwater (kg P eq)	0,00	0,00	0,00	0,00
EP marine (kg N eq)	0,00	0,00	0,00	0,00
EP terrestrial (mol N eq)	0,00	0,00	0,00	0,00
POCP (kg NMVOC eq)	0,00	0,00	0,00	0,00
ADP Elements (kg Sb eq)	0,00	0,00	0,00	0,00
ADP fossil fuels (MJ)	10,40	0,09	-2,59	7,90
WDP (m^3 water eq deprived)	0,05	0,03	-0,02	0,07

Table D.12: Environmental impact of Solitex Fronta Humida waterproof membrane

D.4 Concrete

Table D.12 includes the results of the environmental impact of the concrete. The results presented in the table include the combined results of Argex 4/8, cement and recycled sand. These results are then

presented graphically in Figure 6.4.

Impact Category	A1–A3	C1-C4	D	Total
CC total (kg CO2 eq)	176,1	5,4	-11,1	170,4
CC fossil (kg CO2 eq)	175,9	5,4	-10,7	170,6
CC biogenic (kg CO2 eq)	0,0	0,0	-0,4	-0,4
CC luluc (kg CO2 eq)	0,1	0,0	0,0	0,1
ODP (kg CFC 11 eq)	0,0	0,0	0,0	0,0
AP (mol H+ eq)	3,0	0,0	-1,0	2,1
EP freshwater (kg P eq)	0,0	0,0	0,0	0,0
EP marine (kg N eq)	0,2	0,0	-0,2	0,0
EP terrestrial (mol N eq)	2,1	0,1	-0,4	1,8
POCP (kg NMVOC eq)	0,7	0,0	-0,4	0,3
ADP Elements (kg Sb eq)	0,0	0,0	0,0	0,0
ADP fossil fuels (MJ)	1399,3	98,3	-22,1	1475,5
WDP (m^3 water eq deprived)	15,7	2,4	-1,6	16,5

Table D.13: Environmental impact of the concrete layer